Simulation of NMR Spectra from MD trajectories. Application to Solid State ^{2}H NMR of Deuterated ImTPA Host Guest Crystals

Dennis F. Cook

January 2020

Thesis for Masters By Research

University of East Anglia

School of Chemistry Norwich

Abstract

This work predicts the effects of molecular motions on NMR measurements, namely ^{2}H NMR line shapes arising from quadrupolar coupling (Pake pattern) and T_1 relaxation times directly and completely from the results of all-atom MD simulations. Simulations were performed on a host guest system of ImTPA crystals at two characteristic temperatures. The resulting trajectories have been used for the first time to predict ^{2}H NMR line shapes based on the theoretical and computational methodology originally developed by Oganesyan for the prediction of EPR spectral line shapes from atomistic MD trajectories [1] adapted for predicting NMR spectra.

DFT methods have been employed to optimise the structures of host and guest molecules, generating parameters for the forcefields in MD runs using GROMACS and calculated the quadrupolar coupling tensor components of ^{2}H sites in Imadazolium Ions.

^{2}H NMR spectra were predicted using two approaches; i) direct propagation of the density matrix (DP) for the spin system using the Stochastic Liouville Equation (SEL) [2] and time dependent Liouville superoperator and ii) applying fast motional limit (FML) approximation

which employs the motionally averaged quadrupolar coupling tensor. The results are compared to the experimental measurements available from the literature.

It is concluded that the NMR predictions based on the FML approach provide an adequate representation of the two-states jump motions of the Imidazolium Ions in ImTPA capturing accurately their impact on the NMR line shapes at different temperatures. Predictions by DP method are broadly in agreement with the FML but, in comparison with EPR, require longer trajectories for an adequate spectral simulation.

Predictions of T_1 relaxation times arising from the dynamical modulation of the quadrupolar coupling term in the spin-Hamiltonian are reported at both temperatures for a range of magnetic field strengths using the same MD trajectories.

Access Condition and Agreement

Each deposit in UEA Digital Repository is protected by copyright and other intellectual property rights, and duplication or sale of all or part of any of the Data Collections is not permitted, except that material may be duplicated by you for your research use or for educational purposes in electronic or print form. You must obtain permission from the copyright holder, usually the author, for any other use. Exceptions only apply where a deposit may be explicitly provided under a stated licence, such as a Creative Commons licence or Open Government licence.

Electronic or print copies may not be offered, whether for sale or otherwise to anyone, unless explicitly stated under a Creative Commons or Open Government license. Unauthorised reproduction, editing or reformatting for resale purposes is explicitly prohibited (except where approved by the copyright holder themselves) and UEA reserves the right to take immediate ‘take down’ action on behalf of the copyright and/or rights holder if this Access condition of the UEA Digital Repository is breached. Any material in this database has been supplied on the understanding that it is copyright material and that no quotation from the material may be published without proper acknowledgement.

Contents

Acknowledgments

This work is indebted to the guidance of Dr Vasily Oganesyan who both developed the theoretical groundwork and instructed me on it's implementation, which was instrumental in my ability to complete this project as well as providing general assistance with the organisation of the project and providing regular feedback on my work and thesis as it developed.

Additionally to my secondary supervisor Professor Yaroslav Khimyak who helped me build up my understanding of the wider context of NMR theory and experimental technique as well as helping my surveying of the literature and choice of sample system.

Mrs Pauline Walton and Dr Chris Prior provided vital support for the computational aspect by teaching me how to use bash terminals to access the High Performance Cluster (HPC), which I thank the University of East Anglia for access to, so I could run simulation in the molecular dynamics suite GROMACS and use Gaussview and Amber to develop the required inputs for those systems. While Dr Robert Penfold assisted with the use of MATLAB for coding for the required calculations.

I am also extremely grateful to the emotional support provided by my partner, family and friends especially my mother, Mrs Susan Cook and Ms Ariadne Thompson who have assisted at numerous points with proofreading my work.

List of Figures

List of Tables

List of Symbols and Constants

Symbol	Quantity	S.I units	Value
ω	Frequency	Hz	-
I	Nuclear Spin	-	-
B	Magnetic Field	T	-
γ	Gyromagnetic Ratio	Hz T^{-1}	-
E	Energy	J	-
$\hbar$	Reduced Planck's Constant	J.s	1.055×10^{-34}
h	Planck's Constant	J.s	6.626×10^{-34}
T	Temperature	Kelvin	-
k_B	Boltzmann's Constant	J K^{-1}	1.38×10^{-23}
V	Electric Field Gradient	V m^{-2}	-
q	Electric charge	C	-
r	Distance	m	-
x_a	Distance In Direction a	m	-
ϵ_0	Vacuum Permittivity	F. m^{-1}	8.85×10^{-12}
Tr	Trace of the matrix	-	-
η	Asymmetry	-	-
χ	Quadrupolar Coupling	Hz	-

Table 1: List of Symbols and Constants

Q	Electric Quadrupole Moment	C m^2	-
e	Elementary Charge	C	1.602×10^{-19}
$\hat{H}$	Spin Hamiltonian	J or Hz	
ν	Splitting	Hz	-
t	Time	s	-
k	Reaction Rate	Hz	-
A	Arrhenius Pre-exponential Factor		-
R	Molar Gas Constant	m^2 kg s^{-2} K^{-1} mol^{-1}	8.314
σ	Chemical Shielding	ppm	-
$R_a(\theta)$	Rotation Matrix	-	-
$I(\omega)$	Absorption Intensity	-	-
ρ	Density Operator	-	-
$\hat{\hat{L}}$	Liouville Superoperator	-	-
M	Net Magnetisation	A m^{-1}	-
$\hat{U}$	Identity Operator	-	-
$\hat{S_+}$	Sum of Electron Spin Operators	-	-
N, K	Sets of Coordinates for 2 by 2 Tensor	-	-
G	Autocorrelation Function	-	-
$\hat{X}$	Ensemble Averaged Operator		
τ	Time Step	s	-
$\boldsymbol{\hat{T}}$	Spherical Tensor Operator	-	-
$\boldsymbol{\bar{V}}$	Lattice Tensor	-	-
$\boldsymbol{D}$	Wigner Matrix	-	-
Ω	Set of 3 Euler Angles	-	-
α, λ	Arbitrary Magnetic Interaction	-	-
y	Rank of a Tensor	-	-
τ_c	Correlation Time	s	-

Table 1: List of Symbols and Constants

$\langle ... \rangle$	Ensemble Averaged quantity	-	-
C	Correlation Function	-	-
$\hat{\hat{\Lambda}}$	Time Independent Superoperator	-	-
K_r	Force Constant of a Bond	N m^{-1}	-
b	Equilibrium Bond Length		
K_{ij}^{θ}	Angular Force Constant	N degree^{-1}	-
K_{ijk}^{θ}	Dihedral Angular Force Constant	N degree^{-1}	-
ψ	Dihedral Angle	degrees	-
F	Force	Newtons	-
$\hat{F}$	Fock Operator	-	-
$\hat{h}$	Single Electron Orbitals	-	-
$\hat{J}$	Coulomb Repulsion Operator	-	-
$\hat{K}$	Exchange Operator	-	-
v	Final Velocity	m s^{-1}	-
u	Initial Velocity	m s^{-1}	-
a	Acceleration	m s^{-2}	-
s	Displacement	m	-
N	Number of Particles in the System	-	-
V	Volume	m^3	-
C_v	Heat Capacity	J K^{-1}	-
N_{dif}	Degrees of Freedom	-	-
K	Kinetic Energy	J	-
W	Random Force	N	-
ρ	Density	kg m^{-3}	-
P	Pressure	N m^{-2}	
μ	Pressure Matrix	-	-
β	Isothermal Compressability	Pa^{-1}	-

Table 1: List of Symbols and Constants

R_{QR}	Quadrupolar Relaxation Rate	-	-

Table 1: List of Symbols and Constants

1

Introduction

1.1 NMR

Nuclear Magnetic Resonance Spectroscopy (NMR) [6] is an analytical technique used to investigate the structure and dynamics of a chemical system. These features are investigated by measuring the frequencies, ω, of precession of nuclei in the system around a magnetic field.

This precession occurs in nuclei with non-zero net spin at a rate dependent on the strength of the magnetic field, B, and a fundamental quantity of the isotope involved, the gyromagnetic ratio ,γ [7]. This allows for the presence of specific NMR active nuclei to be identified in the species, including distinguishing between isotopes of the same element with different spins or gyromagnetic ratios [8].

While this is true for a single isolated nucleus it is an incomplete picture, as it assumes the local environment has no effect on the magnetic field experienced by the precessing nuclei. In single crystal NMR the influences of local environment are also important, this introduces interactions with the nuclei and local magnetic field, chemical shielding [9], as well as coupling between pairs of nuclear spins, J coupling [10] through bonds and dipolar coupling [11] through space, and for nuclei with absolute spins greater than $\frac{1}{2}$ coupling between nuclear quadrupoles and electric field gradients in the local structure [12].

These effects introduce additional sensitivity into the NMR spectrum allowing for more details to be determined about the structure. The dependency of chemical shielding on the local environment allows nuclei to be distinguished by their surrounding environment. This includes distinguishing between the head groups of polymers [13] and site specific measurements of isotopic abundance [14]. While dependence on the distances between nuclei in dipolar coupling can measure the distance [15] [16] in molecular structure and similarly J coupling can measure angles in structures [17].

Further there's the potential for orientational dependence, for example chemical shielding around a nucleus is not necessarily the same in all directions, chemical shift anisotropy, leading to a difference in the shielding observed dependent on the orientation of the molecule relative to the external magnetic field. This allows orientations to be distinguished [18]. Beyond the single crystal case, these orientational dependencies can reveal information about order and the distributions of molecular orientations in a larger structure through the broadening of frequencies for each chemical environment [19][20].

These orientations can also be time dependent, where the rates of change in orientation affect the extent of coupling observed. Because of this NMR can be used to study the dynamics of systems [21] [22] [23]. This allows NMR to distinguish between phases by the rates of motion and the range of accessible orientations, for example quadrupolar coupling is observed in solid state NMR but absent in solution. Allowing the detection of phase transition between solid and liquid phases and liquid phases of different orders [24].

Similarly this can be used to detect binding between molecules and the wider structures which has the effect of restricting motions, this is valuable in both an inorganic context, when looking at host guest interaction in zeolites [25] [26] [27], and metal organic frameworks [28] [29]. In an organic context this is useful when studying the binding of molecules to lipid bi-layers [30] [31] [32] and proteins [33].

1.2 Computational Chemistry

The use of computational techniques in chemistry presents a powerful tool for the modeling of chemical systems and the prediction of bulk properties from first principles without relying on experiments. This has several advantages over conventional measurement, for example simulation of high energy systems [34] allows data to be collected on systems that would otherwise be prohibitively difficult to study under laboratory conditions. While computational studies of reaction pathways [35] [36] [37] allow for the prediction of behaviours that can't be monitored as easily experimentally. For example the positions of individual atoms and the properties of extremely short lived excited [38] [39] or transition [40] [41] states.

Oganesyan [1] has developed a technique for the prediction of EPR spectra of spin systems, this approach involves calculating a Liouvillian Superoperator which expresses how the distribution of spins in the system change with time. This Superoperator is the sum of the Superoperators for individual magnetic interactions which for EPR are the Zeeman interaction [42], zero field splitting [43], exchange interactions [44] and hyperfine coupling [45]. This approach has been successfully applied to investigation of structure and dynamics of bio molecules including DNA [46], lipid bi-layers [47] and myoglobin [48].

Calculating the Superoperator for each interaction requires a spherical tensor, dependent on the electron spins in the system, as well as a lattice tensor that describes the surrounding structure and a Wigner matrix modeling the relative orientation of the surrounding structure to the external magnetic field. For NMR, the spin tensors are dependent on nuclear spin and characteristic properties of each isotope only, so are the same for all nuclei of each isotope.

The lattice tensors are more complex to calculate, first involving the optimisation of structure of individual molecules in the system [49] [50] from which the relevant lattice tensors can be calculated. This project focuses on the quadrupolar coupling interaction where the lattice tensor required is the electric field gradient tensor which can be calculated from the distribution of charges in the molecule [51]. While quadrupolar coupling was chosen for this project the approach can be applied analogously to the other magnetic interactions.

Finally the Wigner matrices are derived from molecular dynamics simulations which allow the positions of individual nuclei to be tracked in the form of a trajectory file, this part of the approach is the same for both EPR and NMR [52].

1.3 NMR Measurements

To measure the NMR spectra of a system it is placed in a magnetic field, B_0. B_0 defines the z direction for the experiment and a detector coil is placed perpendicular to B_0 in the x-y plane of this laboratory fixed axis system.

$$B_0 = \begin{bmatrix} 0 \\ 0 \\ B_{0z} \end{bmatrix} \tag{1.1}$$

In the presence of B_0, nuclei with non zero spin, I, in the system precess around the field at a frequency, ω_0, proportional to the strength of the field and γ a characteristic constant for a given isotope, Hz T^{-1}.

$$\omega_0 = B_0 \gamma \tag{1.2}$$

A second magnetic field, B_t, is then applied. B_t is carried by an electromagnetic pulse in the radio frequency, r.f, range, that propagates perpendicular to the z direction in the x-y plane. As it's carried by an oscillating wave, B_t is time dependent, rotating in the x-y plane around the z direction with frequency, ω_t, the same as the frequency of the pulse. This pulse can either be applied as a single continuous wave, which sweeps through a range of frequencies (building up the spectra over a longer time) or can be applied simultaneously in a pulse made up of multiple frequencies at once.

Now it's the resultant of these two fields on the nucleus, B_{eff}, that the nucleus precesses around, which is given by.

$$B_{eff} = \sqrt{\left((B_0(1 - \frac{\omega_t}{\omega_0}))^2 + (B_t)^2\right)} \tag{1.3}$$

[53] Normally $B_0 >> B_t$, meaning that $B_{eff} \approx B_0$, unless ω_t is equal to or almost equal to ω_0, referred to as the pulse being on or near resonance. When the field B_t oscillates at the same rate that the nucleus precesses, $\omega_0 = \omega_t$,

$$B_{eff} = B_t \tag{1.4}$$

the resultant field on the nucleus is B_t which is a constant, B_1, with respect to the nucleus. This negates the effect of B_0 on the nucleus leading it to precess only around B_1. As B_1 is perpendicular to B_0 the precession of the nucleus has been rotated 90° into the plane of the detector coil.

After the pulse, the detector coil placed in the x-y plane is switched on. This coil detects voltage associated with the movement of charges as nuclei precess, which vary with time. For a single type of nucleus the result is a dampened sine-wave, FID, with the same frequency as the frequency of precession.

For multiple types of nuclei precessing simultaneously, the voltage detected in the coil is a superposition of the voltages due to each precession, which are not necessarily of the same frequency. This signal in time can then be converted from the time domain to the frequency domain to separate it into its component frequencies using a Fourier transform. This will correspond to which NMR active nuclei are present in the system.

There's another source of information in the spectra, which comes into effect after the pulse ends. During the pulse, there's an energetic incentive to be aligned with the magnetic field in the x-y plane and the effects of B_0 are negated.

After the pulse this is no longer true and so there's a loss of this alignment, both through realignment with B_0 via T1 relaxation and loss of coherence

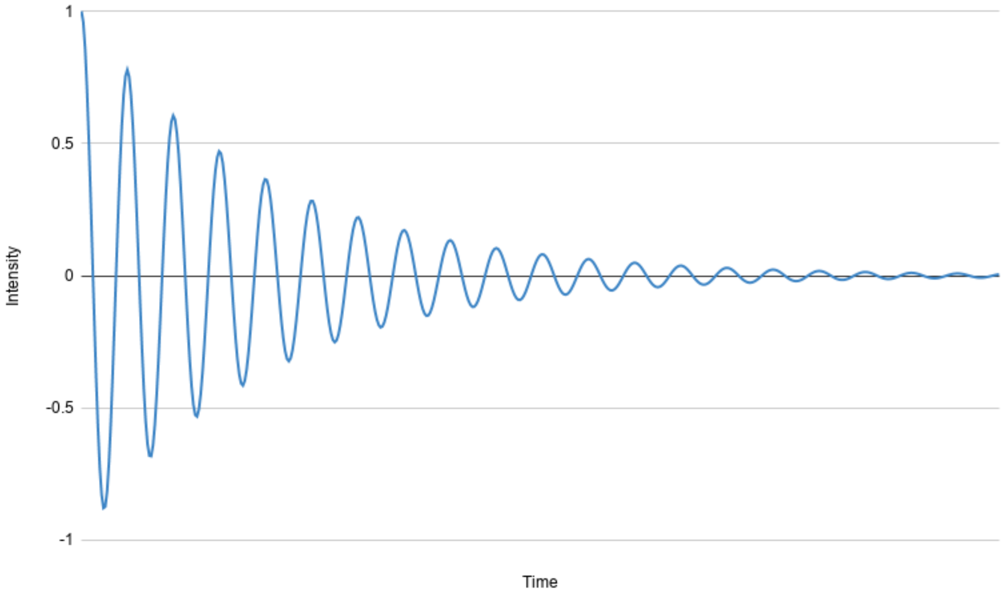

Figure 1.3.1: FID for single NMR active nucleus in the sample. Plotted as $cos(25t)e^t$.

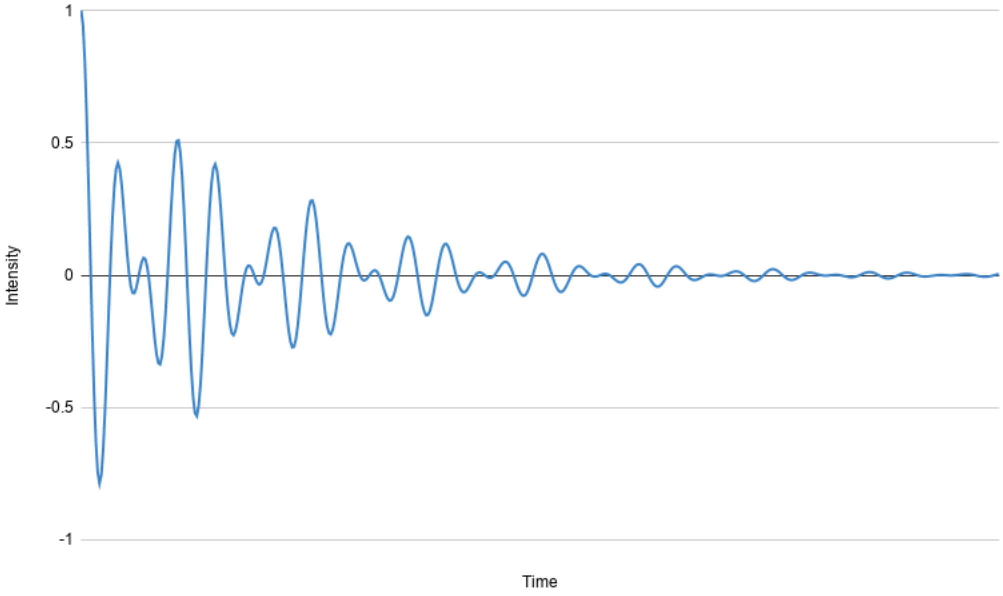

Figure 1.3.2: FID for multiple NMR active nuclei in the same sample with different characteristic frequencies. $(cos(25t) + cos(35t))2e^{-t}$.

in the x-y plane by entropic effects in T2 relaxation. The result of this relaxation is a dampening of the signal detected by the coil in the x-y plane. Where the rates of relaxation reveal information about the system, including how able nuclei in the system are to reorient themselves, which reveals information about the dynamics.

1.4 NMR Theory

1.4.1 Zeeman Splitting

Nucleons, protons and neutrons, possess a quantity called spin of $\frac{1}{2}$. In the nucleus there is a tendency for nucleons of the same type to pair up positive to negative, reducing the net spin, I, of the nucleus. For an even number of both types of nucleon this pairing is complete resulting in $I = 0$.

But for an odd number of either nucleon, or both, the pairing is incomplete resulting in a nucleus with $I \neq 0$. Though at this point the distinction between a positive and negative spin is arbitrary as there's no energy difference between the two.

The two states are no longer degenerate, of equal energy, in the presence of a magnetic field, B_0, where the nuclear spin can be aligned with, or opposed to, the field, and the energy difference between states, ΔE, is given by

$$\Delta E = \Delta m \gamma B_0 \hbar \tag{1.5}$$

Being aligned with the field is lower energy than being opposed to it. $\hbar$ is the reduced Planck's constant and γ is the gyromagnetic ratio, a value for the rate a nucleus rotates at for a given field strength. This energy difference corresponds to a frequency, ω, of radiation that can be absorbed or emitted to transition between states.

$$E = h\omega \tag{1.6}$$

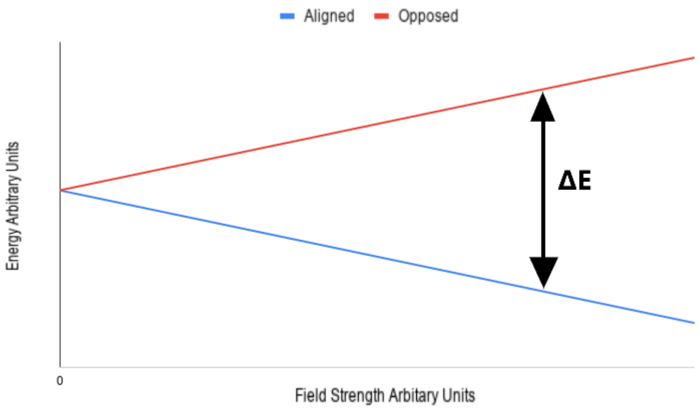

Figure 1.4.1: Increasing ΔE between spins aligned and opposed spins with increasing magnetic field.

Under these conditions the nuclear spins in the species exist in two states with a ratio between the population in the high energy, E_+, and low energy, E_-, states of

$$\frac{E_+}{E_-} = exp\left(\frac{-\Delta E}{k_B T}\right) \tag{1.7}$$

This has a few consequences, as k_B is constant, the two relevant properties are ΔE, proportional to constants and the magnetic field, and temperature T.

As the magnetic field increases, the splitting between states is higher and so the spins tend towards being aligned completely for an infinite magnetic field, while for no field the populations are even, corresponding to the degeneracy mentioned earlier. As for temperature the species approaches equal populations of both spin states as temperature approaches infinity as thermal energy overcomes the energetic incentive to be aligned with the field.

However, this is an incomplete picture as there are additional factors to consider when not dealing with single isolated nuclei in a magnetic field.

1.4.2 Quadrupolar Coupling

Quadrupolar coupling is a interaction, due to the coupling between electric field gradients, V, present in the species and asymmetries in the charge distribution present in certain nuclei.

The electric field gradient is the derivative of the electric field potential at a given point in a species, where the electric field potential for a nuclei is the sum of the potentials V_E due to each surrounding nuclei, i.

$$V_E = \sum_i \frac{1}{4\pi\epsilon_0}.\frac{q_i}{r} \tag{1.8}$$

where ϵ_0 is the permittivity of free space, q is the charge of the nucleus and r is the distance from that charge.

The electric field gradient is also the 2nd derivative with respect to distance in the directions x_a and x_b.

$$V_{ab} = \frac{\partial^2 \boldsymbol{V}}{\partial x_a \partial x_b} \tag{1.9}$$

Which are arranged into a tensor, as with shielding.

$$\boldsymbol{V} = \begin{vmatrix} V_{xx} & V_{xy} & V_{xz} \\ V_{yx} & V_{yy} & V_{yz} \\ V_{zx} & V_{zy} & V_{zz} \end{vmatrix} \tag{1.10}$$

A consequence of the formula for the derivative being the same on exchange of a and b.

$$\frac{\partial^2 V}{\partial x_a \partial x_b} = \frac{\partial^2 V}{\partial x_b \partial x_a} \tag{1.11}$$

Is that

$$V_{ab} = V_{ba} \tag{1.12}$$

meaning that the matrix is symmetrical along its main diagonal.

The axes are conventionally defined as

$$\mid V_{zz} \mid \geq \mid V_{yy} \mid \geq \mid V_{xx} \mid \tag{1.13}$$

and the asymmetry parameter, η, is defined as

$$\eta_V = \frac{V_{yy} - V_{xx}}{V_{zz}} \tag{1.14}$$

which is unitless.

Another feature of this gradient is that the trace of the matrix,

$$Tr(\boldsymbol{V}) = V_{xx} + V_{yy} + V_{zz} = 0 \tag{1.15}$$

This is because the electric field gradient follows the Laplace equation where the sum of the 2nd partial derivatives of V in each direction is 0.

$$\Delta V = \frac{\partial^2 V}{\partial x^2} + \frac{\partial^2 V}{\partial y^2} + \frac{\partial^2 V}{\partial z^2} = 0 \tag{1.16}$$

where Δ is the Laplace operator [54]. If this value was non zero it would result in a net force on the nucleus and the species would not be at equilibrium.

In the principal axis system $\boldsymbol{V}^{PAS}$ of the tensor only the diagonal values of V are non zero.

$$\boldsymbol{V}^{PAS} = \begin{vmatrix} V_{xx} & 0 & 0 \\ 0 & V_{yy} & 0 \\ 0 & 0 & V_{zz} \end{vmatrix} \tag{1.17}$$

But not all species have an electric field gradient. For a gradient to exist over the species there needs to be asymmetry in at least one direction. Otherwise the species possesses an inversion centre and any gradient respective to a nucleus in one part of the molecule is cancelled out by an equal and opposite gradient relative to an equivalent nucleus through the inversion centre and the two orientations are indistinguishable.

As well as specific requirements for the structure of a species, there are also limits on the nuclei that can display quadrupolar coupling. Nuclei have spherical charge distribution when, $\mid I \mid < 1$, but for absolute nuclear spins of 1 or greater the nucleus will be either oblate or prolate with non spherical charge distribution. This produces a quadrupole in the nucleus which can be thought of as two bisecting perpendicular lines of positive and negative charge respectively.

When both requirements are met, the electric field gradient exerts torque on the quadrupole. This results in a change in the frequency of precession of nuclei as the nucleus needs to push with or against this torque. With the frequency accounting for quadrupolar interactions, ω_Q, given by

$$\omega_Q = \omega_0 - \frac{3}{8}\left(\frac{2m-1}{I(2I-1)}\right)\chi(3\cos^2\theta - 1) \tag{1.18}$$

where the angle, θ, is the angle between the quadrupole and the z axis of the external magnetic field, B_0 [55].

This equation also gives the value for the magic angle, where the perturbation term cancels out, at 54.74° degrees. As a consequence spinning the sample sufficiently quickly at an angle of 54.74° eliminates broadening due to quadrupolar coupling.

For the $I = 1$ case, m is 0 or ± 1 corresponding to the spin state of the nucleus, χ is a constant for the system representing the strength of quadrupolar coupling

$$\chi = \frac{e^2 qQ}{\hbar} \tag{1.19}$$

where e is the electron charge, and Q is the nuclear quadrupolar moment and q is an expression of anisotropy in the electron cloud, and θ is the angle in degrees between the quadrupole and B_0 and eq is the anisotropy in the tensor V_{zz}.

$$eq = V_{zz} \tag{1.20}$$

$$\chi = \frac{eV_{zz}Q}{\hbar} \tag{1.21}$$

The Hamiltonian for the energy of this interaction is given by

$$\hat{H}_Q = \frac{eQ}{2I(2I-1)} \cdot \begin{bmatrix} I_x & I_y & I_z \end{bmatrix} \begin{vmatrix} V_{xx} & V_{xy} & V_{xz} \\ V_{yx} & V_{yy} & V_{yz} \\ V_{zx} & V_{zy} & V_{zz} \end{vmatrix} \begin{bmatrix} I_x \\ I_y \\ I_z \end{bmatrix} \tag{1.22}$$

In the simplest quadrupolar case of a spin 1 nucleus, for example deuterium, there are two transitions to consider, -1 to 0 and 0 to 1 of equivalent energy. Assuming all nuclei are in equivalent environments and orientation with isotropic shielding, this results in a peak for each transition.

However in the powder spectrum, where the molecules in the system are distributed evenly across all possible orientations, these two peaks are spread across frequencies corresponding to the range of angles, θ. Between a peak corresponding molecules where V_{zz}^{PAS} is perpendicular to B_0, trailing off to minimum intensity where V_{zz}^{PAS} is perpendicular.

There are three different splittings $\Delta\nu_1$, $\Delta\nu_2$ and $\Delta\nu_3$ in each spectra, values of these splitting being dependent on orientations and motions in the system [56].

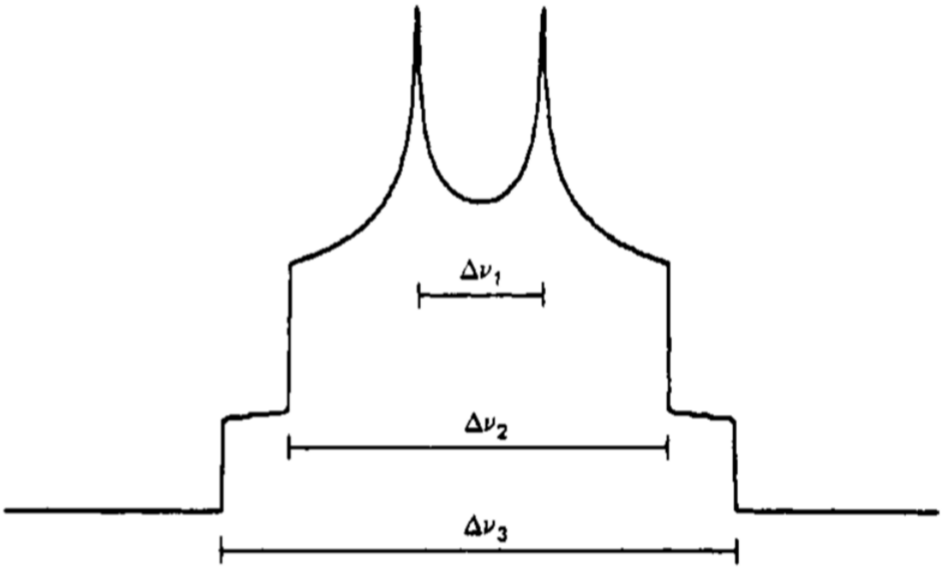

Figure 1.4.2: Pake Pattern with splitting values nu 1, 2 and 3 labeled by Gall et al.

These splitting values are given by

$$\Delta\nu_1 = \frac{3}{8}\chi(1-\eta) \tag{1.23}$$

$$\Delta\nu_2 = \frac{3}{8}\chi(1+\eta) \tag{1.24}$$

$$\Delta\nu_3 = \frac{3}{4}\chi \tag{1.25}$$

1.4.3 What can be distinguished

A key assumption for the above is that two non-equal frequencies can be distinguished, which is not necessarily true. The limit to what can be distinguished is a result of time–energy uncertainty, which is a minimum value of the product of uncertainty in the values of energy and time [57].

$$\Delta E \Delta t \geq \frac{\hbar}{2} \tag{1.26}$$

This means that the more precisely the time is known the less precision there can be in energy measurements, and if uncertainty in energy measurements is greater than the difference in energy between two states, they are indistinguishable. This means for a given frequency difference, $\Delta\nu$, there's a limit to how short lived the shortest lived state can exist for before all that's seen is the average of the two states, referred to as the coalescence time, τ which is the inverse of the rate of interchange between the states, k.

$$\tau_{coalescence} = (\sqrt{2}\pi\Delta\nu)^{-1} = k^{-1} \tag{1.27}$$

And the factors affecting rate can be modeled with the Arrhenius equation,

$$k = A.exp\left(-\frac{E_a}{RT}\right) \tag{1.28}$$

where A is a proportionality constant for a given process, E_a is the activation energy for that process and R is the molar gas constant. Because of these dependencies there are ways to improve the ability of an experiment to distinguish between two states. In the case of chemical shielding the energy difference

$$\hat{H}_\sigma = \hbar\gamma\hat{I}\sigma\hat{B} \tag{1.29}$$

is proportional to the magnetic field strength, allowing larger magnets to increase the resolution. However this is not true in the case of quadrupolar splitting, which is a function of inherent properties in the molecule and not due to the external magnetic field. In both cases the rate dependence on temperature opens the possibility of lowering temperature to slow down the interchange between states. There are two limits to these effects, the fast limit and the rigid limit where

$$k \gg \Delta\nu \tag{1.30}$$

and

$$k \ll \Delta\nu \tag{1.31}$$

respectively.

At the fast limit multiple different transitions display as a single peak and at the rigid limit they appear distinctly. This is also why broadening due to quadrupolar coupling isn't observed in liquid or gaseous state NMR, where rapid molecular tumbling results in such short lived orientations that none can be distinguished and a single distinct average peak is all that is observed.

1.4.4 Definition of Reference Frames

A reference frame is a coordinate system defined by a set of three orthogonal cartesian axes. This project requires conversion between multiple reference frames because the physical quantities used are known and defined in different reference frames. The electric field gradient tensor is known relative to each individual molecule but the degree to which these gradients lead to splitting is dependent on their magnitude relative to the external magnetic field so each individual molecular tensor needs to be rotated into a common frame, that of the magnetic field.

The relevant reference frames in this project are

The Principle Axis System (PAS) defined by features of the molecule

- P$_z$ - The direction of the greatest eigenvalue of the electric field gradient tensor.
- P$_y$ - The direction of the middle eigenvalue of the electric field gradient tensor.
- P$_x$ - The direction of the lowest eigenvalue for the electric field gradient tensor.

The Laboratory Frame (LAB) defined by the external magnetic field and the axis used in GROMACS simulations

- L$_z$ -The direction of the external magnetic field
- L$_y$ and L$_x$ two vectors mutually perpendicular to L$_z$

1.4.5 Transformation between frames

In order to transform one reference frame into another a series of three rotations are needed [58]. Each individual rotation is described by a rotation matrix $R_a(\theta)$ anticlockwise about an axis, a, by an angle of θ. For the x, y and z axis these rotation matrices are.

$$R_x(\alpha) = \begin{bmatrix} 1 & 0 & 0 \\ 0 & cos\alpha & -sin\alpha \\ 0 & sin\alpha & cos\alpha \end{bmatrix} \tag{1.32}$$

$$R_y(\beta) = \begin{bmatrix} cos\beta & 0 & sin\beta \\ 0 & 1 & 0 \\ -sin\beta & 0 & cos\beta \end{bmatrix} \tag{1.33}$$

$$R_z(\gamma) = \begin{bmatrix} cos\gamma & -sin\gamma & 0 \\ sin\gamma & cos\gamma & 0 \\ 0 & 0 & 1 \end{bmatrix} \tag{1.34}$$

These rotations may either be active, A, or passive, P. Active rotations involve the movement of a rigid body within the reference frames. As opposed to passive rotations where the frames themselves are rotated while the body, in this case a molecule, remains static. For conversion between reference frames passive rotations are used.

For converting from X, Y and Z in the Principle Axis System to the laboratory frame.

$$\begin{bmatrix} X_{LAB} \\ Y_{LAB} \\ Z_{LAB} \end{bmatrix} = P_{rotatedX_3Y_2Z_1}(\gamma, \beta, \alpha) \begin{bmatrix} X_{PAS} \\ Y_{PAS} \\ Z_{PAS} \end{bmatrix} \tag{1.35}$$

three steps are required.

1. Rotation about the Z$_{PAS}$ axis by an angle of α rotates xyz to $x'y'z'$

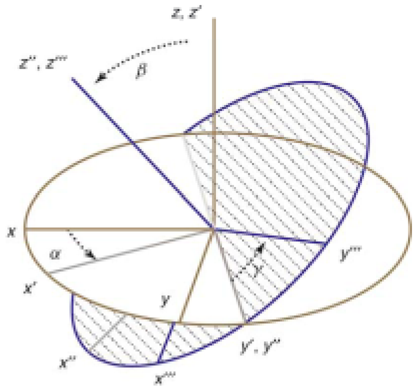

Figure 1.4.3: Transformation between two frames by three rotations [3].

where $z = z'$.

$$\begin{bmatrix} x' \\ y' \\ z' \end{bmatrix} = \begin{bmatrix} cos\alpha & -sin\alpha & 0 \\ sin\alpha & cos\alpha & 0 \\ 0 & 0 & 1 \end{bmatrix} \begin{bmatrix} x \\ y \\ z \end{bmatrix} \tag{1.36}$$

2. Rotation about the the new axis y' by an angle β where $y' = y''$.

$$\begin{bmatrix} x'' \\ y'' \\ z'' \end{bmatrix} = \begin{bmatrix} cos\beta & 0 & sin\beta \\ 0 & 1 & 0 \\ -sin\beta & 0 & cos\beta \end{bmatrix} \begin{bmatrix} x' \\ y' \\ z' \end{bmatrix} \tag{1.37}$$

3. And finally rotation about x'' axis by an angle of γ where $x'''y'''z'''$ are the lab frame $X_{LAB}Y_{LAB}Z_{LAB}$.

$$\begin{bmatrix} x''' \\ y''' \\ z''' \end{bmatrix} = \begin{bmatrix} 1 & 0 & 0 \\ 0 & cos\gamma & -sin\gamma \\ 0 & sin\gamma & cos\gamma \end{bmatrix} \begin{bmatrix} x'' \\ y'' \\ z'' \end{bmatrix} \tag{1.38}$$

These transformations can then be expressed as a single 2nd rank Wigner

D matrix, which takes the form.

$$\begin{bmatrix} (\frac{1+cos\beta}{2})^2e^{-2i(\alpha+\gamma)} & -\frac{1+cos\beta}{2}sin\beta e^{-i(2\alpha+\gamma)} & \sqrt{\frac{3}{8}}sin^2\beta e^{-i2\alpha} & -\frac{1-cos\beta}{2}sin\beta e^{i(-2\alpha+\gamma)} & (\frac{1-cos\beta}{2})^2e^{2i(-\alpha+\gamma)} \\ \frac{1+cos\beta}{2}sin\beta e^{-i(2\alpha+\gamma)} & [cos^2\beta-\frac{1-cos\beta}{2}]e^{i(\alpha+\gamma)} & -\sqrt{\frac{3}{8}}sin(2\beta)e^{-i\alpha} & [\frac{1-cos\beta}{2}-cos^2\beta]e^{i(-\alpha+\gamma)} & -\frac{1-cos\beta}{2}sin\beta e^{i(-\alpha+2\gamma)} \\ \sqrt{\frac{3}{8}}sin^2\beta e^{-i2\gamma} & \sqrt{\frac{3}{8}}sin(2\beta)e^{-i\gamma} & \frac{3cos^2\beta-1}{2} & -\sqrt{\frac{3}{8}}sin(2\beta)e^{i\gamma} & \sqrt{\frac{3}{8}}sin^2\beta e^{i2\gamma} \\ \frac{1-cos\beta}{2}sin^2\beta e^{i(\alpha-2\gamma)} & [\frac{1+cos\beta}{2}-cos^2\beta]e^{i(2\alpha-\gamma)} & \sqrt{\frac{3}{8}}sin^2\beta e^{i\alpha} & [cos^2\beta-\frac{1-cos\beta}{2}e^{i(\alpha+\gamma)}] & -\frac{1+cos\beta}{2}sin\beta e^{i(\alpha+2\gamma)} \\ (\frac{1-cos\beta}{2})^2e^{2i(\alpha-\gamma)} & (\frac{1-cos\beta}{2})sin\beta e^{i(2\alpha-\gamma)} & \sqrt{\frac{3}{8}}sin^2\beta e^{i2\alpha} & (\frac{1+cos\beta}{2})sin\beta e^{i(2\alpha+\gamma)} & (\frac{1+cos\beta}{2})^2e^{2i(\alpha+\gamma)} \end{bmatrix} \tag{1.39}$$

The terms of which are found in the tensor components for the magnetic interactions.

1.5 Spectra Prediction From Direct Propagation

The method of prediction for EPR, which is a sister technique to NMR, reported in [1] was adapted for the purpose of simulation of Pake pattern line shapes arising from ^{2}H quadrupolar coupling interactions. A brief overview of this method is given below.

1.5.1 The Density Operator

The formal solution to the Stochastic Liouville Equation is given by the following expression for the density operator at a given time, found by evolution of the density operator at thermal equilibrium, $\rho(0)$, using the Liouville Superoperator $\hat{\hat{L}}$.

$$\boldsymbol{\rho(t)} = \left\langle exp\left(-i\int_0^t \hat{\hat{L}}(\tau)d\tau\right)\right\rangle \rho(0) \tag{1.40}$$

where $\langle ... \rangle$ is an average across the entire ensemble of particles in the system. The density operator at thermal equilibrium is a description of the superposition of different spins in the system [59].

The density matrix $\rho(0)$ satisfies the following requirements.

- The trace is 1 as the sum of the proportions of nuclei in each spin state is 1.
- The matrix is hermitian, meaning it is equal to it's conjugate transpose.

For $I = 1$ and at thermal equilibrium ρ is $\rho(0)$ a 3 by 3 matrix of the states

$-1, 0$ and $+1$ in the z direction.

$$\boldsymbol{\rho}(0) = \begin{bmatrix} p_+ & 0 & 0 \\ 0 & p_0 & 0 \\ 0 & 0 & p_- \end{bmatrix} \tag{1.41}$$

1.5.2 The Liouvillian

The Liouville Superoperator, $\hat{\hat{L}}$, is an operator that differentiates the density operator at a given time as expressed in the von Neumann form of the SLE, which is explicitly dependent on time.

$$\frac{d\rho(t)}{dt} = \hat{\hat{\boldsymbol{L}}}(t).\boldsymbol{\rho(t)} \tag{1.42}$$

Where the product of the Liouville Superoperator and density matrix at a given time is the commutator of the spin Hamiltonian, $\hat{H}$, and density operator at a given time.

$$\hat{\hat{\boldsymbol{L}}}(t).\boldsymbol{\rho(t)} = [\hat{H}(t), \rho(t)] \tag{1.43}$$

This Superoperator, $\hat{\hat{L}}$, for a given magnetic interaction, α, summed over the spins in the system, P, the ranks, y, of the tensors involved and the indexes of those tensors n, m, k is dependent on

$$\hat{\hat{L}}^{\alpha}(t) = \lambda_{\alpha} \sum_{P} \sum_{y} \sum_{n,m,k} \hat{\hat{T}}_{n}^{y\alpha P} \bar{V}_{-k}^{\alpha y} D_{km}^{y}(\Omega_{P \to M}) D_{mn}^{y}(\Omega_{M \to L}(t)) \tag{1.44}$$

- λ_{α} a constant for a given magnetic interaction.
- $\hat{\hat{\boldsymbol{T}}}$ a spherical Superoperator for the given interaction, a function of the spin operators present in the system.

- $\bar{\boldsymbol{V}}$ a lattice tensor representing the interaction between the spins and the molecular structure, expressed in the principle axis frame, these are not necessarily spherical and so may have orientational dependence.

- $\boldsymbol{D}^y_{km}(\Omega_{P\to M})$ a time independent Wigner matrix that expresses the passive rotation for the transformation between the principle frame and a frame for the molecule, this is a function of three Euler angles.

- $\boldsymbol{D}^y_{mn}(\Omega_{M\to L})(t)$ a time dependent Wigner matrix that maps a frame for the molecule to the laboratory frame.

Though this expression can be simplified for systems where the principle frame is chosen to be coincident with the molecular frame, an assumption which can be made for small rigid molecules, in which case D^y_{km} can be neglected and only the time dependent Wigner matrix is needed.

$$\hat{\hat{L}}^{\alpha}(t) = \lambda_\alpha \sum_P \sum_y \sum_{n,m,k} \hat{\hat{T}}^{y\alpha P}_n \bar{V}^{\alpha y}_{-k} D^y_{mn}(\Omega_{M\to L}(t)) \tag{1.45}$$

1.5.3 Intensity

This intensity in the spectrum, $I(\omega)$, as a function of frequency, is given by the real part of the integral

$$I(\omega) = \mathrm{Re} \int_0^\infty exp(-i\omega t) \left\langle M_+(t) \right\rangle \mathrm{d}t \tag{1.46}$$

while the imaginary part gives the gradient of this intensity

$$\frac{\mathrm{d}I(\omega)}{\mathrm{d}\omega} = \mathrm{Im} \int_0^\infty exp(-i\omega t) \left\langle M_+(t) \right\rangle \mathrm{d}t \tag{1.47}$$

The magnetization, M_+, of the system is proportional to

$$\langle M_+(t)\rangle \propto Tr(\hat{\hat{I}}_{sum}\rho(t)) \tag{1.48}$$

where $\hat{\hat{I}}_{sum}$ is a Superoperator of the sum of spin operators in the system and $\rho(t)$ is the density operator at a given time. Tr defines the trace of a given matrix, which is the sum of the matrix's diagonal elements. The sum of the spin operators in the system is given by

$$\hat{I}_{sum} = \sum_i \hat{I}^i_{sum} = \frac{1}{\sqrt{2}}\sum_i(\hat{I}^i_x + i\hat{I}^i_y) \tag{1.49}$$

and

$$\hat{\hat{I}}_{sum} = \hat{I}_+ \otimes \hat{U} - \hat{U} \otimes \hat{I}_{sum} \tag{1.50}$$

where $\hat{U}$ is the identity operator with the same dimensions as $\hat{I}_{sum}$ and $\otimes$ is the Kronecker product. For a 3 by 3, n by n, matrix

$$\hat{A} = \begin{bmatrix} A_{11} & A_{12} & A_{13} \\ A_{21} & A_{22} & A_{23} \\ A_{31} & A_{32} & A_{33} \end{bmatrix} \tag{1.51}$$

the superoperator takes the form of a 9 by 9 matrix ,n^2 by n^2.

$$\hat{\hat{A}} = \begin{bmatrix} 0 & -A_{21} & -A_{31} & A_{12} & 0 & 0 & A_{13} & 0 & 0 \\ -A_{12} & (A_{11-22}) & -A_{32} & 0 & A_{12} & 0 & 0 & A_{13} & 0 \\ -A_{13} & -A_{22} & (A_{11-33}) & 0 & 0 & A_{12} & 0 & 0 & A_{13} \\ A_{21} & 0 & 0 & (A_{22-11}) & -A_{21} & -A_{31} & A_{23} & 0 & 0 \\ 0 & A_{21} & 0 & -A_{12} & 0 & -A_{32} & 0 & A_{23} & 0 \\ 0 & 0 & A_{21} & -A_{13} & -A_{23} & (A_{22-33}) & 0 & 0 & A_{23} \\ A_{31} & 0 & 0 & A_{32} & 0 & 0 & (A_{33-11}) & -A_{21} & -A_{31} \\ 0 & A_{31} & 0 & 0 & A_{32} & 0 & -A_{12} & (A_{33-22}) & -A_{32} \\ 0 & 0 & A_{31} & 0 & 0 & A_{32} & -A_{13} & -A_{23} & 0 \end{bmatrix} \tag{1.52}$$

1.5.4 Nyquist-Shannon Sampling Theorem

In order for the half-Fourier transform (equation 1.46) to fully capture motions in the system in the time domain and convert them into the frequency domain there are two requirements that need to be met. Measurements need to be taken for a sufficient amount of time and sufficiently often [60]. The length of time the simulations are run for must be greater than the reciprocal of the resolution in the frequency domain.

$$T \geq \frac{1}{\delta\omega} \tag{1.53}$$

While the measurement need to happens at least as often as the required resolution in the time domain. In terms of simulation how often the measurement is taken is equivalent to the discrete time step, Δt, used for propagation of the density matrix.

$$\Delta t \leq \delta t \leq \frac{1}{\Delta\omega} \tag{1.54}$$

where $\Delta\omega$ is the width of the entire spectrum in the frequency domain.

1.5.5 Hamiltonian

In EPR the spin Hamiltonian, $\hat{H}$, is a value for the energy of the system, modeled as the sum of Hamiltonians for different spin interactions, α. This can be done equivalently in NMR where the interactions are chemical shielding between nuclei and external magnetic fields mitigated by local fields, J coupling between nuclei connected by bonds, dipole coupling between nuclear dipoles over space, and quadrupolar coupling between nuclear quadrupoles and electric field gradients that exist across the molecule.

$$\hat{H} = \sum_{\alpha} \hat{H}^{\alpha} = \gamma\hbar \sum_{I} \hat{I}^{I} \boldsymbol{\sigma} B + \pi \sum_{I_1, I_2} I_1 \boldsymbol{J}^{I_1 I_2} I_2 + \sum_{I_1 I_2} + I_1 \boldsymbol{D}^{I^1 I^2} I_2 + \sum_{I} \boldsymbol{I V I} \frac{eQ}{2I(21-1)} \tag{1.55}$$

Where, $\boldsymbol{\sigma}$, $\boldsymbol{J}$, $\boldsymbol{D}$ and $\boldsymbol{V}$ are magnetic tensors that describe the interactions between spins and magnetic fields, pairs of spins though bond and space and spins with electric field gradients respectively.

The Hamiltonians for each of these interactions, α, can in turn be modeled as the sum of products of the irreducible components of a spherical tensor operator $\hat{\boldsymbol{T}}$ and lattice tensor $\boldsymbol{V}$ multiplied by a constant λ dependent on which magnetic interaction is involved.

$$\hat{H}^{\alpha}(t) = \lambda_{\alpha} \sum_{y} \sum_{n=-y}^{y} (-1)^{n} \hat{T}_{n}^{(\alpha.y)} V_{-n}^{(\alpha,y)}(t) \tag{1.56}$$

For Quadrupolar interactions the spherical components of the spin operator $\hat{T}$ are

$$\hat{T}_0^{Q(2)LAB} = \frac{1}{\sqrt{6}}\left(3\hat{I}_z^2 - \hat{\boldsymbol{I}}^2\right) \tag{1.57}$$

$$\hat{T}_{\pm1}^{Q(2)LAB} = \mp\frac{1}{2}\left(\hat{I}_z\hat{I}_\pm + \hat{I}_\pm\hat{I}_z\right) \tag{1.58}$$

$$\hat{T}_{\pm2}^{Q(2)LAB} = \mp\frac{1}{2}\hat{I}_\pm^2 \tag{1.59}$$

And the components of the lattice tensor are

$$V_0^{(2)PAS} = \sqrt{\frac{3}{2}}V_{zz} \tag{1.60}$$

$$V_{\pm1}^{(2)PAS} = 0 \tag{1.61}$$

$$V_{\pm2}^{(2)PAS} = -\frac{1}{2}V_{zz}\eta \tag{1.62}$$

However these lattice tensor components are given in the principle axis frame, PAS, of the electric field gradient $\boldsymbol{V}$.

$\boldsymbol{V}^{PAS}$ is transformed into $\boldsymbol{V}^{LAB}$ by the multiplication of it's components with the Wigner matrix $D^2(\Omega_{M\to L})$ for transformation from the magnetic to laboratory frame.

$$V_n^{(2)LAB} = \sum_{m=-2}^{2} V_m^{(2)PAS} D_{mn}^{(2)}(\Omega_{M\to L}) \tag{1.63}$$

For Quadrupolar coupling the interactions are all 2nd rank. This is due to the electric field gradient having a trace of zero. This limits the equation to

$$\hat{H}^Q(t) = \lambda_Q \sum_{n=-2}^{2} (-1)^n \hat{T}_n^{(Q,2)} \boldsymbol{V}_{-n}^{(Q,2)P}(t) \tag{1.64}$$

Where λ_Q is a constant relevant to the quadrupolar interaction.

$$\lambda_Q = \frac{eQ}{2I(2I-1)\hbar} \tag{1.65}$$

This is further simplified by the High-Field approximation.

1.5.6 The High-Field Approximation

The High-Field approximation assumes that energy difference due to Zeeman splitting is significantly larger than any interactions from internal fields, for example quadrupolar coupling, and as such these internal effects can be treated as small perturbations on the Zeeman splitting. This means that only terms in the perturbing Hamiltonian that commute with the Zeeman splitting are significant to the overall energy, these are the secular terms.

In terms of the Hamiltonian equations this is the equivalent of the magnetic field being entirely in the z direction and so only nuclear spins in that direction are significant to the energy difference between spin states.

$$\hat{H}_Q = \frac{eQ}{2I(2I-1)}.\begin{bmatrix} 0 & 0 & I_z \end{bmatrix}\begin{vmatrix} V_{xx} & V_{xy} & V_{xz} \\ V_{yx} & V_{yy} & V_{yz} \\ V_{zx} & V_{zy} & V_{zz} \end{vmatrix}\begin{bmatrix} 0 \\ 0 \\ I_z \end{bmatrix} \tag{1.66}$$

$$\hat{H}_Q = \frac{eQ}{2I(2I-1)}.{I_z}^2 V_{zz} \tag{1.67}$$

In terms of spherical tensor components this means that only $\hat{I}_z$ is non zero.

$$\hat{I}_{\pm} = \hat{I}_x \pm i\hat{I}_y = 0 \tag{1.68}$$

and

$$\hat{\boldsymbol{I}} = \hat{I}_z \tag{1.69}$$

This is equivalent to

$$\hat{T}_0^{Q(2)Lab} = \frac{1}{\sqrt{6}}(3\hat{I}_z^2 - \hat{\boldsymbol{I}}) \tag{1.70}$$

$$\hat{T}_{\pm1}^{Q(2)Lab} = 0 \tag{1.71}$$

$$\hat{T}_{\pm2}^{Q(2)Lab} = 0 \tag{1.72}$$

Which removes the $n \neq 0$ terms from the Hamiltonian.

$$\hat{H}^Q(t) = \lambda_Q \hat{T}_0^{(Q,2)} \sum_{m=-2}^{2} V_m^{(2)PAS} D_{m0}^{(2)}(\Omega_{M\to L}) \tag{1.73}$$

Where the summation over m gives

$$\sum_{m=-2}^{2} V_m^{(2)PAS} D_{m0}^{(2)}(\Omega_{M\to L}) = \sqrt{\frac{3}{2}} V_{zz} \left(D_{00}^2(\Omega_{M\to L}) - \frac{\eta}{\sqrt{6}}(D_{-20}^2(\Omega_{M\to L}) + D_{20}^2(\Omega_{M\to L})) \right) \tag{1.74}$$

Which can be simplified by defining the combination of Wigner matrices under the high-field assumption as $\boldsymbol{D}_0$.

$$\boldsymbol{D}_0 = \left(D_{00}^2(\Omega_{M\to L}) - \frac{\eta}{\sqrt{6}}(D_{-20}^2(\Omega_{M\to L}) + D_{20}^2(\Omega_{M\to L})) \right) \tag{1.75}$$

Further simplifying the Quadrupolar Hamiltonian to.

$$\hat{H}^Q(t) = \lambda_Q \frac{1}{2}(3\hat{I}_z^2 - \hat{\boldsymbol{I}}) V_{zz} \boldsymbol{D}_0 \tag{1.76}$$

1.5.7 Averaging and Rediagionalisation of the Hamiltonian

There are two equivalent approaches to averaging the Hamiltonian, and by extension the Liouvillian, across either the ensemble or time. In the cartesian expression the electric field gradient tensor is averaged, $\hat{I}$ is constant so doesn't need to be averaged.

$$\left\langle \hat{H}^{Q} \right\rangle = \hat{I} \left\langle \boldsymbol{V} \right\rangle \hat{I} \tag{1.77}$$

Whereas in terms of spherical tensors, it's the Wigner matrices for the transformation between reference frames that are averaged.

$$\left\langle \boldsymbol{D}_h \right\rangle = \left\langle \big(D^2_{0h}(\Omega_{M\to L}) \big\rangle - \frac{\eta}{\sqrt{6}} (\big\langle D^2_{-2h}(\Omega_{M\to L}) \big\rangle + \big\langle D^2_{2h}(\Omega_{M\to L}) \big\rangle) \right) \tag{1.78}$$

$$\left\langle \hat{H}^{Q} \right\rangle = \frac{1}{2}(3\hat{I}_z^2 - \hat{\boldsymbol{I}}) V_{zz} \left\langle \boldsymbol{D}_0 \right\rangle \tag{1.79}$$

Importantly the averaging of tensors that are diagonal in their principle axis system can lead to non diagonal tensors, which need to be rediagionalised through the use of an operator R and its transpose R^T which are function of the directions of the normalised principle values of the relevant tensors $\bar{v}_{xx}$, $\bar{v}_{yy}$ and $\bar{v}_{zz}$.

$$\boldsymbol{V}_d = R \left\langle \boldsymbol{V} \right\rangle R^T \tag{1.80}$$

An advantage of the random distribution of orientations in the systems is that the orientations of the averaged EFG tensors for each molecule are themselves averaged out across the system, this means that orientations of specific molecular EFG tensors aren't needed.

1.5.8 Autocorrelation Functions

The auto-correlation function $G(\Delta t)$ is another ensemble averaged quantity. For a time dependent function, $f(t)$, the autocorrelation function is.

$$G(\Delta t) = \langle f(t) f(t + \Delta t) \rangle \tag{1.81}$$

[53] where the autocorrelation function for a given time difference is the ensemble average of the product of the function, f, before and after that time difference. The more disordered the system the more the function for different molecules will cancel each other out resulting in a lower value for G for any given time step.

Similarly $G(\tau)$ decreases exponentially with time for isotropic rotational diffusion dependent on the correlation time of the molecules, τ_c, as more rapid molecular motions lead to faster averaging of molecular positions and more cancellation.

$$G(\tau) = exp\left(-\frac{\mid \tau \mid}{\tau_c}\right) \tag{1.82}$$

Eventually this value reaches a plateau where the autocorrelation function stops decreasing with time, at this point the coherence between orientations has been completely lost.

The relevant function in this case is a function of the angle between the z axes in the two reference frames.

$$f(\beta) = \frac{3cos^2\beta - 1}{2} \tag{1.83}$$

1.5.9 Fast Motional Limit Prediction

[1] also provides a general equation for the prediction of motional line shapes under FML. In this case it is assumed that molecular motions have correlation times, τ_c, significantly shorter than the propagation time step, Δt, and as such the ensemble average at any time will be constant. This allows for the prediction of the spectra from the formula (23) in [1] adapted for the quadrupolar case by neglecting all terms where rank $\gamma \neq 2$.

$$I(\omega) = \mathbf{Re}Tr(\hat{\hat{I}}_{+}(\omega\hat{\hat{I}} - i\hat{\hat{\Lambda}}_0 - i\hat{\hat{\Lambda}}^2_{N(2)} \langle \boldsymbol{D}_0 \rangle + \hat{\hat{\Lambda}}^2_{N(2)}\hat{\hat{\Lambda}}^2_{K(2)}\lambda)^{-1}\rho(0)) \tag{1.84}$$

where $N(2)$ and $K(2)$ are combinations of indices for a 5 by 5 matrix (-2:2, -2:2). $\hat{\hat{\Lambda}}$ is a time independent super operator.

$$\hat{\hat{\Lambda}}^{Q2}_{nm} = \sum_{q,k} \hat{\hat{T}}^{(Q,2)}_{q} V^{(Q,2)PAS}_{-k} D^2_{km}(\Omega_{P\to M}) D^2_{nq}(\Omega_{D\to L}) \tag{1.85}$$

Where the Wigner matrix $D^2_{nq}(\Omega_{D\to L})$ is a time independent mapping of the director frame, the frame in which simulation takes place, onto the laboratory frame.

λ is the decay function, the integral of ensemble averaged autocorrelation function for the function $f(\Omega)$.

$$\lambda = \int_0^{\infty} \langle f(\Omega(0) f(\Omega(\tau))\rangle \, d\tau \tag{1.86}$$

Where $f(\Omega)$ is the difference between a set of Wigner matrix elements and the average of those Wigner Matrix elements.

$$f(\Omega) = \boldsymbol{D}_0 - \langle \boldsymbol{D}_0 \rangle \tag{1.87}$$

As the autocorrelation function for the system decays λ tends to 0 at which point the system is completely motionally averaged, leaving only the time independent terms

$$I(\omega)_{FullMotionalAveraging} = \mathbf{Re}Tr(\hat{\hat{I}}_{+}(\omega\hat{\hat{I}} - i\Lambda_0 - i\hat{\hat{\Lambda}}^{2}_{N(2)}\left\langle \boldsymbol{D}_0 \right\rangle)^{-1}\rho(0)) \tag{1.88}$$

Under the high field assumption Λ is further simplified. Λ only has value when $q = 0$ reducing it to

$$\hat{\hat{\Lambda}}^{Q2}_{nm} = \hat{\hat{T}}^{(Q,2)}_{0} \sum_{k} V^{(Q,2)PAS}_{-k} D^{2}_{km}(\Omega_{P\to M}) D^{2}_{n0}(\Omega_{D\to L}) \tag{1.89}$$

And as before the summation over k simplifies the entire expression to.

$$\hat{\hat{\Lambda}}^{Q2}_{nm} = \frac{1}{2}(3\hat{I}^{2}_{z} - \hat{\boldsymbol{I}})V_{zz}\left\langle \boldsymbol{D}_m \right\rangle D^{2}_{n0}(\Omega_{D\to L}) \tag{1.90}$$

The advantage of this method as opposed to direct propagation is that it uses significantly shorter simulation times. Averaging of transformation from the magnetic to laboratory frame can be done using single molecular trajectories, as opposed to direct propagation which requires concatenation of all molecules in the system into a single trajectory to extend the simulation time.

1.5.10 Orientational Averaging of the Quadrupolar Spectra

There are two factors that average the orientational dependence in the quadrupolar Hamiltonian. The distributions of orientation across molecules in the system at any single time, static averaging, and the range of orientations any single molecule takes over time, motional averaging.

1.5.11 Static Averaging

In the rigid regime the molecules are functionally static on the NMR time scale resulting in splitting values that are the equivalent to the values predicted by the electric field gradient tensor in the principle axis frame, averaged using the probability distribution of orientations in the system.

$$\nu_1 = \pm V_{xx} = \pm\frac{3}{8}\chi(1-\eta) \tag{1.91}$$

$$\nu_2 = \pm V_{yy} = \pm\frac{3}{8}\chi(1+\eta) \tag{1.92}$$

$$\nu_3 = \pm V_{zz} = \pm\frac{3}{4}\chi \tag{1.93}$$

The result is the distinctive Pake Pattern.

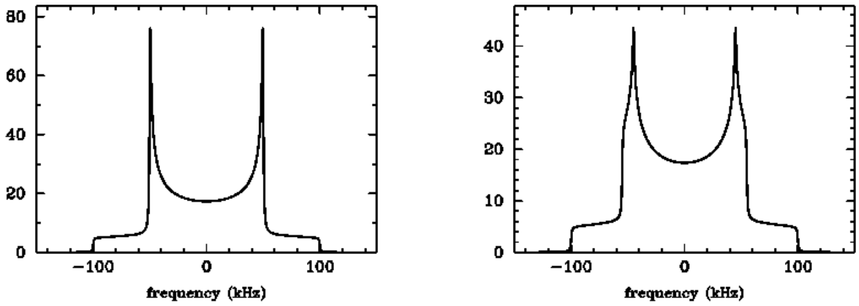

Figure 1.5.1: Quadrupolar spectra showing static averaging (Pake Pattern), with no 0 (left) and 0.1 (right) asymmetry. Simulated with NMR-WEBLAB [4]

.

1.5.12 Motional averaging

The effect of motion on the spectra is to further reduce this splitting. Gall et al [56] discuss two common types of motions.

Fast Flips

Fast flips are significant because they change the orientation of individual molecules providing an additional source of averaging which further reduces the extent of quadrupolar coupling in the NMR spectra. This is distinct from continuous motions, as two or more orientations are relatively long lived compared to the intermediate positions [61].

In the Fast Flips regime, the system swaps between a limited number of orientations which has the effect of partially averaging the electric field gradient tensor. For two orientations, a and b, the flip angle between them, θ, is the angle between the z principle axis of $\boldsymbol{V}^a$ and $\boldsymbol{V}^b$.

The flip averaged tensor $\boldsymbol{V}^F$ is then the average of $\boldsymbol{V}^a$and $\boldsymbol{V}^b$ when they are rotated into their midpoint by $\pm\frac{\theta}{2}$ perpendicular to the plane of the flip angle (x-z plane in this case) respectively.

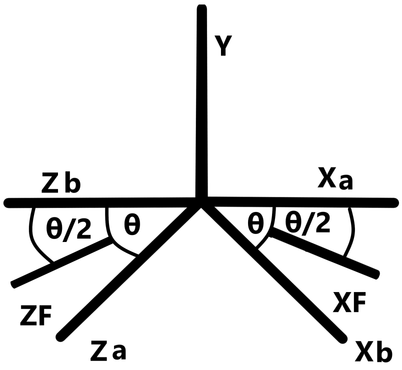

Figure 1.5.2: Diagram showing the averaging of the directions of the x and z axis between tensors $\boldsymbol{V}^a$ and $\boldsymbol{V}^b$ for V^F

Then when static averaging is applied to this averaged tensor the resulting components of the averaged tensor for a flip angle are

$$\nu_1 = \pm V_{xx}^F = \pm V_{xx} cos^2\frac{\theta}{2} - V_{zz} sin^2\frac{\theta}{2} \tag{1.94}$$

$$\nu_2 = \pm V_{yy}^F = \pm V_{yy} \tag{1.95}$$

$$\nu_3 = V_{zz}^F = \mp V_{xx} sin^2\frac{\theta}{2} - V_{zz} cos^2\frac{\theta}{2} \tag{1.96}$$

[62]

This reduces the splitting in the directions in the plane of the flip, but leaves the splitting in the direction perpendicular to the flip unchanged. Essentially each molecule is now treated as static and in the average of the two positions it occupies.

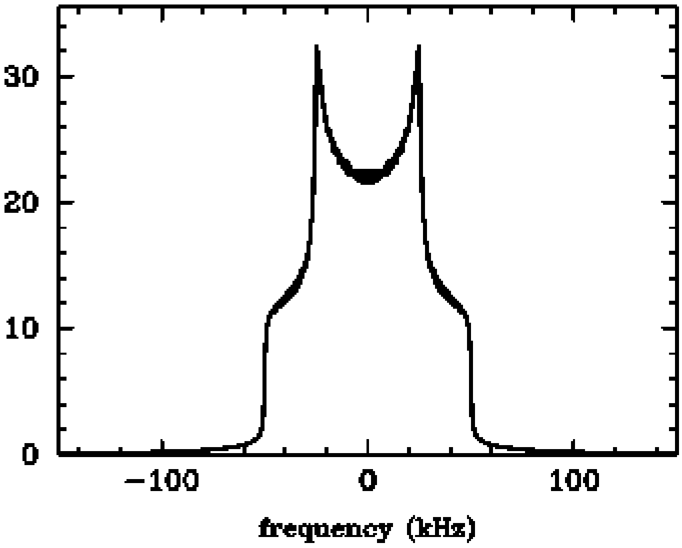

Figure 1.5.3: Spectrum simulated for a 90 degree flip between two sites with no asymmetry. [4]

For a flip in the x-z plane this results in contraction of the outer and inner most splitting but not the middle splitting value.

Rapid Rotation

The effect of rapid rotation is to further average the interaction tensor $\boldsymbol{V}$ by transforming it into the rotational frame $\boldsymbol{V^R}$ where α and β are Euler angles that relate these two frames.

$$\nu_1 = \nu_2 = V^R_{xx} = V^R_{yy} = \frac{1}{2}(1 - cos^2\alpha sin^2\beta)A_{xx} + \frac{1}{2}(1 - sin^2\beta)A_{yy} + \frac{1}{2}(sin^2\beta)A_{zz} \tag{1.97}$$

$$\nu_3 = V^R_{zz} = sin^2\beta cos^2\alpha V_{xx} + sin^2\beta sin^2\alpha V_{yy} + cos^2\beta V_{zz} \tag{1.98}$$

[62] This results in only two splitting as the rotation completely averages the splitting in its plane.

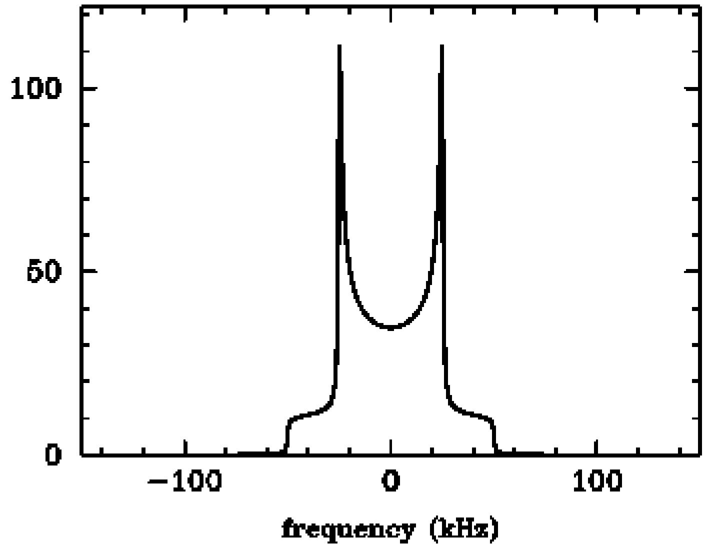

Figure 1.5.4: Spectrum simulated for rapid rotation about a 90 degree angle.[4]

1.6 The Sample System

The sample system of imidazolium ions in a hydrogen terephthalate lattice, as studied by Shi et al. [5], was chosen for simulation in this work for numerous reasons.

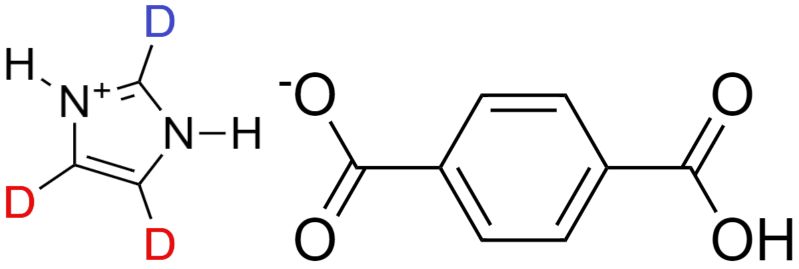

Figure 1.6.1: Im 1-d_3 isomorph (left), with site 1 in blue and sites 2 & 3 in red, and TPA (right)

The availability of experimental data in the source literature includes a series of spectra at temperatures between 300 K and 450 K that all show the distinctive Pake pattern, associated with quadrupolar coupling, but also show features that depend on motion to varying extents.

This provides a valuable opportunity to compare the results of simulations to experimental data, in this case the simulations can be validated by their ability to reproduce both the commonalities, Pake pattern, and differences, the extend of motional averaging, between spectra.

However, there are limitation to these experimental spectra, as spectra are measurements of the bulk system. This means, the individual deuterium sites in isomorphs with multiple deuterium nuclei can't be distinguished, Shi et al. assume these produce equivalent spectra but this assumption can be checked by simulating the spectrum due to each site individually.

In the model proposed by Shi et al to explain this behaviour, imidazolium ions undergo rapid 95° flips around an axis perpendicular to the plane of the molecule at 450 K which do not happen at 300 K. These flips would have an identical effect on motional averaging at each site and would produce the observed splitting but MD presents an opportunity to directly observe simulated molecular motions. And through the use of autocorrelation functions performed on individual bond angles in the system the order and degree of motional averaging can be quantified individually.

This project focuses on the 1-d_3 isotopologue with 3 deuterium atoms in the Imidazolium ions and none in the lattice. This choice of isomorph provides two distinct chemical environments, site 1 and sites 2 and 3, to study which can potentially be distinguished by collecting data on each individually.

It's also important to consider other contributions to the NMR spectra that may complicate or obscure observations of deuterium signals. In terms of other constituents of the system there's atomic hydrogen, carbon, oxygen (exclusively in the HTP lattice) and nitrogen. The two considerations here are whether these will produce signals on their own and whether there will be any interaction between the deuterium of interest and other spins in the Im cation. Both ^{12}C and ^{16}O are spin 0 and so neither produce NMR signals or couple with other spins. However, ^{1}H and ^{14}N have spins of $\frac{1}{2}$ and 1 respectively so there is potential for dipole-dipole and J coupling as well as the nuclei producing their own signals.

The potential for NMR signals from other Nuclei is not a concern as the two nuclei in question have gyromagnetic ratios of 3.08 (^{14}N) and 42.6 MHz T^{-1} (^{1}H) both sufficiently different from the value of 6.54 MHz T^{-1} for ^{2}D that neither chemical shift (on the order of KHz) or quadrupolar effects (on the order of 100s of KHz for organic systems) would result in nitrogen or hydrogen signals in the range that the deuterium signal would be observed. While J coupling is only on the order of Hz and so would result in changes below the required resolution for this work and so can be ignored.

As well as the physical properties of the system that give rise to behaviour that can potentially be reproduced in this project, it is also key to consider the computational cost of running the simulations. The two important computational operations in this case are the optimisation of the structure and the MD simulations themselves. For both of these smaller molecules reduce the number of calculations that need to be completed, for optimisation this affects the accuracy by limiting the extent to which the assumptions underlying HF optimisation need to be applied, while for MD this is largely a question of the time it takes to run simulations. Im is a 10 nuclei cation while TPA consists of 13 nuclei both sufficiently small for HF optimization to produce accurate values. And the number of atoms in a system with on the order of 100 of each molecule would only be 2300 atoms, allowing for the behaviour of multiple copies of each molecule to be observed for microseconds within reasonable simulation times.

When fitting the rates of motion to the Arrhenius equation Shi et al. calculated an activation energy, $E_a = 52.1$ KJ mol^{-1}, and rate constant , $A = 7.44 \times 10^{12}$ s $^{-1}$.

Giving a rate of

$$k = A.exp\left(\frac{-E_a}{RT}\right) \tag{1.99}$$

With a factor between the two rates of

$$\frac{k_{T1}}{k_{T2}} = exp\left(\frac{-E_a}{R}\left(\frac{1}{T1} - \frac{1}{T2}\right)\right) \tag{1.100}$$

which for the values above gives a difference between rates of a factor on the order of 1000 times faster at 450 than 300K.

At 450K these values predict a rate of $k_{450} = 6.66 \times 10^6 s^{-1}$ or 6.66 MHz as opposed to $k_{300} = 6.66$ kHz.

However, this is not necessarily a complete picture, as it assumes the activation energy of jumps is constant which is not necessarily true as Shi et al. also found evidence for multiple phases of the structure, where the phases show different amounts of hydrogen bonding between the guest and host crystal. This data can in turn be checked and potentially confirmed by physically counting the number of flips that appear within a given time scale.

An assumption made by Shi et al. in their simulation was that the electric field gradients at these nuclei are axially symmetric, $\eta = 0$. This is something that can be checked by the output of HF optimisation as it has implications for the amount of discontinuities shown in the spectra.

Temperature	ν_1 kHz	ν_2 kHz	ν_3 kHz
300 K	±63	±84	±140
450 K	±26	±43	±68

Table 1.1: Shi et al. splitting values

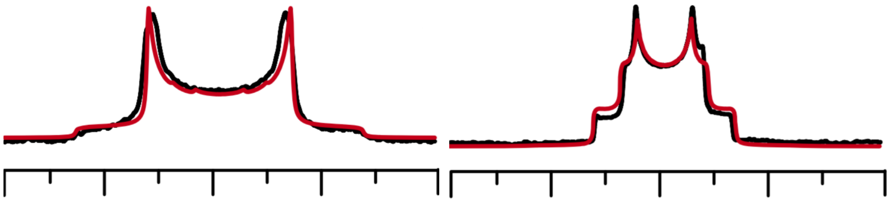

Figure 1.6.2: Shi et al. measured (black) and simulated (red) spectra at 300 K (left) and 450 K (right)

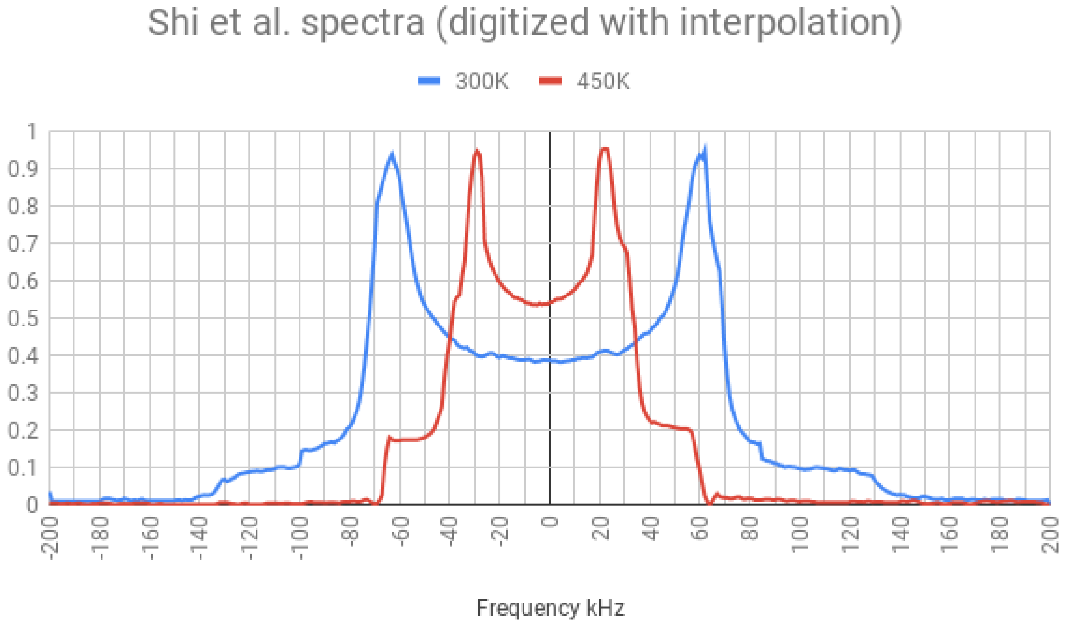

Figure 1.6.3: Experimental spectra of ImTPA from Shi et al [5]. (digitized) at 300K (blue) and 450K(red).

2

Molecular Dynamics Simulations

2.1 Perpetration of inputs

Molecular dynamics simulations in this project are run in GROMACS [63] which is software that simulates molecular dynamics using classical mechanics.

GROMACS simulations begin with atoms in a periodic box. This periodic box and its contents are defined in a .gro or .pdb file which contains the atom types and locations of each atom as well as the size of the box.

For this product the structure file was built using the structures Shi.et.al[5] contributed to the Cambridge Crystallographic Data Centre, specifically CCDC 1493605, which gives the unit cell for the triply deuterated structure from which the entire structure can be derived. By repeating this cell with four instances of each molecule three times in each direction, a periodic box with 108 of both molecules is created.

The bulk structure is modelled as repeated identical copies of this periodic box, as a consequence of this any atoms that leave the periodic box in one direction will be replaced by the same atom entering from the opposite direction as it leaves an identical box on the other side. This means the number of atoms in the periodic box is constant.

In addition to this structure, a force-field, .itp, is required. This contains the parameters for calculation of potential energy in the system. The potential energy, E, is modeled as the sum of bonded and non-bonded interactions.

$$E = \sum_{Bonds} K_r(r - r_{eq})^2 + \sum_{Angles} K_\theta(\theta - \theta_{eq})^2 + \\ \sum_{Dihedral} \frac{V_n}{2}[1 + cos(n\phi - \gamma)] + \sum_{Non-bonded} (\frac{C_{ij}^{(12)}}{R_{ij}^{12}} - \frac{C_{ij}^{(6)}}{R_{ij}^{6}} + \frac{q_i q_j}{\epsilon R_{ij}}) \quad (2.1)$$

2.1.1 Bonded Interactions

The bonded interactions in a system are calculated between bonded sets of two (bonds) three (angles) and four (dihedrals)atoms.

For the bonds between pairs of atoms, i and j, the force on each atom is given by the deviation of the bond length r_{ij} from it's equilibrium value, b_{ij} squared multiplied by the force constant for the bond.

$$F_i(r_{ij}) = \frac{1}{2}k_{ij}^b(r_{ij} - b_{ij})^2 = -F_j \quad (2.2)$$

Similarly for angles between the bonds $i - j$ and $j - k$, it's the deviation of the bond angle from it's equilibrium value giving a potential of

$$V_a(\theta_{ijk}) = \frac{1}{2}k_{ijk}^\theta(\theta_{ijk} - \theta_{ijk}^0)^2 \quad (2.3)$$

and the 2nd derivative of potential gives the force on each atom.

$$F_i = -\frac{dV_a(\theta_{ijk})}{dR_i} \tag{2.4}$$

$$F_k = -\frac{dV_a(\theta_{ijk})}{dR_k} \tag{2.5}$$

$$F_j = -F_i - F_k \tag{2.6}$$

The same principle is true for the dihedral and improper dihedral angles which are interactions between four atoms i, j, k and l

The dihedral angle,ϕ, is the angle between the planes ijk and jkl where atom i is bonded to atom j which in turn is bonded to atom k which is bonded to atom l.

In this case the potential energy is given by

$$V_d(\phi_{ijkl}) = k_\phi(1 + cos(n\phi - \phi_0)) \tag{2.7}$$

[63]

where k_ϕ is the force constant for the dihedral angle, ϕ_0 is the equilibrium value and n is an integer value for the periodicity around the jk bond.

While an improper dihedral angle corresponds to an arrangement where one atom i is bonded to atoms j, k and l which are not bonded to each other, forming a structure like a triangular based pyramid. The improper dihedral is the angle between the plane formed by jkl, the base of the pyramid, and one of the sides ijk.

The potential of this is given by

$$V_{id}(\psi_{ijkl}) = k_{\psi}(\psi_{ijkl} - \psi_0)^2 \tag{2.8}$$

2.1.2 Non-bonded Interactions

The non-bonded interactions are interactions between all atoms within a cut off distance of each other and functions of that distance, R, where the net potential, V, on atom, i, due to the sum of it's potential from each interaction with the other atoms, j.

$$V(r_1 ... r_N) = \sum_{ij} V_{ij}(R_{ij}) \tag{2.9}$$

And the force, F_i on the atom i is the sum over all other atoms j of the derivatives of that potential.

$$F_i = -\sum_j \frac{dV_{ij}(r_{ij})}{dr_{ij}} \frac{R_{ij}}{r_{ij}} \tag{2.10}$$

Where R is the vector form of distance r so that $\frac{R_{ij}}{r_{ij}}$ defines the distance the over which the force acts.

The interactions that make up this non-bonded potential between two given atoms are.

The Lennard-Jones interaction

$$F_{LJ}(r_{ij}) = (12\frac{C_{Aij}^{(12)}}{r_{ij}^{13}} - 6\frac{C_{Bij}^{(6)}}{r_{ij}^{7}})\frac{R_{ij}}{r_{ij}} \tag{2.11}$$

Where $C_{ij}^{(12)}$ and $C_{ij}^{(6)}$ are properties of the atoms involved, the distance at which the Lennard Jones potential around a given atom is zero.

And coulombic interactions between atoms which carry charge, q, with a force on i of.

$$F_i(r_{ij}) = f\frac{q_i q_j}{\epsilon_r r_{ij}^2}\frac{R_{ij}}{r_{ij}} \tag{2.12}$$

Where f is.

$$f = \frac{1}{4\pi\epsilon_0} \tag{2.13}$$

Where ϵ_0 is vacuum permittivity and ϵ_r is the relative dielectric constant.

However for both of these interactions there's a potential issue, because the force is proportional to distance there's no point where the potential is completely zero. There will be interactions between atom i and it's reflections in the copies of the periodic box. For this reason a cut off distance is introduced which ignores the potential due to atoms beyond a certain distance. This distance is less than the dimensions of the periodic box ensuring no interaction between instances of the same atom.

It's the force-field that stores the partial charges on each atom for these calculation and also stores the equilibrium bond lengths and angles for calculation of the bonded interactions.

2.1.3 Force-field and Topology Creation of Im and TPA

The force-field was built in the AMBER program Antechamber [64] derived fully from ab initio methods.

AMBER identifies the atom types within a single IM and TPA and the bonding between them. From which the partial charges and equilibrium bond lengths can be calculated, from the molecule in the form of a molecule structure file antechamber generates a Gaussian input file. Then ab initio calculation at the Hartree-Fock level of theory (6-31G*) calculates the molecular orbitals for the system.

2.1.4 Hartree-Fock Minimization

The Hartree-Fock [65] method is an iterative process to calculate the wavefunction of electrons in a system. Starting with the coordinates of atomic nuclei, which are assumed to be stationary, the electrons are added as single electron orbitals, $\hat{h}$. For each electron, i, there is a Fock operator, $\hat{F}$.

$$\hat{F}(i) = \hat{h}(i) + \sum_{J=1}^{\frac{n}{2}} [2\hat{J}_j - \hat{K}_j] \tag{2.14}$$

where n is the number of electrons, $\frac{n}{2}$ is the number of orbitals and $\hat{J}$ and $\hat{K}$ are operators for interactions with other electrons in the system, coulomb repulsion and exchange respectively.

$\hat{F}$ can then be diagonalized to produce a new set of orbitals that account for the interactions between electrons that were absent in the initial $\hat{h}$ operators.

These new orbitals can then be used to produce a new Fock matrix.

Once the force-field is made it is then combined with the structure file to produce a topology file, .top and position restraint file .itp. The topology file contains the positions of each element as well as the force-field to be used and the inputs for that force-field, the partial charges, bond lengths and various angles. From these components simulations can then be run.

The coordinates and partial charges of the atoms, in angstroms and electron charges, of the optimised structure produced in Gaussian are

Atom	X	Y	Z	Partial Charge
C1	0.68	0.98	0	0.058
C2	-0.68	0.98	0	0.058
N1	-1.07	-0.35	0	-0.534
C3	0	-1.14	0	0.329
N2	1.07	-0.35	0	-0.534
H1	2.03	-0.68	0	0.415
D1	1.39	1.80	0	0.257
D2	-1.39	1.80	0	0.257
H2	-2.03	-0.68	0	0.415
D3	0	-2.22	0	0.279

Table 2.1: Gaussian optimised Im structure

2.1.5 Electric Field Gradient Calculation

From these partial charges the electric field can be calculated at any point in space. For each nuclei this is the sum of the potentials due to the partial charges, q, on each other nuclei at the position of that nuclei a distance r from the nuclei.

$$V_E = \sum_i \frac{1}{4\pi\epsilon_0} . \frac{q_i}{r} \tag{2.15}$$

And the gradient is then the 2nd derivative with respect to each pair of directions, xyz.

2.2 Running Simulations

GROMACS simulates molecular motions by using the equations described above to calculate the potentials and forces acting on each atom in a system which then lead to the movement of those atoms. Using Newton's equations and the 's,u,v,a,t' (displacement, initial velocity, final velocity, acceleration and time) equations.

$$v = u + at \tag{2.16}$$

$$s = ut + \frac{1}{2}at^2 \tag{2.17}$$

$$s = vt - \frac{1}{2}at^2 \tag{2.18}$$

$$s = \frac{1}{2}(u + v)t \tag{2.19}$$

$$v^2 = u^2 + 2as \tag{2.20}$$

However, this presents an issue. As the potentials are position dependent any alteration to their positions due to the forces acting on them will then alter those potentials.

2.2.1 Leapfrog Algorithm

The solution is to use a leapfrog algorithm [66] where the acceleration of atoms due to the forces on them are assumed to be constant for a small time difference Δt. So that the change in velocity between $t - \frac{\Delta t}{2}$ and $t + \frac{\Delta t}{2}$ can be calculated.

$$v(t + \frac{\Delta t}{2}) = v(t - \frac{\Delta t}{2}) + a(t)\Delta t \tag{2.21}$$

From these velocities the change in position, x, over a time step can also be calculated

$$x(t + \Delta t) = x(t) + v(t + \frac{\Delta t}{2})\Delta t \tag{2.22}$$

and then from these new positions the forces can be recalculated and the process repeats.

2.2.2 Run Files .mdp

Each run in GROMACS is described by a .mdp file this file defines the parameters for simulation including.

nstep: The number of simulation steps.

pbc: The type and dimensions of the periodic box

Δt: The time interval per step, multiplied by the number of steps to give the simulation duration.

Integrator: The algorithms used for integrating Newton's equations.

cutoff: The method used for limiting the range of non-bonding interactions. Followed by the specific distances to cut off given interactions.

tcoupl: Thermostat used to regulate temperature in the system

pcoupl: Barostat used to regulate pressure in the system.

2.2.3 Minimisation

Before the main molecular dynamics simulations can be run the system needs to undergo energy minimisation to release strain in the system, followed by temperature and pressure equilibration. Each step takes the form of a run with it's own .mdp file.

Energy minimisation reduces potential energy in the system to ensure the full run happens on a system that's representative of the real system, for example avoiding situations where multiple atoms occupy the same position.

A common method for energy minimisation is the steepest descent method

[67]. Starting with atoms in position r_n the forces, F, and potential energy are calculated leading to a new set of positions r_{n+1}.

$$r_{n+1} = r_n + \frac{F_n}{max(\mid F_n \mid)} h_n \tag{2.23}$$

Where $max(\mid F_n \mid)$ is the maximum value for force and h_n is the maximum value for displacement both set in the .mdp file.

The two sets of positions are then compared in terms of their potential energy. If the change has reduced the potential in the system then the process repeats with the new positions and a larger value for h_n while if the potential energy has not decreased then the process repeats with the original positions and a constricted h_n

The .mdp file for energy used for minimisation used the following parameters.

- Integrator = Steep ; Use the steepest descent algorithm
- emtol = 1000.0 ; Stop minimization when the maximum force ¡ 1000.0 kJ/mol/nm
- nsteps = 50000 ; Maximum number of (minimization) steps to perform
- nstlist = 1 ; Frequency to update the neighbour list and long range forces
- cutoff-scheme = Verlet
- ns_type = grid ; Method to determine neighbour list (simple, grid)
- coulombtype = PME ; Treatment of long range electrostatic interactions

- rcoulomb = 1.0 ; Short-range electrostatic cut-off
- rvdw = 1.0 ; Short-range Van der Waals cut-off
- pbc = xyz ; Periodic Boundary Conditions (yes/no)

2.2.4 NVT Equilibration

After energy minimisation the next step is an NVT run which keeps the number of particles in the box and the volume of the box constant and regulates the average temperature with a thermostat. With the heavy atoms constrained by a .itp file, to prevent large scale structural changes, the system is run to allow the temperature to reach the required value.

As an example thermostat is the Andersen thermostat which regulates temperature by periodically randomising the velocity of some or all particles in the system using the Boltzmann distribution of expected energies at the target temperature to determine the likelihood of a particle having a given velocity. Though this method is not compatible with restraints.

Alternatively the Berendsen thermostat gradually changes the temperature towards the goal T_0 at a rate defined by the current temperature and time constant, τ.

$$\frac{dT}{dt} = \frac{T_0 - T}{\tau} \tag{2.24}$$

This is done by scaling the velocities of particles in the system by a factor λ

$$\lambda = \left[1 + \frac{n_{TC}\Delta t}{\tau_T}\left(\frac{T_0}{T(t - \frac{1}{2}\Delta t)}\right)\right]^{\frac{1}{2}} \tag{2.25}$$

where

$$\tau = \frac{2C_{V\tau_T}}{N_{df}k} \tag{2.26}$$

C_V is the system's heat capacity and N_{df} is the number of degrees of freedom in the system.

The .mdp file for this run needs to define

- The thermostat used
- If the system contains a single group for temperature coupling or multiple groups
- The target temperature for each of the groups to be temperature couples

For the Andersen thermostat

- How frequently to randomize the velocities of particles
- The portion of particle velocities to randomise each time some are randomised

For the Berendsen thermostat

- The time constant, τ
- How often the temperature is coupled, n_{TC} (every n steps)
- A factor representing how much of the temperature added or removed from the system is instead gained as potential energy τ_T

However the Berendsen thermostat requires correction as it doesn't produce the correct distribution of kinetic energy only giving the correct average. This is covered which by velocity-rescaling temperature coupling which modifies the kinetic energy K in the system via a random force W.

$$dK = (K_0 - K)\frac{dt}{\tau_T} + 2\sqrt{\frac{KK_0}{N_{df}}}\frac{dW}{\sqrt{\tau_T}} \tag{2.27}$$

The end result of this equilibration is a system with an average temperature with minimal temperature fluctuation.

For this project the NVT run at 300K uses the following parameters.

- integrator = md ; leap-frog integrator
- nsteps = 50000 ; 2 * 50000 = 100 ps
- dt = 0.002 ; 2 fs
- nstxout = 500 ; save coordinates every 1.0 ps
- nstvout = 500 ; save velocities every 1.0 ps
- nstenergy = 500 ; save energies every 1.0 ps
- nstlog = 500 ; update log file every 1.0 ps
- continuation = yes ; Restarting after minimization
- constraint_algorithm = lincs ; holonomic constraints
- constraints = all-bonds ; all bonds (even heavy atom-H bonds) constrained
- lincs_iter = 1 ; accuracy of LINCS
- lincs_order = 4 ; also related to accuracy
- cutoff-scheme = Verlet

- ns_type = grid ; search neighboring grid cells
- nstlist = 10 ; 20 fs, largely irrelevant with Verlet scheme
- rcoulomb = 1.0 ; short-range electrostatic cutoff (in nm)
- rvdw = 1.0 ; short-range van der Waals cutoff (in nm)
- coulombtype = PME ; Particle Mesh Ewald for long-range electrostatics
- pme_order = 4 ; cubic interpolation
- fourierspacing = 0.16 ; grid spacing for FFT
- tcoupl = V-rescale ; modified Berendsen thermostat
- tc-grps = System ;Non-Protein ; two coupling groups - more accurate
- tau_t = 0.1 ;0.1 ; time constant, in ps
- ref_t = 300 ;300 ; reference temperature, one for each group, in K

2.2.5 NPT Equilibration

Now that the temperature is constant, in addition to the volume and number of particles, the system can be equilibrated in terms of pressure, P, and density ρ. For this run in addition to temperature coupling a pressure coupling barostat is introduced.

Parinello-Rahman pressure coupling scales the dimensions of the simulation box with volume V, and dimensions represented by a matrix b, in order for pressure to reach a target pressure P_{ref}. [63]

Where the 2nd derivative of box dimensions with time is then given by.

$$\frac{db^2}{dt^2} = V\boldsymbol{W}^{-1}\boldsymbol{b}'^{-1}(P - P_{ref}) \tag{2.28}$$

Where $\boldsymbol{W^{-1}}$ is a matrix parameter representing the strength of the coupling interaction with elements given by.

$$(W^{-1})_{ij} = \frac{4\pi^2\beta_{ij}}{3\tau_p^2 L} \tag{2.29}$$

Where β is isothermal compressibility of the system in directions i and j, τ_p is the pressure time constant and L is the largest element of matrix b.

In addition to the values defined for the NVT run the system NPT mdp file also needs to define

- The target pressure
- How often the pressure is coupled τ_p
- The compressability
- Whether pressure is isotropic, semi-isotropic (axially symmetric) or anisotropic.

And as such uses the same file as above with the following additions

Pressure coupling is on

- pcoupl = Parrinello-Rahman ; Pressure coupling on in NPT
- pcoupltype = isotropic ; uniform scaling of box vectors
- tau_p = 2.0 ; time constant, in ps

- ref_p = 20 ; reference pressure, in bar
- compressibility = 4.5e-5 ; isothermal compressibility of the system, bar$\hat{-}$1
- refcoord_scaling = com{}

2.2.6 Simulation run

Simulations were performed on the same system equilibrated at two different temperatures, 300K and 450K. Each simulation is run for a total 5μs with the first 0.5μs being used to ensure the system is fully equilibrated while the remaining 4.5μs are used for spectra prediction.

2.2.7 Processing Outputs

The output of the simulation relevant for this project is the .xtc file, which stores the cartesian coordinates of each atom at each time step, in this case each picosecond, ps. But for further processing this can be reduced to one frame every 20ps and 10ns respectively.

The coordinates for each of the 108 molecules in the dt= 10ns .xtc file (451 frames) can then be concatenated together into a single trajectory for a total of 4.9 μ s of simulation time and 48708 frames.

However there's an important caveat, concatenating the molecules together with respect to the Laboratory frame will result in discontinuities, where the molecules rapidly reorient when one molecule's frames end and the others begin. If the molecules are all independently oriented at the initial time step then their final positions won't necessarily correlate which could artificially accelerate any loss of order.

The solution is the introduction of an additional frame for each molecule, which is defined by the molecule's initial position, then for each molecule the changes in position can be tracked relative to that molecule's initial position limiting the discontinuities. As well as this the first frame of each molecule is rotated to match the last frame of the previous molecule.

The next step is to validate the system using a combination of inspection in VMD [68] and the plotting of autocorrelation functions. This has been performed using the appropriate cartesian transformations resulting in a single continuous trajectory.

2.2.8 VMD Validation

VMD is software used to visualise molecular dynamics, starting with a .gro or .pdb file for the system and then loading the trajectory file for a simulation run into it.

This also allows for the tracking of single Im cations to view their individual motions at both temperatures.

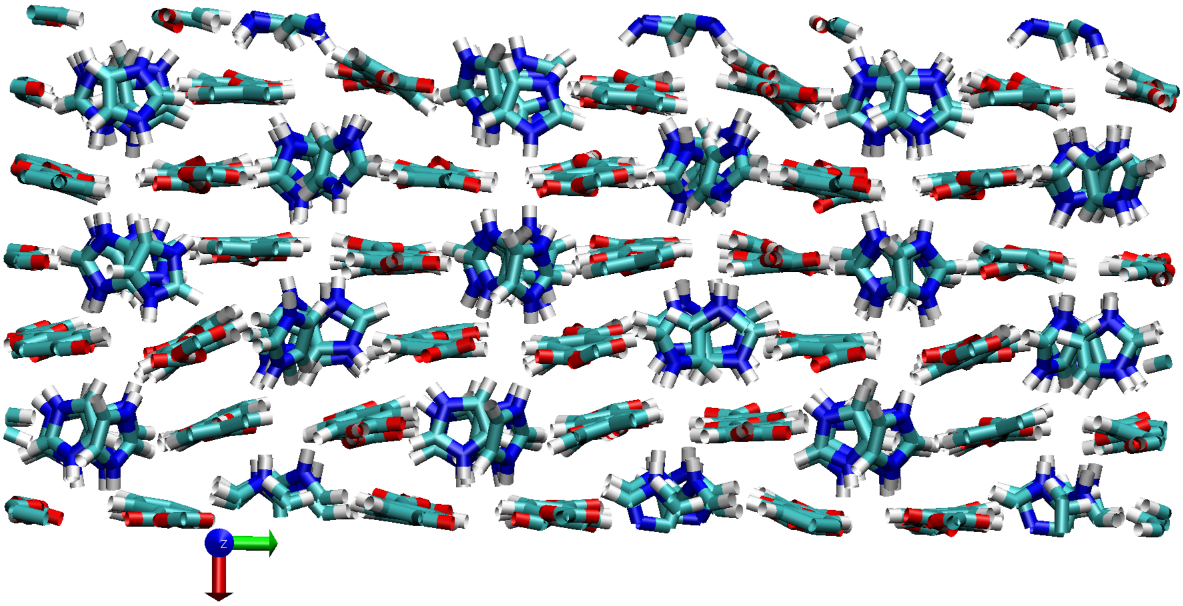

Figure 2.2.1: ImTPA system at 300K, frame 100. Showing the LAB frame

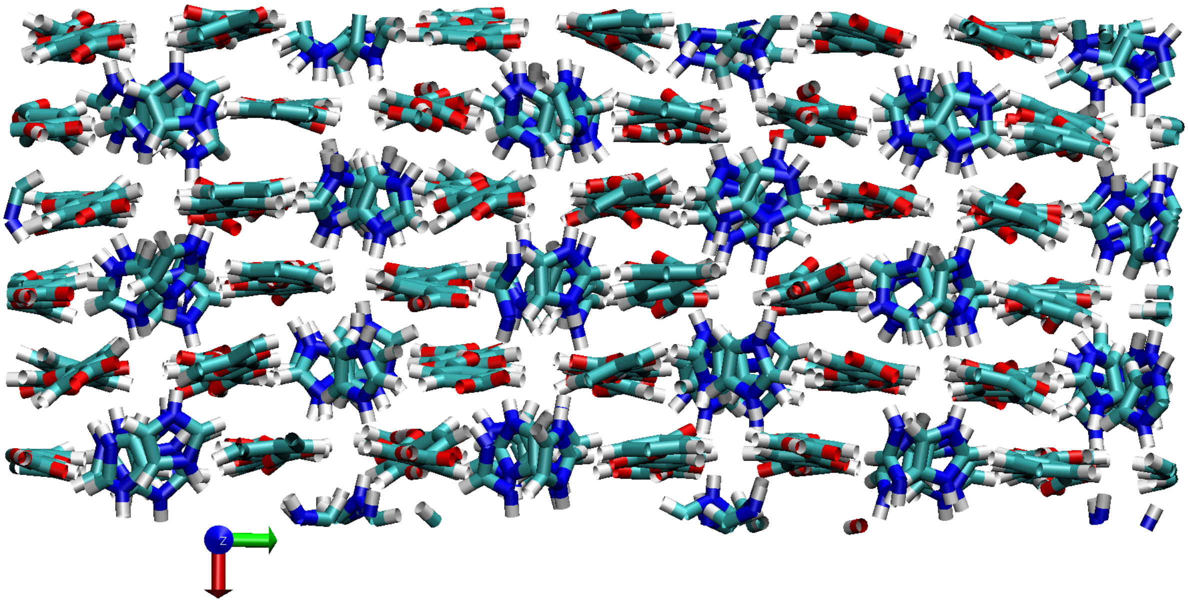

Figure 2.2.2: ImTPA system at 450K, frame 100. Showing the LAB frame

2.2.9 T1 Relaxation

T_1 relaxation is the realignment of magnetisation with B_0 after the pulse is no longer being applied. In terms of magnetization, M, it is the restoration of the equilibrium magnetization in the z direction $M_{z,eq}$. After a pulse that turns the magnetization of the species 90°, $M_z(0) = 0$, the magnetization in z as a function of time is

$$M_z(t) = M_{z,eq}(1 - e^{\frac{-t}{T_1}}) \tag{2.30}$$

The relaxation rate in the z direction is given by the Bloch equation [69].

$$\frac{\partial M_x(z)}{\partial t} = \gamma(M(t) \times B(t))_z - \frac{M_z(t) - M_0}{T_1} \tag{2.31}$$

This occurs by multiple mechanisms at different rates with the overall relaxation rate, R, being the sum of the rates via each mechanism. For this project, the contribution of quadrupolar relaxation is considered, though an analogous treatment works for other sources of relaxation including chemical shift anisotropy.

$$\frac{1}{T_1} = R = \sum_{\alpha} R_{\alpha} \tag{2.32}$$

where T_1 is the inverse of the sum of rates of each contributing mechanism, R.

The quadrupolar relaxation rate for $I = 1$ is given by

$$R_{QR} = \frac{3}{2}\pi^2(1 + \frac{\eta^2}{3})\chi^2 \times [J(\omega_0) + 4J(2\omega_0)] \tag{2.33}$$

[70]

Where $J(\omega_0)$ is a one sided Fourier transform of the autocorrelation function for the molecular motions

$$J(\omega) = \int_0^\infty C_2(t) cos(\omega t) dt \tag{2.34}$$

[71]

In this case the relevant motions are the orientations of the principle axis of the quadrupolar coupling tensor to the external magnetic field, described by the 2nd order Legendre polynomial of the angle between the principle axes θ.

$$P_2(\theta) = \frac{1}{2}(3cos(\theta)^2 - 1) \tag{2.35}$$

which is the same as the $\boldsymbol{D}^2_{00}$ term of the Wigner matrix.

3

Methods - Calculations

3.1 The Hamiltonian

Under the high-field assumption the quadrupolar Hamiltonian is

$$\hat{H}^Q(t) = \lambda_Q \frac{1}{2}(3\hat{I}_z^2 - \hat{\boldsymbol{I}})V_{zz}\boldsymbol{D}_0 \tag{3.1}$$

Where

$$\lambda_Q = \frac{eQ}{2I(2I-1)\hbar} \tag{3.2}$$

Which for $I = 1$ deuterium reduces to

$$\lambda_Q = \frac{eQ}{2\hbar} \tag{3.3}$$

$$\hat{H}^Q(t) = \frac{eQ}{4\hbar}(3\hat{I}_z^2 - \hat{\boldsymbol{I}})V_{zz}\boldsymbol{D}_0 \tag{3.4}$$

Where the spin matrix elements for $\hat{I}$ are

$$\hat{\boldsymbol{I}} = \begin{bmatrix} 1 & 0 & 0 \\ 0 & 0 & 0 \\ 0 & 0 & -1 \end{bmatrix} \tag{3.5}$$

$$\hat{I}_z^2 = \begin{bmatrix} 1 & 0 & 0 \\ 0 & 0 & 0 \\ 0 & 0 & 1 \end{bmatrix} \tag{3.6}$$

$$\hat{H}^Q(t) = \frac{eQ}{4\hbar} \begin{bmatrix} 2 & 0 & 0 \\ 0 & 0 & 0 \\ 0 & 0 & 4 \end{bmatrix} V_{zz}\boldsymbol{D}_0 \tag{3.7}$$

$$\hat{H}^Q(t) = \frac{eQ}{\hbar} \begin{bmatrix} \frac{1}{2} & 0 & 0 \\ 0 & 0 & 0 \\ 0 & 0 & 1 \end{bmatrix} V_{zz}\boldsymbol{D}_0 \tag{3.8}$$

3.2 Calculation of Lattice Tensors in the principle axis frame

The lattice tensors $\boldsymbol{V}^{PAS}$ are dependent on the components of the electric field gradient in the principle axis system of each nuclei. As the sample contains three different Deuterium nuclei this is calculated for each independently. Calculations were performed in Gaussian [72] by minimising the energy of electrons in the system using the Hartree-Fock method discussed earlier.

$$V_0^{(2)PAS} = \sqrt{\frac{3}{2}}V_{zz} \tag{3.9}$$

$$V_{\pm1}^{(2)PAS} = 0 \tag{3.10}$$

$$V_{\pm2}^{(2)PAS} = -\frac{1}{2}V_{zz}\eta_\lambda \tag{3.11}$$

3.3 Transformation of V into the Laboratory Frame

The transformation of V_{zz} into the required reference frames is given by $\boldsymbol{D}_0$ which is a function of the Wigner matrix elements dependent on

$$D^2_{00} = \frac{3cos^2\beta - 1}{2} \tag{3.12}$$

$$D^2_{\pm 20} = \sqrt{\frac{3}{8}} sin^2\beta e^{\mp i2\gamma} \tag{3.13}$$

Where β is the angle between the z axes of the PAS and LAB frames and γ is the angle between the y axes.

3.4 Calculation of Wigner Matrix Elements

In the method developed by Oganesyan for EPR spectra simulations from MD, two sets of Wigner matrices are used. The first maps the magnetic frame onto the molecular frame and the second maps the molecular frame onto the laboratory frame.

However it's possible to simplify this to one frame, assuming that the molecular frame is chosen to coincide with the magnetic frame, which would be true if the molecule is rigid, which is an assumption made for the Im$^+$ cation.

In this case the vectors used to track the movement of the $\boldsymbol{V}$ tensor in the laboratory frame are

- z^{PAS} - The normalized vector product of the C-C and/or C-N bonds, orthogonal to the plane of the molecule.

- x^{PAS} - The normalized projection of the C-D bond in the plane of the molecule
- y^{PAS}- the normalized cross product of z and x.

Though conventionally the PSA is defined with z pointing along the C-D bond, for the purpose of tracking the motions in simulation these are equivalent approaches as it's the changes in orientation over the course of the simulation that are of interest.

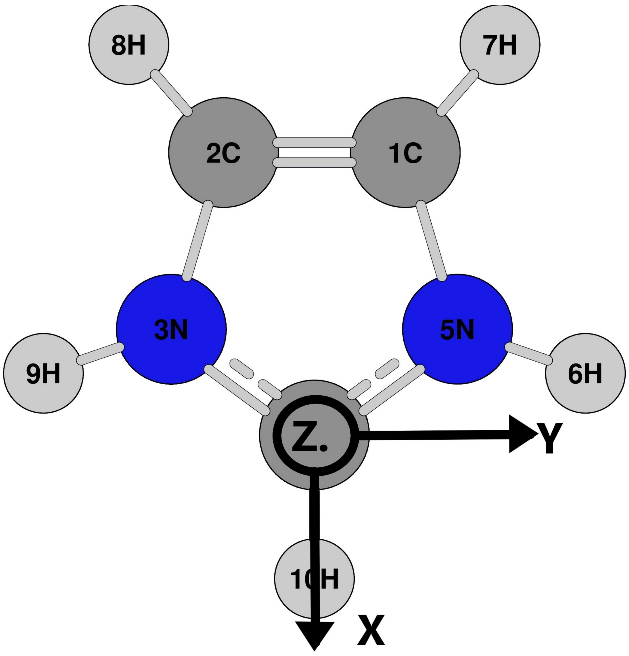

Figure 3.4.1: Diagram of Im+ cation optimised structure with x axis (along the C-D bond) z axis (out of the page) and y axis (cross product of x and z) for site 1.

From these vectors the projection cosines between the vectors that define the two frames were calculated. The x, y and z direction in the principle axis system each have components in the x, y and z directions of the Laboratory frame.

$$x^{PAS} = \begin{bmatrix} x^{PAS}_{x^{LAB}} \\ x^{PAS}_{y^{LAB}} \\ x^{PAS}_{z^{LAB}} \end{bmatrix} \tag{3.14}$$

3.5 Calculation of the Liouvillian

The Liouvillian for quadrupolar coupling can then be calculated for each spin, P, in the system where many of the same assumptions and apply. As with the Hamiltonian for the same interaction only the 2nd rank components are non-zero, as the electric field gradient is traceless, and high-field approximation limits the Liouvillian to $n = 0$. Which for the small and rigid Im cation with the principle and molecular frame being coincident leaves.

$$\hat{\hat{L}}^{PQ}(t) = \hat{\hat{T}}^{2Q}_{0} \lambda_Q \sum_{m,k} \bar{V}^{Q2}_{-k} D^{2}_{m0}(\Omega_{M \to L}(t)) \tag{3.15}$$

3.6 Evolution of the Density Matrix in DP approach

The Liouvillian is then averaged across the system to calculate the density matrix as a function of time.

$$\rho(t) = \left\langle exp\left(-i \int_0^t \hat{\hat{L}}^{Q}(\tau) d\tau\right)\right\rangle \rho(0) \tag{3.16}$$

3.7 Calculation of the Spectrum

From which the spectrum can be calculated by

$$I(\omega) = \mathrm{Re} \int_0^\infty exp(-i\omega t) \left\langle M_+(t) \right\rangle \mathrm{d}t \tag{3.17}$$

Where the magnetization M_+ is proportional to the trace of the super operator

$$\langle M_+(t) \rangle \propto Tr(\hat{\hat{I}}_+ \rho(t)) \tag{3.18}$$

$$\hat{I}_{tot} = \sum_i \hat{I}^i_{tot} = \frac{1}{\sqrt{2}} \sum_i (\hat{I}^i_x + i\hat{I}^i_y) \tag{3.19}$$

Simulations were performed using the general purpose SpinMolDyn simulation suite originally developed by Oganesyan,[1], in MATLAB for prediction of EPR spectra from MD and recently extended to NMR prediction (Copyright University of East Anglia).

4

Results and Discussion

In aiming to demonstrate the applicability of MD simulations to the prediction of NMR spectra line shapes there are several key results that reveal the degree to which MD simulations can produce agreement with experimental data. As well as exciting cases where MD simulations can study behaviour that wouldn't otherwise be experimentally accessible to support or contest theoretical models.

4.1 EFG tensor

The principle values of the EFG tensor calculated in Gaussian in atomic units from the HF optimised structure are.

i	$V_{zz}^{PAS}, \delta_\lambda$	V_{yy}^{PAS}	V_{xx}^{PAS}	η	Tr	χ kHz
1	-0.292	0.162	0.130	0.110	0	196
2	-0.299	0.165	0.134	0.104	0	201
3	-0.299	0.165	0.134	0.104	0	201
Site 1 to 2/3 ratio	0.98	0.97	0.98			

Table 4.1: EFG tensor values for Imidazolium Ion

These values are consistent with the observation that positions 2 and 3 in the Im molecule are symmetrical and supports the findings of Shi et al. that these nuclei all produce equivalent spectra, as their electric field gradients in each direction are all within 3% of each other. But it's worth noting these values are taken in the PAS of each deuterium site so don't account for differences in orientation between the sites or differences in mobility of the sites. The orientational differences aren't significant because the distribution of molecular orientations over the system will average out the orientations of each site to the same extent. This is sufficient evidence to conclude that these sites will produce the same spectra in the static regime but can't be used to reach the conclusion that the spectra in the context of motional averaging will be uniform across all sites.

From these tensor values calculated in Gaussian the quadrupolar coupling constant, χ, asymmetry parameter, η, and trace of the tensor were calculated.

The trace is 0 at all sites, which is evidence that the optimisation of the

Site	ν_1 kHz	ν_2 kHz	ν_3 kHz
1	±65	±82	±147
2-3	±67	±84	±150

Table 4.2: Splitting predictions at 300 K

electronic structure in Gaussian has been successful as it means there's no net force due to the electric field potential that would result in a change of that structure.

The values for V_{zz}^{PAS} have been used to calculate the quadrupolar coupling constant which for all three sites is approximately 200 kHz and can in turn be used to calculate the expected static splitting, ν_3, for each site. As the values for V_{yy} and V_{xx} are also known, the asymmetry was also calculated, giving values of approximately 10% in each case, importantly this disagrees with the assumption of axial symmetry made by Shi et al. that was used in their simulations of spectra. Additionally, from the asymmetry parameter and V_{zz}^{PAS}, ν_2 and ν_1 were calculated for the static regime. These static values closely match the values measured by Shi et al for the system at 300 K.

This supports the validity of computational approaches to prediction of static splitting but is insufficient to reach conclusions about molecular motions.

4.2 Autocorrelation Functions

ACFs were calculated for the D^2_{00} Wigner matrix element ($f(\beta)$ as defined in equation 1.83) for each cartesian axis in the PAS averaged among all molecule for each site at both temperatures with a length of 3 μs. From these plots the correlation time can be estimated, as can the order parameter from the square root of the Autocorrelation that the function levels off to.

Temperature	Site	Order x	Order y	Order z	τ_z ns	τ_y ns	τ_z ns
300 K	1	0.77	0.81	0.84	1 - 10	1 - 10	1 - 10
	2	0.76	0.76	0.81	1 - 10	1 - 10	1 - 10
	3	0.81	0.77	0.77	1 - 10	1 - 10	1 - 10
450 K	1	0.76	0.81	0.81	1 - 10	1 - 10	1 - 10
	2	0.42	0.42	0.77	730	730	1 - 10
	3	0.45	0.45	0.77	800	800	1 - 10

Table 4.3: Autocorrelation Data

At site 1 all six autocorrelation functions show rapid relaxation within 10 ns to order parameters between 0.75 and 0.85, with the primary distinction being the smoothness of the function, which shows less random variation at 450 K than 300 K. This indicates that temperature does not introduce additional sources of motional averaging, but that the motions that cause this averaging are happening faster, leading to less variation in the autocorrelation function with time.

There are two possible explanations for the initial ns scale relaxation both at site 1 and the other sites. Either rapid librational motions in the system, or alternatively this is the system equilibrating during the MD simulation run. That the system has undergone energy minimisation followed by temperature and pressure equilibration is evidence against the

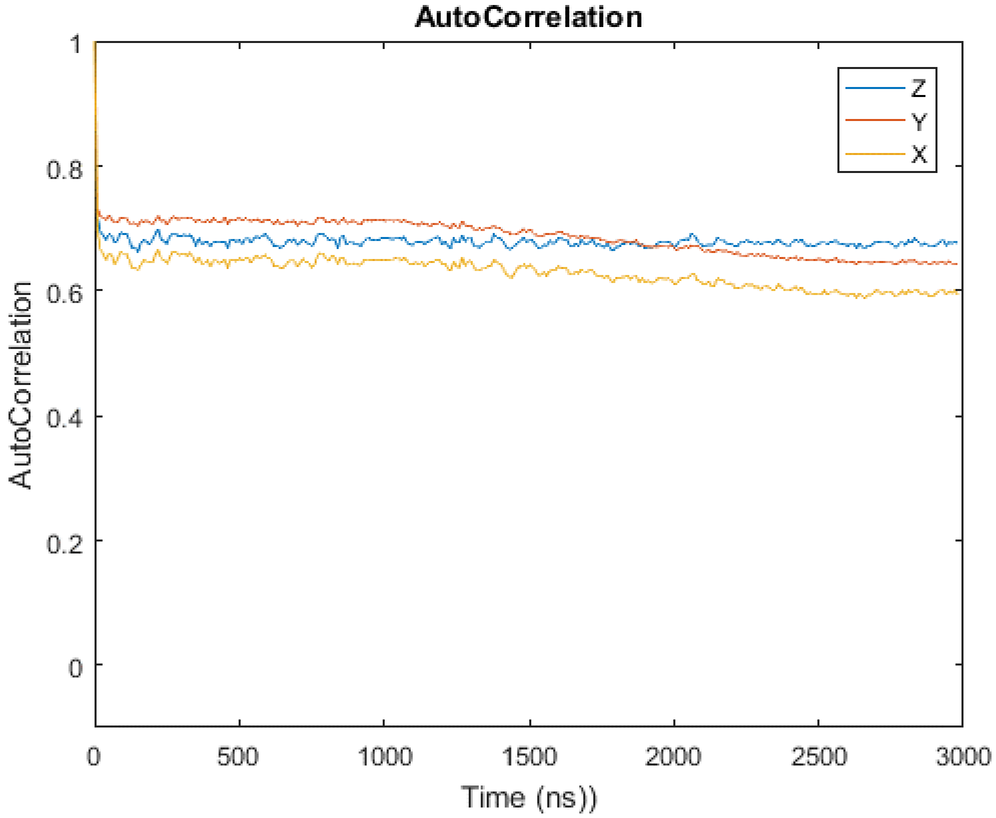

Figure 4.2.1: ACF for Site 1 at 300 K.

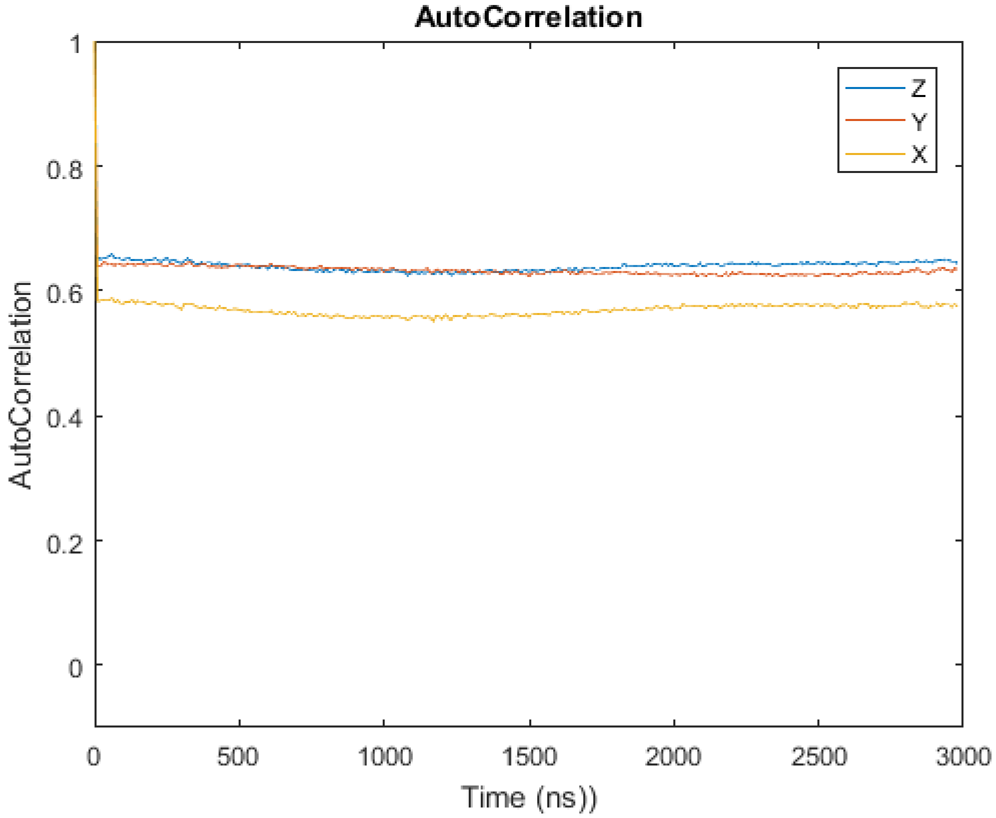

Figure 4.2.2: ACF for Site 1 at 450 K.

second case.

Additionally the fact this has happened after the first 0.5 μs of simulation, which weren't included in calculations of autocorrelation functions, is evidence in support of them being librational as opposed to due to equilibration, as the observed relaxation happens on the ns scale and so would be expected to have resolved within the first 0.5 μs where as librational motions would be a persistent feature of the system at all times in the simulation.

There's minimal difference between the three directions, though at both temperatures there is slightly less order in the x direction than in the y or z direction which are closer together. The difference between these order parameters is lower at the higher temperature though the exact cause of this, whether it's a fundamental difference in the behaviour of those axes or to an extent random, is unclear at this point.

Key here is that neither spectra for site 1 show any evidence of the flips that would be expected under the model proposed by Shi et al despite the overall spectra Shi et al. produced showing motional averaging due to the flips which undermines the conclusion that these sites behave equivalently. Which would be true if the rotation happened around an axis perpendicular to the plane of the molecule.

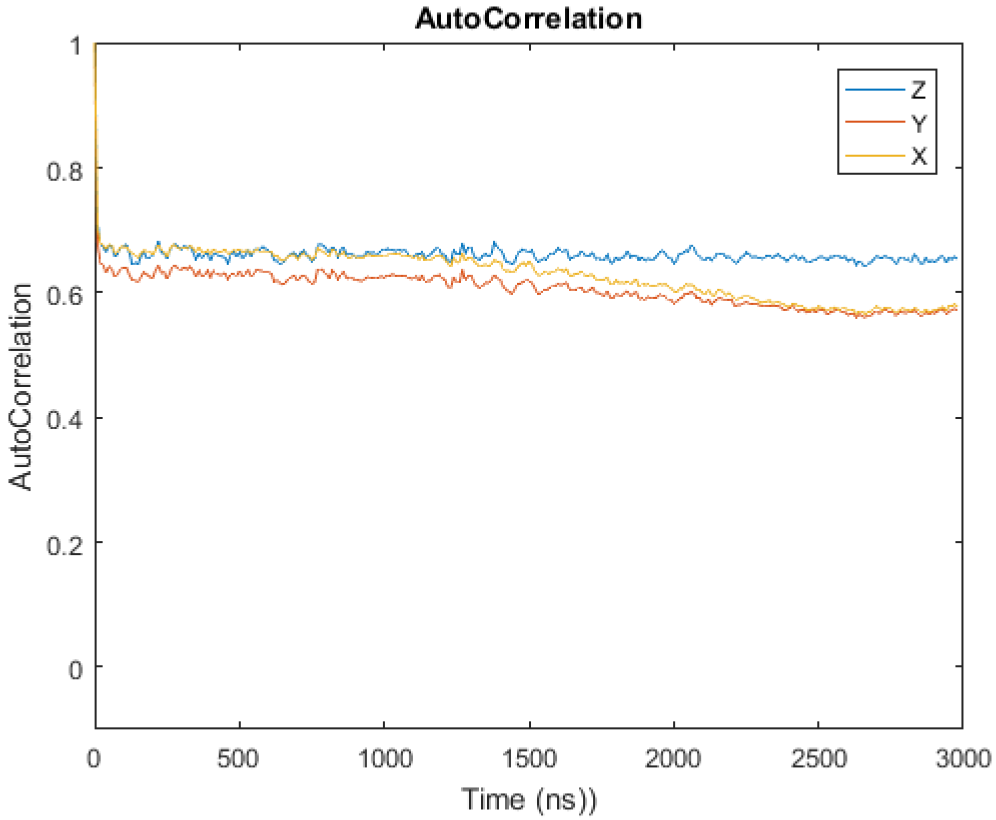

Figure 4.2.3: ACF for Site 2 at 300 K.

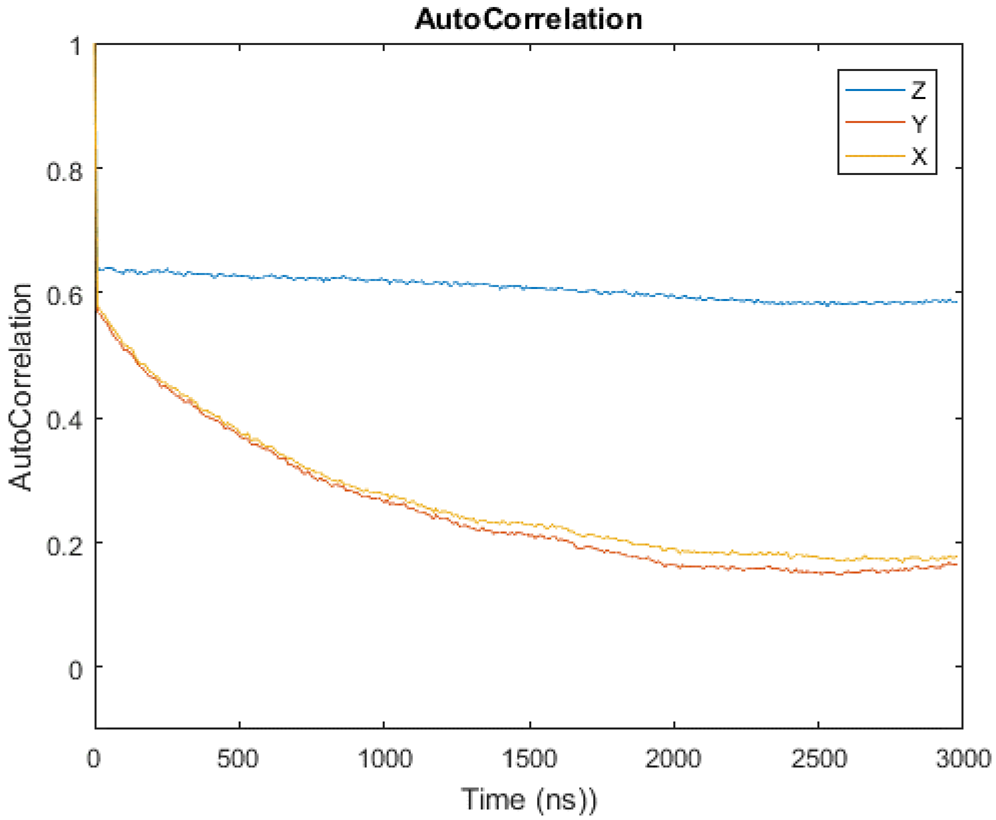

Figure 4.2.4: ACF for Site 2 at 450 K.

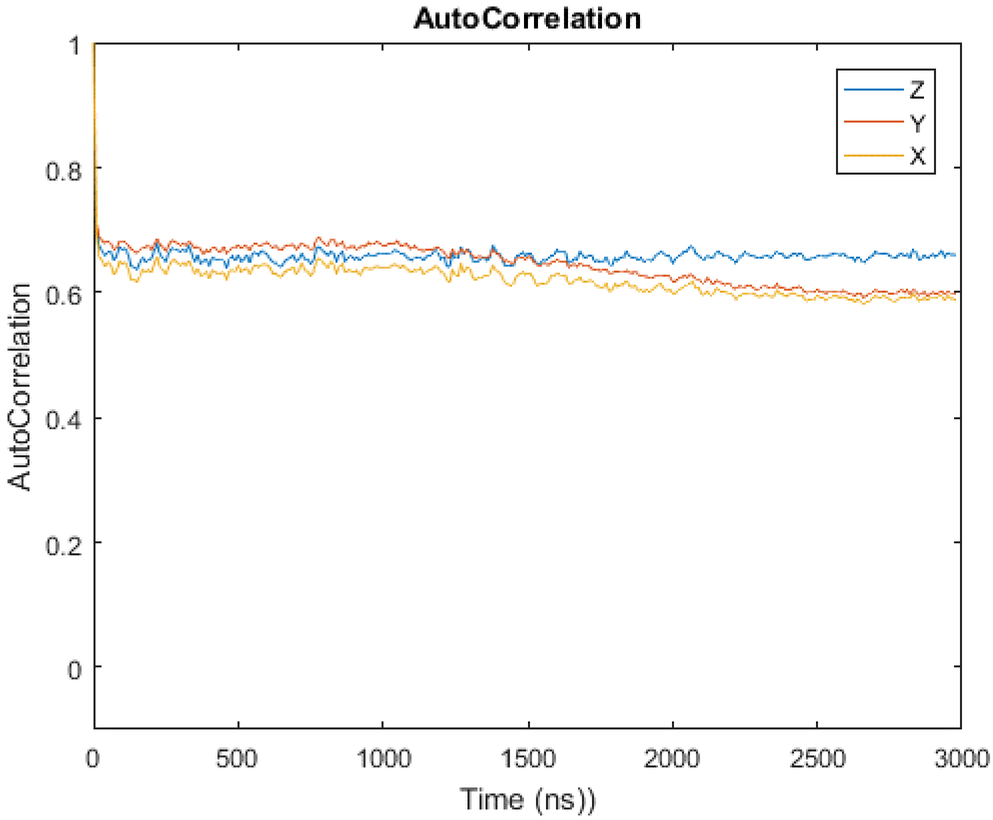

Figure 4.2.5: ACF for Site 3 at 300 K.

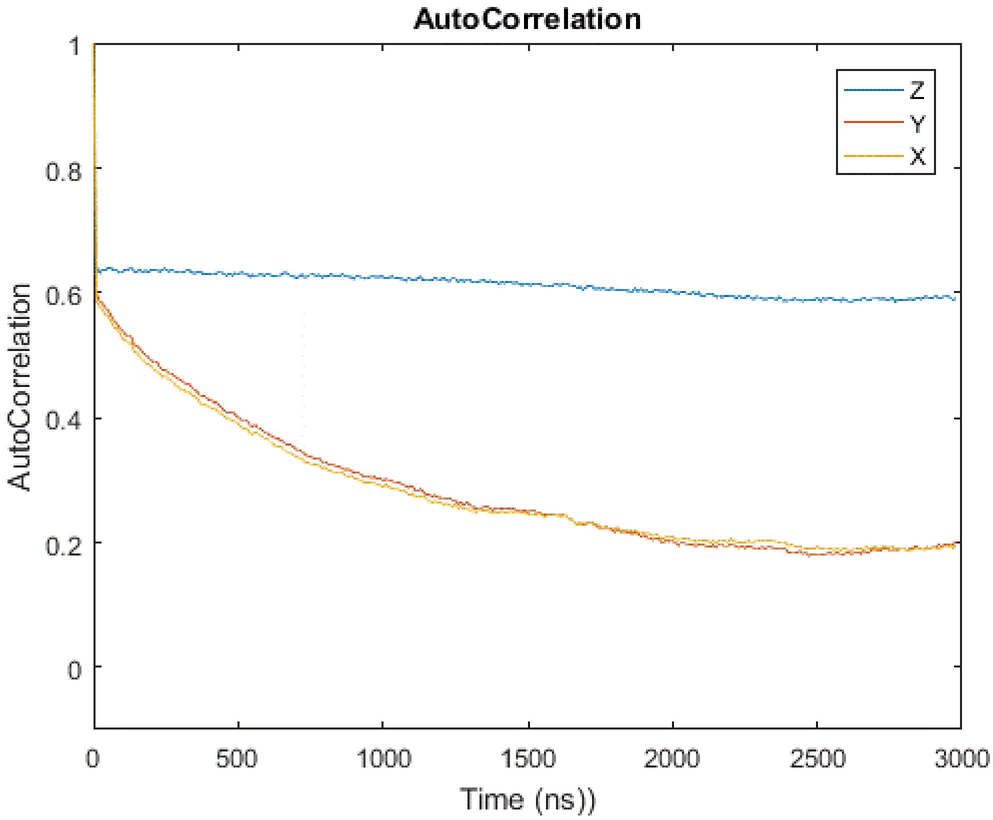

Figure 4.2.6: ACF for Site 3 at 450 K.

Sites 2 and 3 show a similar pattern at 300 K with the order parameters falling within the same range and with the same rapid relaxation within 10 ns to a leveled order parameter. This supports the equivalence of the motional behaviour of the three sites at 300 K and the three direction in the system. Interestingly the same pattern of the z direction relative to the molecule being more ordered compared to x and y is consistent between all three sites at 300 K indicating this may be more than random variation due to limited sample sizes, sites 2 and 3 also show less distinction between the x and y directions with both having identical order parameters as opposed to site 1 where the y direction is more distinct from the x direction.

A drastic difference between sites 2 and 3 compared to site 1 at 450 K is found in the distinction between the z axis and the x and y axes. In addition to the same rapid relaxation within 10 ns to the 300 K order parameter for all axes, there's a second relaxation that occurs in the x and y direction over orders of magnitude longer times, 730 to 800 ns, to an order parameter of between 0.4 and 0.45 at which point the x and y axis of the same site are indistinguishable.

This decrease in order parameter is clear evidence of additional sources of motional averaging, at 450 K for sites 2 and 3, where the inverse of these correlation times gives rates of 1.37 and 1.25 MHz for sites 2 and 3 respectively which are on the same order of magnitude as the flip rate proposed by Shi et al.

Further, that this relaxation happens in two axes but not the third is support for motions that happen exclusively in the x-y plane perpendicular to the z axis. This would be consistent with the expected behaviour of flips occurring in the plane of the molecule which z^{PAS} as defined in this work is perpendicular to, hence why it's the z axis that

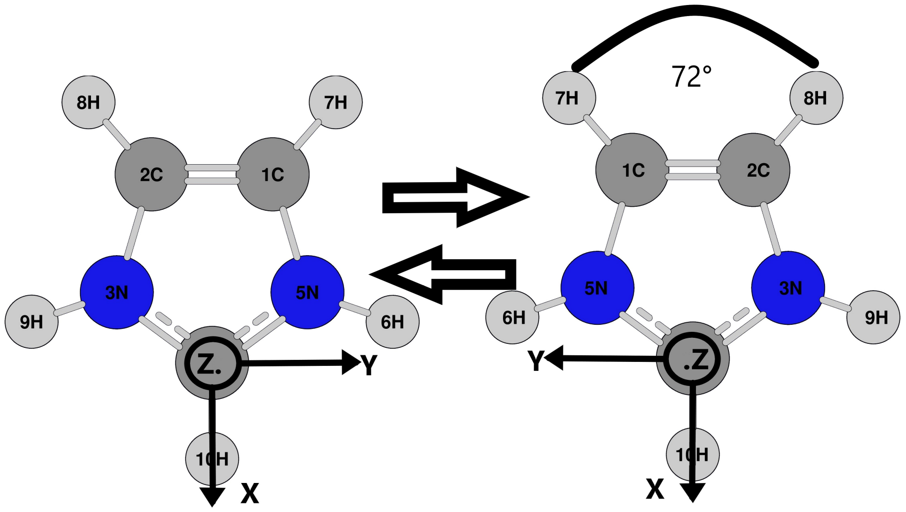

Figure 4.2.7: Flip diagram for proposed alternative flip model of flips taking place around the x axis of site 1.

doesn't show the additional relaxation.

This ability to distinguish between sites using the data produced by MD simulations is significant as it helps challenge assumptions of uniformity between sites that can't be distinguished experimentally.

This leads to the proposal of an alternative model to the one suggested by Shi et al [5] of in plane flips, that takes account of the distinction between sites. In this model the molecule flips 180 degrees around an axis co-linear with the C-D bond of site 1. Which suggests the presence of hydrogen bonding at site 1, as seen in the Shi et al paper, to the TPA lattice that restricts the motions of the Im cation preventing in plan rotations.

The effects of this flip is to invert the z axis at each site as well as the y axis of site 1, but leaving the x axis of site 1 unchanged. The x and y axis of the PAS at sites 2 and 3 are both rotated by 72°.

The function that the autocorrelation is taken for is D^2_{00}, which is dependent on $\cos^2\theta$. In the cases of the inversions of each z axis, and y at site 1, this doesn't affect the autocorrelation as D^2_{00} is periodic over 180°and so unaffected. In the reference frame of sites 2 and 3 this would be equivalent to a flip in the x y plane of 72° analogous to the model in [62].

4.3 VMD Check

By inspecting the .xtc visually in VMD it's possible to check both the arrangement of molecules in space and the motions of individual molecules. Visual inspection shows that at both temperatures the structure forms a host guest system of Im ions in hexagonal cells of the TPA lattice. However, the alignment between the TPA ions in the lattice appears more disordered at the higher temperature. These systems also show apparently random distributions of Im ions within the cells which matches observations of splitting demonstrating the Pake pattern in the 300 K spectra.

Additional features can be discovered by watching the molecules in motion. Specifically flips can be checked for and counted by focusing on a single Im molecule in the host guest structure, an example of these motions is shown in figures 4.3.1-10 where it can be seen that both temperatures display random motions between frames.

While at 450 K, as well as random motions, there are more clear changes in the orientation of the ring in the plane it's being viewed from. However these are ambiguous in terms of whether they represent rapid flips or liable motions. This can be quantified by counting the observed number of these orientational changes for every 10th molecule over 1 μs (100 frames).

While this is ultimately a rough estimate, as there's ambiguity in identifying flips visually, these results generally agree with the conclusion that flips don't happen at 300 K (100 kHz being the minimum detectable rate if one of the ten molecules flipped once) and happen significantly more at 450 K.

This rate estimate can further be compared to the rate predicted for 450 K

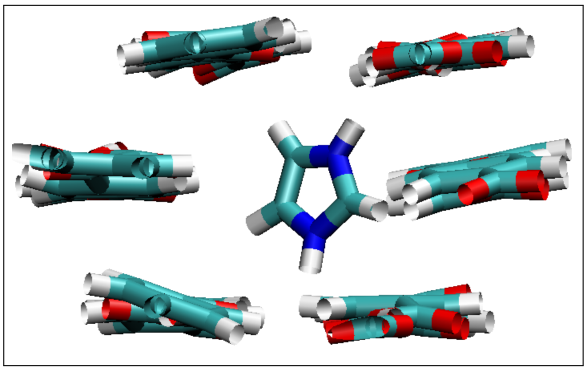

Figure 4.3.1: 300 K, t = 0

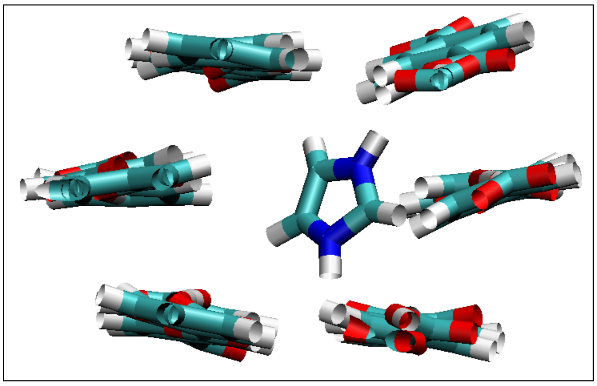

Figure 4.3.2: 300 K, t = 100ns

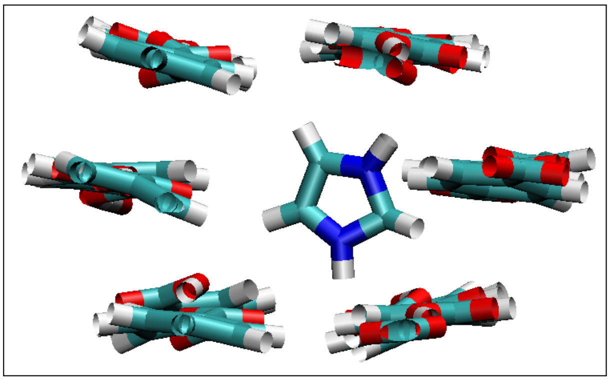

Figure 4.3.3: 300 K, t = 200ns

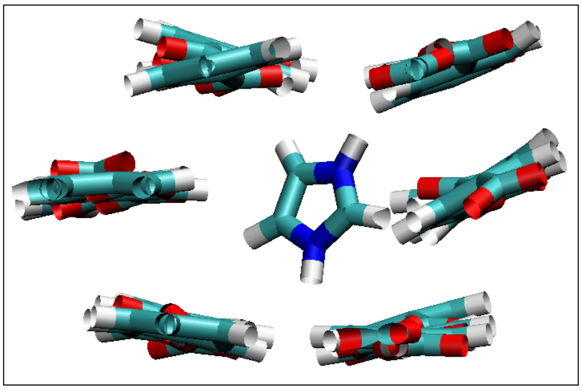

Figure 4.3.4: 300 K, t = 300ns

Figure 4.3.5: Four frames of the system at 300 K, 100ns (10 frames) apart.

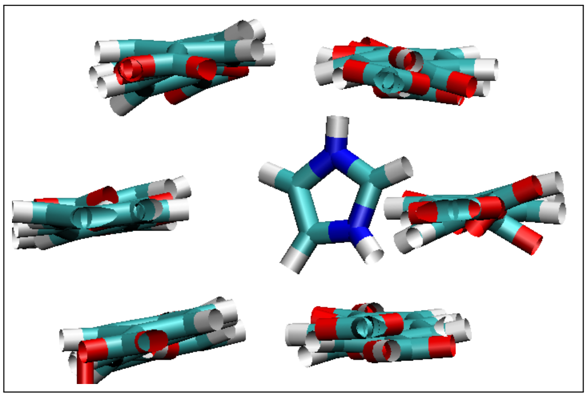

Figure 4.3.6: 450 K, t = 0

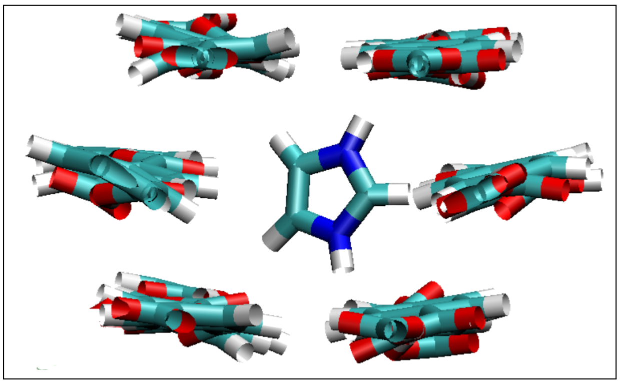

Figure 4.3.7: 450 K, t = 100 ns

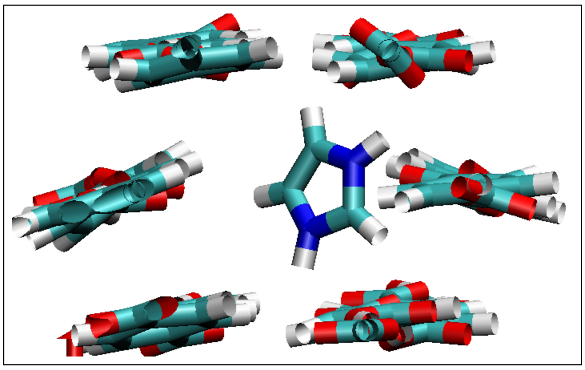

Figure 4.3.8: 450 K, t = 200 ns

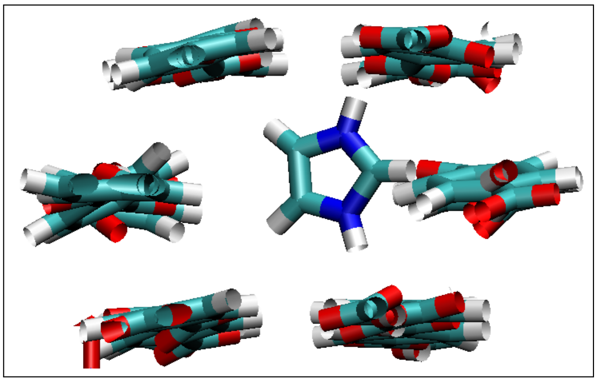

Figure 4.3.9: 450 K, t = 300 ns

Figure 4.3.10: Four frames of the system at 450 K, 100ns (10 frames) apart.

Molecule id	Flip per μs at 300 K	450 K
110	0	4
120	0	1
130	0	2
140	0	0
150	0	1
160	0	0
170	0	0
180	0	0
190	0	0
200	0	2
Average	0	1
ω k Hz	<100	1000

Table 4.4: Flip rate comparison for each temperature.

from the values given by Shi et al for activation energy $E_a = 52.1$ kj mol^{-1} and the pre-expinential factor 7.44×10^{12} s^{-1}. Which at 450 K gives a rate of approximately 6.70 MHz so the estimate given by the counting frames is low but on the same order of magnitude and either rate would be sufficient to qualify for the fast flips regime.

VMD also allows for the alternative model to be tested as well. By labeling the deuterium nuclei at sites 2 and 3 as L and R, symmetrical flips can be observed in the spectra as a reversal of those two labels an example of which is shown in figures 4.3.11 and 4.312.

These flips where observed at 450 K happening in under 10 ns (between two single frames) indicating they are fast on the NMR time scale which is supporting evidence for their role in motional averaging via flips that leave site 1 unchanged.

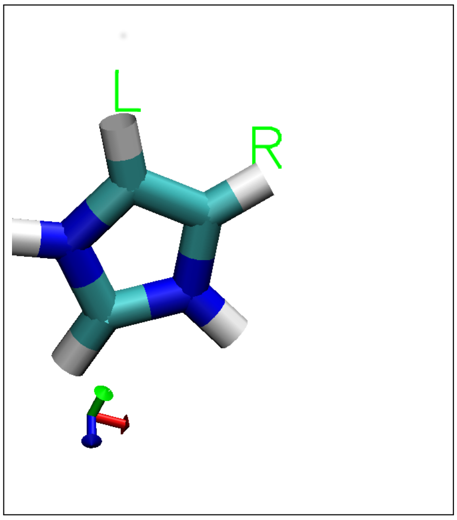

Figure 4.3.11: Single Im cation at 450 K, time 100 ns with sites 2 and 3 labeled L and R respectively, with the laboratory axis for reference.

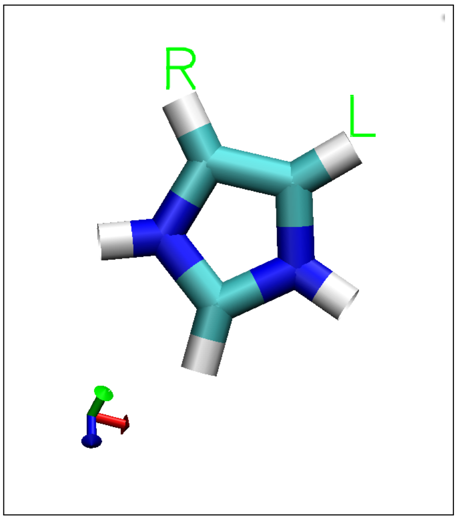

Figure 4.3.12: Second frame of the same Im cation 10 ns (1) frame later, showing 180° around the site 1 C-D bond.

4.4 Spectra Predictions

The spectra for each position were predicted by both FML and DP methods.

4.4.1 FML

First the spectrum for each individual site was calculated at the two characteristic temperatures.

At 300 K the three sites all show the expected characteristic Pake pattern and site 1 is in close agreement with sites 2 and 3 which are coincident. The differences are most noticeable for ν_1 where site 1 is within the splitting for sites 2 and 3, the opposite is true for ν_2, and ν_3 is equal for all sites.

At 450 K the three sites show strong agreement as well, sites 2 and 3 are again coincident while site 1 shows greater ν_3 and ν_2 with the three sites

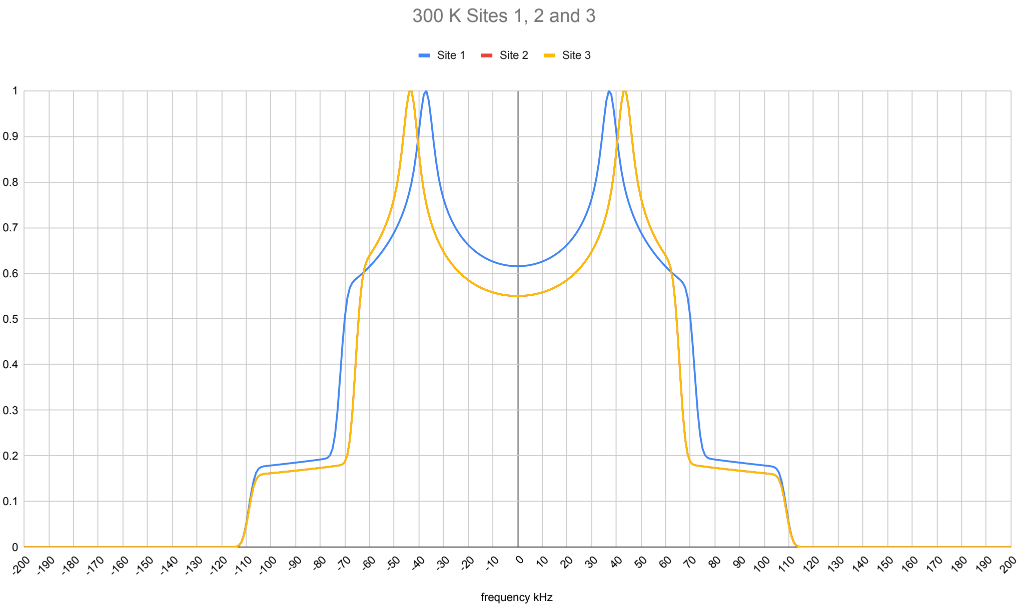

Figure 4.4.1: Spectra for the three deuterium sites at 300 K via FML. With sites 2 and 3 coincident.

Figure 4.4.2: Spectra for the three deuterium sites at 450 K via FML. With sites 2 and 3 coincident.

being the same in terms of ν_1. All three sites display the expected pattern for flip averaging

However it's curious that site 1 displays motional flip averaging when evidence of these flips isn't seen in the autocorrelation function for that site. This suggest a source of averaging not present at 300 K or visible in the autocorrelation functions behind this behaviour.

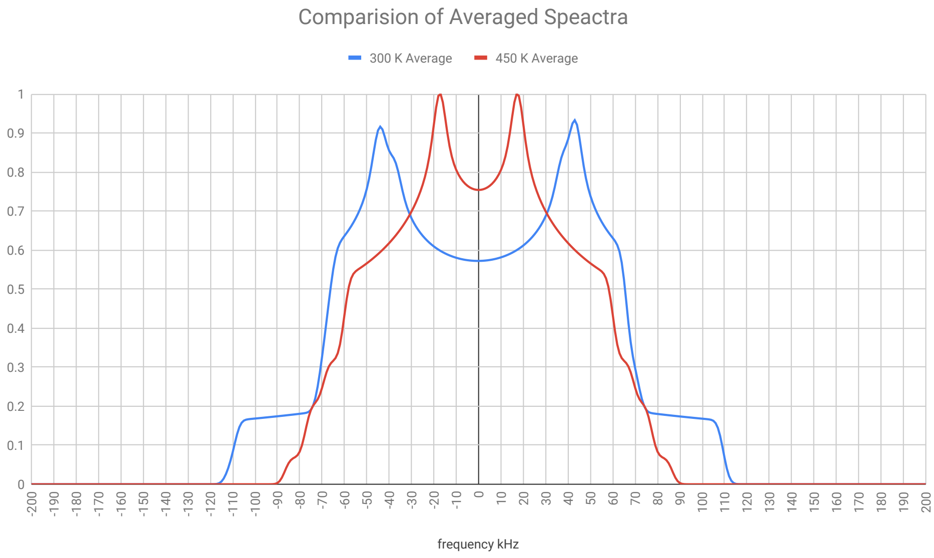

Figure 4.4.3: Comparison between the three site averages of the spectra at the two characteristic temperatures.

Temperature	ν_1 kHz	ν_2 kHz	ν_3 kHz
300 K	37	71	109
450 K	17	69	87

Table 4.5: Averages of 300 K and 450 K Spectra

These spectra are then averaged for comparison to the each other. Key here is that there's a reduction in splitting values ν_3 and ν_1, the inner and outer components. This reduction is evidence of additional motional averaging at 450 K which matches the behaviour seen in the autocorrelation function of the x and y axes for sites 2 and 3. That this reduction is negligible (71 to 69) in the splitting value associated with V_{yy} is evidence that this motion happens perpendicular to the y axis of the PAS.

This provides evidence for flips, though for sites 2 and 3 doesn't distinguish between the motions proposed by Shi et al. and by this work, so doesn't help with resolving the disagreement between the conclusions of the autocorrelation functions and these simulated spectra.

However, it also implies a disagreement between the labeling of directions of the PAS and the molecular features used to track these motions. If the flips occur perpendicular to the y axis then V_{yy}, the middle splitting value, doesn't appear to be in the plane of the molecule.

Next the averaged spectra for each temperature is compared to digitisation of the spectra measured by Shi et al.

Thought the spectra at 300 K broadly match there are key differences. The digitized spectrum shows greater values for splitting with low intensity motions at the edges of the spectrum, attributed to a rigid component of the system by Shi et al that has not been accounted for in this work. Additionally the digitized spectra are not symmetrical around the mid point at 0, unlike the spectra simulated by this work. The digitized spectra is generally wider than the simulated one and doesn't show the asymmetry as clearly.

At 450 K the difference is reversed, with the digitized spectra being significantly narrower than the predictions made by this work and doesn't as clearly display the expected pattern.

Overall there's a consistent pattern of FML based prediction producing general agreement with experimental data for this system including modeling the expected reduction in splitting due to flip averaging. This technique provides evidence in support of the flips happening in the system at 450 K including that these flips happen within a specific plane.

It also provides the ability to distinguish between different deuterium sites with individual plots, which is something that's not accessible experimentally when taking NMR measurements of the bulk system where the signals of different sites are aggregated.

This demonstrates the potential of FML to reproduce experimental data and further to offer insight on a molecular scale to enhance understanding from experimental data. This is accomplished using only a short simulation time and averaged values for Wigner matrices from a single molecular trajectory.

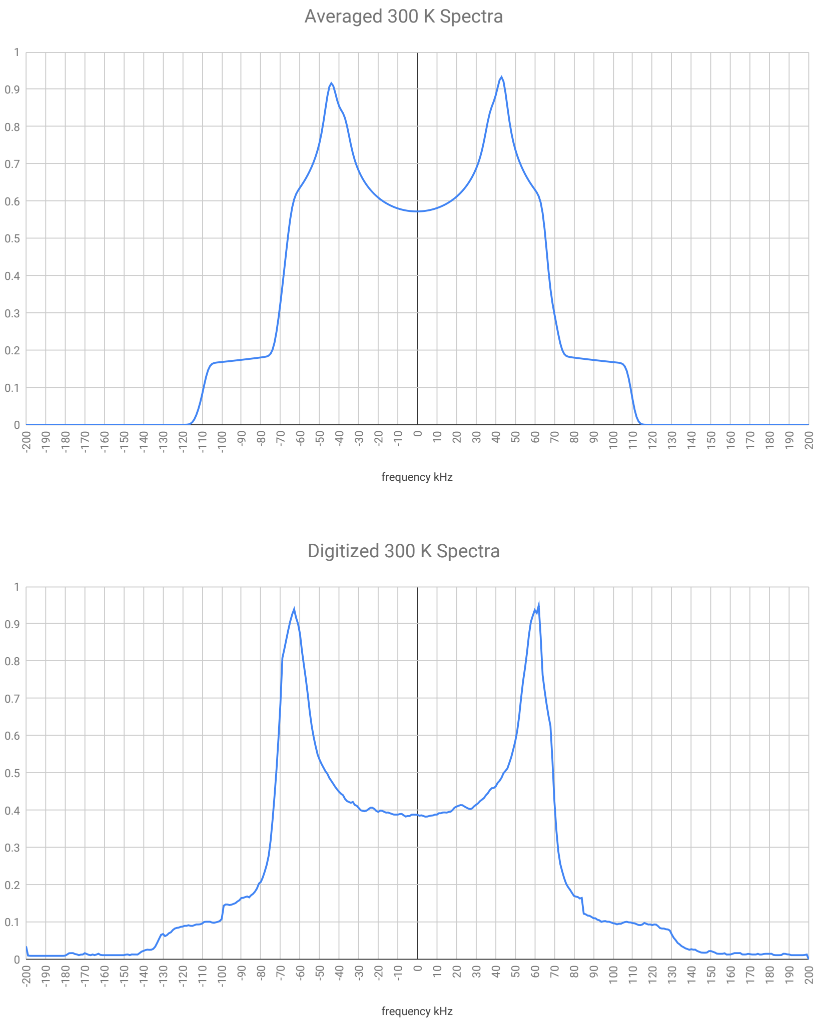

Figure 4.4.4: Comparison of average and digitised spectra at 300 K.

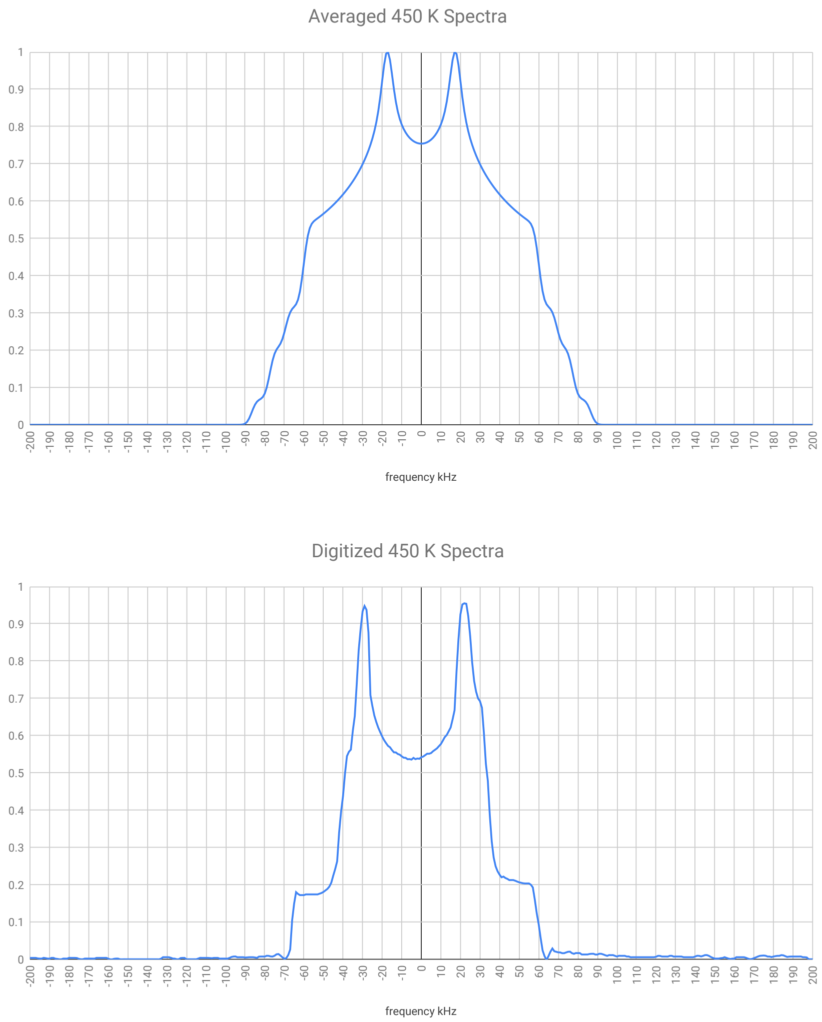

Figure 4.4.5: Comparison of averaged and digitised 450 K spectra.

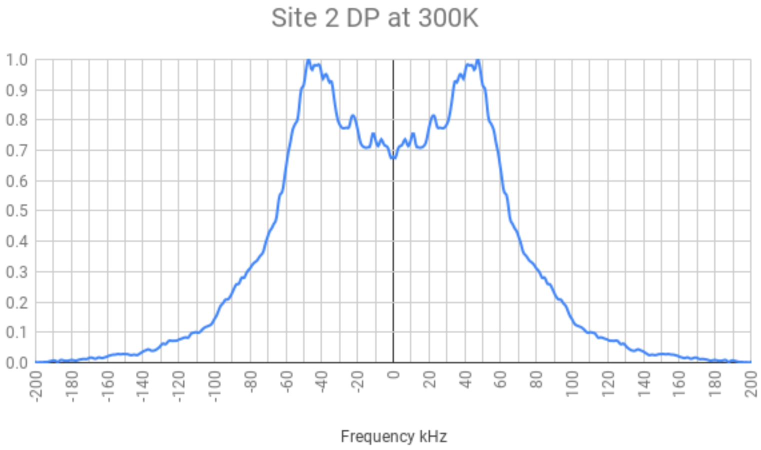

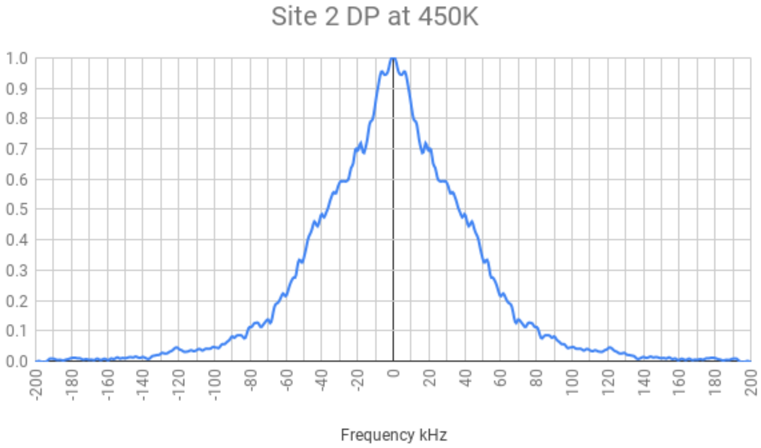

Figure 4.4.6: Comparison of Site 2 spectra from DP between temperatures.

4.4.2 DP

In contrast to FML the spectra produced by the DP method only very qualitatively match the expected spectra, this is attributed to insufficient simulation time for sampling, leading to a poor signal to noise ratio making it difficult to take any readings of ν values.

However it's possible to break these spectra down into two components corresponding to the two transitions in the $I = 1$ quadrupolar nucleus $(-1 \rightarrow 0)$ and $(0 \rightarrow +1)$.

What can be seen from these contributions is a broad tendency for the

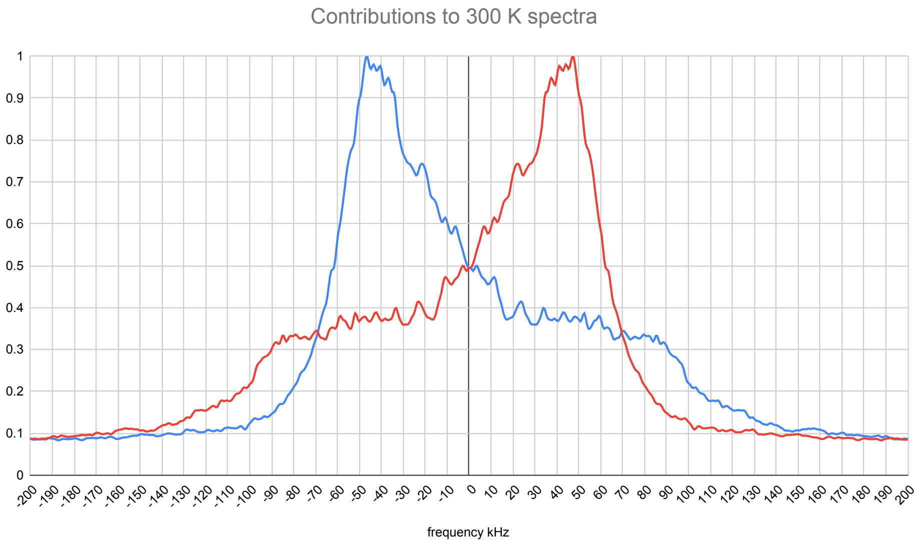

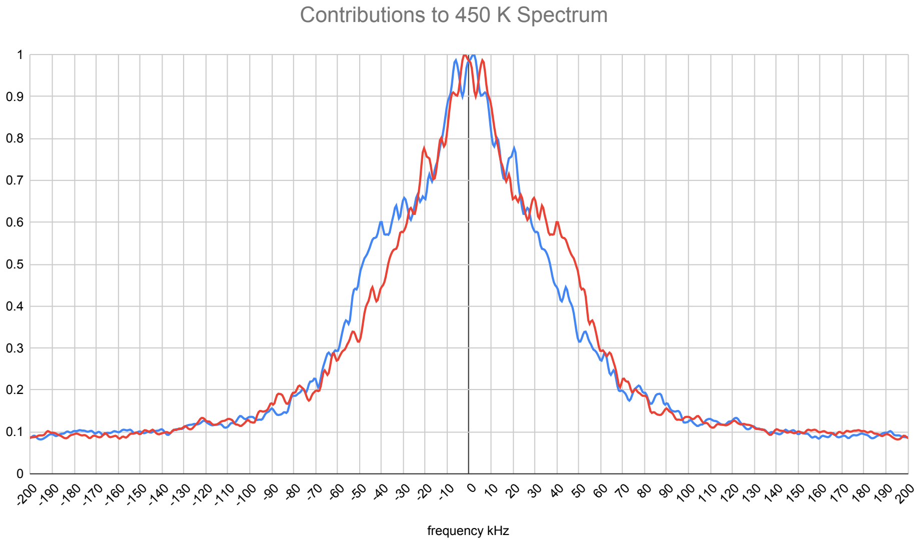

Figure 4.4.7: Contributions to the site 2 spectra. -1 to 0 (red) and 0 to 1 (blue).

splitting between the two transitions to decrease with temperature which is consistent with the behaviour observed in the FML prediction and experimental spectra.

This demonstrates a weakness of direct propagation as a method for the prediction of spectra that make it difficult to judge its applicability to this problem without further testing. The existence of noise also indicates the employed MD trajectory is of insufficient length to resolve spectral features in DP simulations, e.g. the splitting of inner peaks.

4.5 Prediction of T_1 relaxation time from MD

Relaxation times were predicted for all three sites at both temperatures for magnetic field strengths ranging from 0 to 15 tesla.

The predicted relaxation times as a function of field strength divide the three sites at two temperatures into two groups. Those with short relaxation times that reach a maximum of approximately 0.1 ms and then don't vary as the field increases, sites 2 and 3 at 450 K, and those with greater relaxation time for all field strengths and much more oscillation in that relaxation as field strength varies, all three sites at 300 K, with site 1 at 450 K showing close to the same relaxation times as 300 K but with less oscillation though still more than the other 450 K sites.

As χ and η aren't temperature dependent, these are the results of the differences in autocorrelation function. As such it's to be expected that the same division between these plots exists between the sites that do and don't show correlation times of 730 and 800 ns in their autocorrelation functions. The effect of this motional averaging appears to be to allow for faster relaxation. While this is a demonstration of the use of MD simulations it is not independent conformation of its validity as consistency between autocorrelation functions and predicted T_1 is a consequence of autocorrelation functions being used to produce T_1 not necessarily the correctness of either.

However, the demonstration of the technique does open up the opportunity for further research and testing by making relaxation time measurements of systems at variable temperatures and field strengths.

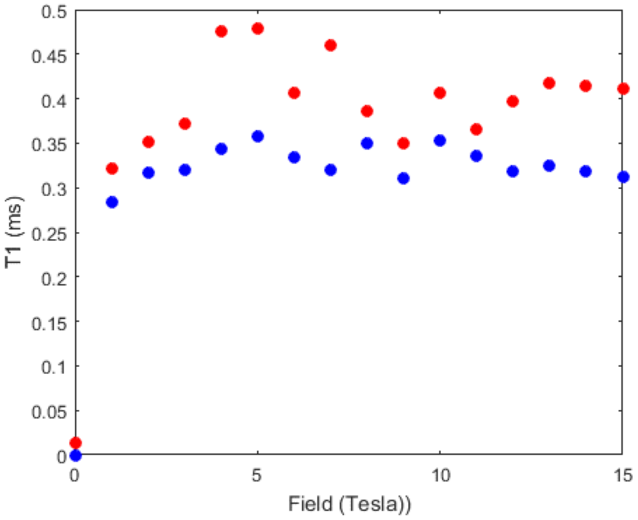

Figure 4.5.1: Relaxation time prediction time for site 1 at 300K (red) and 450K (blue)

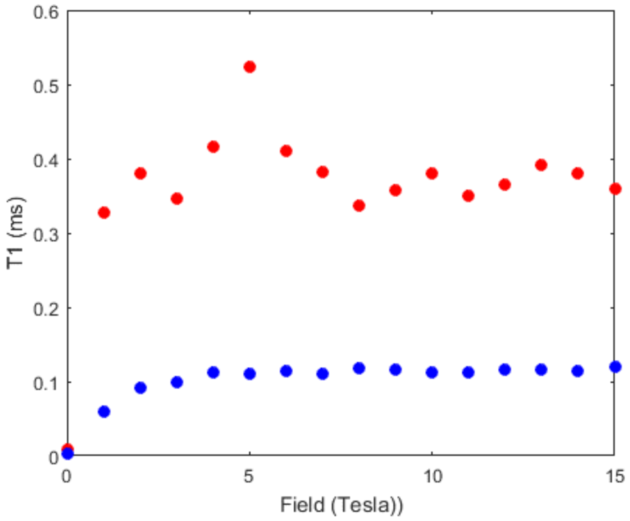

Figure 4.5.2: Relaxation time prediction time for site 2 at 300K (red) and 450K (blue)

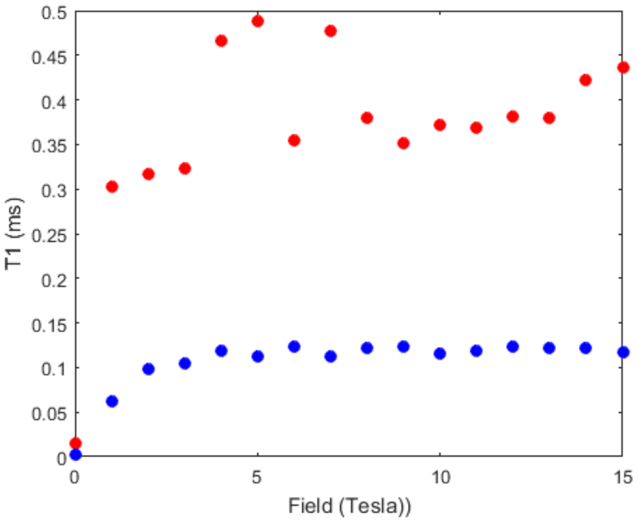

Figure 4.5.3: Relaxation time prediction time for site 3 at 300K (red) and 450K (blue)

This method is also applicable to T_2 relaxation which is analogous to T_1 relaxation but dependent on a different combination of power spectra [70].

5

Conclusion

The task of using MD to produce predictions of ^{2}D quadrupolar coupling NMR line shapes for a host guest ImTPA system was approached by two methods.

FML produced spectral predictions that showed the expected lines shapes at the two characteristic temperature for the system, including recreating static quadrupolar coupling and motional averaging leading to good qualitative agreement with the spectra available in the literature. This was demonstrated to be possible from a limited single molecule MD trajectory through the use of statistical averaging to give a representative sample of the distribution of orientations in the bulk structure.

In contrast the results from DP methods were inconclusive, producing spectra with insufficiently good signal to noise ratios for data collection, this was attributed to an insufficiently long molecular trajectory even with concatenation, which highlights a difficulty in using adapted EPR methods to systems where the relevant motions are on a longer time scale. As such this is an area where further study would be required.

Further, the outputs of these simulations were used to produce site specific autocorrelation functions and predictions of T_1 relaxation times. This site specific analysis highlights a strength of computational chemistry to study individual components of a system whose properties would otherwise be averaged out. Importantly, this can be seen in the comparison of autocorrelation functions between sites that Shi et al.[5] assumed to be equivalent that shows a distinction in the motions those sites undergo providing evidence against their proposed model, which was in turn backed up by visual evidence from VMD of flips.

This method was carried out entirely from first principles aside from the input of initial positions of atoms as a short cut to structure optimisations available via the CCDC, using fundamental physical constants and characteristic qualities of the nuclei involved from which DFT methods produced all of the required inputs for simulation which in turn produced the required outputs using the values in the force field and Newton's equations of motions, employed in MD methods. In addition to a demonstration of this method for quadrupolar coupling, this approach would be equally applicable to other magnetic interactions, for example chemical shift, by using the corresponding tensor, in the same way this method has been used previously for EPR interactions.

A

Appendix

A.1 Output of Gaussian NMR Optimisation

```
Entering Gaussian System, Link 0=g09
 1multiplicity_after_op_2_for_dft_op_2L.com
Output=/gpfs/home/dck13qfu/Imadazonium_Duterated_1ch
arge_
1multiplicity_after_op_2_for_dft_op_2L.log
Initial command:
/gpfs/software/gaussian/09-c01/g09/l1.exe /local/Gau-
6804.inp
-scrdir=/local/
Entering Link 1 = /gpfs/software/gaussian/09-c01/g09/l1.exe
PID=      6806.

Copyright (c) 1988,1990,1992,1993,1995,1998,2003,2009,2011,
Gaussian, Inc.  All Rights Reserved.

This is part of the Gaussian(R) 09 program.  It is based on
the Gaussian(R) 03 system (copyright 2003, Gaussian, Inc.),
```

```
the Gaussian(R) 98 system (copyright 1998, Gaussian, Inc.),
the Gaussian(R) 94 system (copyright 1995, Gaussian, Inc.),
the Gaussian 92(TM) system (copyright 1992, Gaussian,
Inc.),
the Gaussian 90(TM) system (copyright 1990, Gaussian,
Inc.),
the Gaussian 88(TM) system (copyright 1988, Gaussian,
Inc.),
the Gaussian 86(TM) system (copyright 1986, Carnegie
Mellon
University), and the Gaussian 82(TM) system (copyright
1983,
Carnegie Mellon University). Gaussian is a federally
registered trademark of Gaussian, Inc.

This software contains proprietary and confidential
information, including trade secrets, belonging to Gaussian,
Inc.

This software is provided under written license and may be
used, copied, transmitted, or stored only in accord with that
written license.

The following legend is applicable only to US Government
contracts under FAR:

RESTRICTED RIGHTS LEGEND
```

```
Use, reproduction and disclosure by the US Government is
subject to restrictions as set forth in subparagraphs (a)
and (c) of the Commercial Computer Software - Restricted
Rights clause in FAR 52.227-19.

Gaussian, Inc.
340 Quinnipiac St., Bldg. 40, Wallingford CT 06492


---------------------------------------------------------------
Warning -- This program may not be used in any manner
that competes with the business of Gaussian, Inc. or will
provide assistance to any competitor of Gaussian, Inc.  The
licensee of this program is prohibited from giving any
competitor of Gaussian, Inc. access to this program.  By
using this program, the user acknowledges that Gaussian,
Inc. is engaged in the business of creating and licensing
software in the field of computational chemistry and
represents and warrants to the licensee that it is not a
competitor of Gaussian, Inc. and that it will not use this
program in any manner prohibited above.
 ---------------------------------------------------------------
 \clearpage
Cite this work as:
Gaussian 09, Revision C.01,
M. J. Frisch, G. W. Trucks, H. B. Schlegel, G. E. Scuseria,
M. A. Robb, J. R. Cheeseman, G. Scalmani, V. Barone, B.
Mennucci,  G. A. Petersson, H. Nakatsuji, M. Caricato, X. Li,
```

```
H. P. Hratchian, A. F. Izmaylov, J. Bloino, G. Zheng, J. L.
Sonnenberg, M. Hada, M. Ehara, K. Toyota, R. Fukuda, J.
Hasegawa, M. Ishida, T. Nakajima, Y. Honda, O. Kitao, H.
Nakai, T. Vreven, J. A. Montgomery, Jr., J. E. Peralta, F.
Ogliaro, M. Bearpark, J. J. Heyd, E. Brothers, K. N. Kudin, V.
N. Staroverov, T. Keith, R. Kobayashi, J. Normand, K.
Raghavachari, A. Rendell, J. C. Burant, S. S. Iyengar, J.
Tomasi, M. Cossi, N. Rega, J. M. Millam, M. Klene, J. E.
Knox, J. B. Cross, V. Bakken, C. Adamo, J. Jaramillo, R.
Gomperts, R. E. Stratmann, O. Yazyev, A. J. Austin, R.
Cammi, C. Pomelli, J. W. Ochterski, R. L. Martin, K.
Morokuma, V. G. Zakrzewski, G. A. Voth, P. Salvador, J. J.
Dannenberg, S. Dapprich, A. D. Daniels, O. Farkas, J. B.
Foresman, J. V. Ortiz, J. Cioslowski, and D. J. Fox, Gaussian,
Inc., Wallingford CT, 2010.
```

```
******************************************
Gaussian 09:  EM64L-G09RevC.01 23-Sep-2011
                8-Aug-2019
******************************************
%chk=Imadazonium.chk
-----------------------------------------
# nmr=giao b3lyp/6-31g(d) prop=(read,efg)
-----------------------------------------
1/38=1/1;
2/12=2,17=6,18=5,40=1/2;
3/5=1,6=6,7=1,11=2,16=1,25=1,30=1,74=-5/1,2,8,3;
4//1;
```

```
5/5=2,38=5/2;

8/6=1,10=90,11=11/1;

10/13=100,45=16/2;

6/7=2,8=2,9=2,10=2,14=1,15=1,28=1/1,2;

99/9=1/99;

---------------------

DFT optimisatised NMR

---------------------

Charge =  1 Multiplicity = 1

Symbolic Z-Matrix:

C                     0.68166   0.97815   0.00005

C                    -0.68169   0.97813   0.00007

N                    -1.07432  -0.34847   0.00002

C                     0.00001  -1.14277  -0.0001

N                     1.07433  -0.34843  -0.00003

H                     2.03375  -0.6796   -0.00007

H(Iso=2)              1.39   1.80    0.00

H(Iso=2)             -1.39   1.80   0.00

H                    -2.03372  -0.67966   0.00003

H(Iso=2)              0.00  -2.22  -0.00


                         Input orientation:

---------------------------------------------------------------------

Center     Atomic      Atomic             Coordinates (Angstroms)

Number     Number       Type             X           Y           Z

---------------------------------------------------------------------

1          6           0          0.681658     0.978152     0.000050

2          6           0         -0.681688     0.978131     0.000069
```

```
3           7           0        -1.074316   -0.348465    0.000016

4           6           0         0.000012   -1.142774   -0.000099

5           7           0         1.074327   -0.348433   -0.000034

6           1           0         2.033749   -0.679602   -0.000065

7           1           0         1.392890    1.789600    0.000088

8           1           0        -1.392937    1.789564    0.000130

9           1           0        -2.033722   -0.679664    0.000029

10           1           0         0.000047   -2.222671   -0.000183

 ---------------------------------------------------------------------

Distance matrix (angstroms):

1           2           3           4           5

1  C    0.000000

2  C    1.363346   0.000000

3  N    2.200763   1.383479   0.000000

4  C    2.227772   2.227769   1.336079   0.000000

5  N    1.383480   2.200764   2.148643   1.336088   0.000000

6  H    2.139228   3.181458   3.125655   2.085813   1.014970

7  H    1.079027   2.227635   3.264725   3.246371   2.161635

8  H    2.227630   1.079027   2.161640   3.246369   3.264724

9  H    3.181453   2.139224   1.014964   2.085796   3.125649

10  H    3.272592   3.272598   2.160302   1.079897   2.160288

                    6           7           8           9          10

6  H    0.000000

7  H    2.551011   0.000000

8  H    4.223619   2.785827   0.000000

9  H    4.067471   4.223616   2.551018   0.000000

10  H    2.552843   4.247156   4.247168   2.552859   0.000000

Stoichiometry    C3H5N2(1+)
```

```
Framework group  C1[X(C3H5N2)]

Deg. of freedom    24

Full point group                C1      NOp   1

Largest Abelian subgroup        C1      NOp   1

Largest concise Abelian subgroup C1     NOp   1

                         Standard orientation:

 ---------------------------------------------------------------------

 Center     Atomic      Atomic             Coordinates (Angstroms)

 Number     Number       Type             X           Y           Z

 ---------------------------------------------------------------------

1          6           0        -0.681675   -0.978140    0.000050

2          6           0         0.681671   -0.978143    0.000069

3          7           0         1.074322    0.348446    0.000016

4          6           0         0.000008    1.142774   -0.000099

5          7           0        -1.074321    0.348452   -0.000034

6          1           0        -2.033737    0.679638   -0.000065

7          1           0        -1.392922   -1.789576    0.000088

8          1           0         1.392905   -1.789589    0.000130

9          1           0         2.033734    0.679628    0.000029

10          1           0        -0.000008    2.222671   -0.000183

 ---------------------------------------------------------------------

 Rotational constants (GHZ):

8.4754635      7.6817047      4.0295432

Standard basis: 6-31G(d) (6D, 7F)

There are    85 symmetry adapted basis functions of A

symmetry.

Integral buffers will be    131072 words long.

Raffenetti 2 integral format.
```

```
Two-electron integral symmetry is turned on.

85 basis functions,   160 primitive gaussians,

85 cartesian basis functions

18 alpha electrons       18 beta electrons

nuclear repulsion energy       172.7668505020 Hartrees.

NAtoms=   10 NActive=   10 NUniq=   10 SFac= 1.00D+00

NAtFMM=

60 NAOKFM=F Big=F

One-electron integrals computed using PRISM.

NBasis=    85 RedAO= T  NBF=    85

NBsUse=    85 1.00D-06 NBFU=    85

Harris functional with IExCor=  402 diagonalized for initial

guess.

ExpMin= 1.61D-01 ExpMax= 4.17D+03 ExpMxC= 6.27D+02

IAcc=

1 IRadAn=         1 AccDes= 0.00D+00

HarFok:  IExCor=  402 AccDes= 0.00D+00 IRadAn=         1

IDoV= 1

ScaDFX=  1.000000  1.000000  1.000000  1.000000

FoFCou: FMM=F IPFlag=           0 FMFlag=      100000

FMFlg1=           0

NFxFlg=           0 DoJE=T BraDBF=F KetDBF=T FulRan=T

Omega=  0.000000  0.000000  1.000000  0.000000  0.000000

ICntrl=

500 IOpCl=  0

NMat0=    1 NMatS0=    1 NMatT0=    0 NMatD0=    1

NMtDS0=

0 NMtDT0=    0
```

```
I1Cent=           4 NGrid=           0.

Petite list used in FoFCou.

Initial guess orbital symmetries:

Occupied  (A) (A) (A) (A) (A) (A) (A) (A) (A) (A) (A) (A)

(A) (A) (A) (A) (A) (A)

Virtual   (A) (A) (A) (A) (A) (A) (A) (A) (A) (A) (A) (A)

(A) (A) (A) (A) (A) (A) (A) (A) (A) (A) (A) (A)

(A) (A) (A) (A) (A) (A) (A) (A) (A) (A) (A) (A)

(A) (A) (A) (A) (A) (A) (A) (A) (A) (A) (A) (A)

(A) (A) (A) (A) (A) (A) (A) (A) (A) (A) (A) (A)

(A) (A) (A) (A) (A) (A) (A)

The electronic state of the initial guess is 1-A.

Requested convergence on RMS density matrix=1.00D-08

within 128

cycles.

Requested convergence on MAX density matrix=1.00D-06.

Requested convergence on             energy=1.00D-06.

No special actions if energy rises.

Keep R1 ints in memory in canonical form, NReq=7709885.

Integral accuracy reduced to 1.0D-05 until final iterations.

Initial convergence to 1.0D-05 achieved.  Increase integral

accuracy. SCF Done:  E(RB3LYP) =  -226.592173173     A.U.

after   12 cycles Convg  =    0.4674D-08  -V/T =  2.0099

Range of M.O.s used for correlation:     1    85

NBasis=    85 NAE=    18 NBE=    18 NFC=     0 NFV=     0

NROrb=     85 NOA=    18 NOB=    18 NVA=    67 NVB=    67

Differentiating once with respect to magnetic field using

GIAOs.
```

```
Electric field/nuclear overlap derivatives assumed to be

zero.

Keep R3 ints in memory in canonical form, NReq=7504090.

FoFCou: FMM=F IPFlag=           0 FMFlag=           0

FMFlg1=           0

NFxFlg=           0 DoJE=F BraDBF=F KetDBF=T FulRan=T

Omega=  0.000000  0.000000  1.000000  0.000000  0.000000

ICntrl=    6100 IOpCl=  0

NMat0=    1 NMatS0=    1 NMatT0=    0 NMatD0=    1

NMtDS0=    0

NMtDT0=    0

I1Cent=           7 NGrid=          10.

Symmetry not used in FoFCou.

There are     3 degrees of freedom in the 1st order CPHF.

IDoFFX=0.

3 vectors produced by pass  0 Test12= 4.02D-14 3.33D-08

XBig12=

2.57D+00 9.78D-01.

AX will form     3 AO Fock derivatives at one time.

3 vectors produced by pass  1 Test12= 4.02D-14 3.33D-08

XBig12= 1.71D-

03 1.84D-02.

3 vectors produced by pass  2 Test12= 4.02D-14 3.33D-08

XBig12= 5.51D-

06 1.38D-03.

3 vectors produced by pass  3 Test12= 4.02D-14 3.33D-08

XBig12= 7.78D-

09 3.50D-05.
```

```
3 vectors produced by pass  4 Test12= 4.02D-14 3.33D-08

XBig12= 2.07D-

11 2.80D-06.

1 vectors produced by pass  5 Test12= 4.02D-14 3.33D-08

XBig12= 7.11D-

14 1.25D-07.

Inverted reduced A of dimension    16 with in-core refinement.

Calculating GIAO nuclear magnetic shielding tensors.

SCF GIAO Magnetic shielding tensor (ppm):

1  C    Isotropic =    74.3719   Anisotropy =   117.4075

XX=    64.9658   YX=    -4.8060   ZX=    -0.0010

XY=    -5.9855   YY=     5.5064   ZY=     0.0093

XZ=    -0.0058   YZ=     0.0090   ZZ=   152.6436

Eigenvalues:     5.0208    65.4515   152.6436

2  C    Isotropic =    74.3730   Anisotropy =   117.4050

XX=    64.9686   YX=     4.8049   ZX=    -0.0018

XY=     5.9848   YY=     5.5074   ZY=     0.0079

XZ=     0.0035   YZ=     0.0087   ZZ=   152.6430

Eigenvalues:     5.0219    65.4541   152.6430

3  N    Isotropic =    91.6771   Anisotropy =   161.1263

XX=    11.0854   YX=   -34.7846   ZX=    -0.0053

XY=   -37.8892   YY=    64.8512   ZY=     0.0069

XZ=     0.0001   YZ=     0.0075   ZZ=   199.0946

Eigenvalues:    -7.2319    83.1685   199.0946

4  C    Isotropic =    66.4742   Anisotropy =   115.6612

XX=    37.9074   YX=     0.0011   ZX=    -0.0023

XY=     0.0013   YY=    17.9335   ZY=     0.0120

XZ=    -0.0014   YZ=     0.0146   ZZ=   143.5816
```

```
Eigenvalues:    17.9335    37.9074   143.5816
5  N    Isotropic =    91.6736   Anisotropy =   161.1267
XX=    11.0804   YX=    34.7871   ZX=    -0.0037
XY=    37.8907   YY=    64.8491   ZY=     0.0094
XZ=    -0.0083   YZ=     0.0080   ZZ=   199.0914
Eigenvalues:    -7.2380    83.1675   199.0914
6  H    Isotropic =    23.0683   Anisotropy =     7.6231
XX=    27.7100   YX=    -1.2640   ZX=     0.0002
XY=    -1.5510   YY=    23.6517   ZY=    -0.0004
XZ=     0.0002   YZ=    -0.0004   ZZ=    17.8433
Eigenvalues:    17.8433    23.2113    28.1504
7  H    Isotropic =    24.6285   Anisotropy =     3.2939
XX=    25.8760   YX=     0.9977   ZX=     0.0001
XY=     0.1090   YY=    26.5015   ZY=    -0.0004
XZ=    -0.0001   YZ=    -0.0004   ZZ=    21.5078
Eigenvalues:    21.5078    25.5532    26.8244
8  H    Isotropic =    24.6285   Anisotropy =     3.2940
XX=    25.8761   YX=    -0.9977   ZX=     0.0001
XY=    -0.1091   YY=    26.5015   ZY=    -0.0004
XZ=     0.0003   YZ=    -0.0004   ZZ=    21.5078
Eigenvalues:    21.5078    25.5532    26.8245
9  H    Isotropic =    23.0685   Anisotropy =     7.6233
XX=    27.7103   YX=     1.2640   ZX=     0.0002
XY=     1.5511   YY=    23.6518   ZY=    -0.0003
XZ=     0.0003   YZ=    -0.0003   ZZ=    17.8433
Eigenvalues:    17.8433    23.2114    28.1507
10  H    Isotropic =    24.1056   Anisotropy =     4.2627
XX=    24.5759   YX=     0.0002   ZX=     0.0001
```

```
XY=     0.0001   YY=    26.9474   ZY=    -0.0005

XZ=     0.0001   YZ=    -0.0001   ZZ=    20.7934

Eigenvalues:    20.7934    24.5759    26.9474

End of Minotr Frequency-dependent properties file   721

does not exist.

End of Minotr Frequency-dependent properties file   722

does not exist.




**********************************************************************
 *



            Population analysis using the SCF density.



**********************************************************************
 *




Orbital symmetries:

Occupied  (A) (A) (A) (A) (A) (A) (A) (A) (A) (A) (A) (A)

(A) (A) (A) (A) (A) (A)

Virtual   (A) (A) (A) (A) (A) (A) (A) (A) (A) (A) (A) (A)

(A) (A) (A) (A) (A) (A) (A) (A) (A) (A) (A) (A)

(A) (A) (A) (A) (A) (A) (A) (A) (A) (A) (A) (A)

(A) (A) (A) (A) (A) (A) (A) (A) (A) (A) (A) (A)
```

```
(A) (A) (A) (A) (A) (A) (A) (A) (A) (A) (A) (A)

(A) (A) (A) (A) (A) (A) (A)

The electronic state is 1-A.

Alpha  occ. eigenvalues --

-14.62592 -14.62591 -10.49323  -10.43710 -10.43639

Alpha  occ. eigenvalues --

-1.26837  -1.13549  -0.98576 -0.88513 -0.83878

Alpha  occ. eigenvalues --

-0.79428  -0.72914  -0.67200  -0.67103 -0.65502

Alpha  occ. eigenvalues --

-0.64559  -0.53823  -0.45927

Alpha virt. eigenvalues --

-0.21116  -0.16562  -0.12646  -0.08742  -0.06164

Alpha virt. eigenvalues --

-0.03181  -0.02621  -0.00318   0.01211   0.10761

Alpha virt. eigenvalues --

0.12474   0.21682   0.29254   0.31772   0.34766

Alpha virt. eigenvalues --

0.36546   0.37313   0.38928   0.39344   0.39996

Alpha virt. eigenvalues --

0.42114   0.54361   0.55877   0.58796   0.61068

Alpha virt. eigenvalues --

0.63042   0.65819   0.68458   0.72043   0.73806

Alpha virt. eigenvalues --

0.79945   0.95822   1.00144   1.06619   1.07429

Alpha virt. eigenvalues --

1.09378   1.11460   1.14105   1.18355   1.29910

Alpha virt. eigenvalues --
```

```
1.30301   1.41268   1.56221   1.70785   1.76340

Alpha virt. eigenvalues --

1.82354   1.82736   1.90383   1.97632   1.99656

Alpha virt. eigenvalues --

2.02749   2.05919   2.10786   2.11173   2.32312

Alpha virt. eigenvalues --

2.33979   2.43132   2.45773   2.46544   2.71258

Alpha virt. eigenvalues --

2.80807   2.81709   3.63662   3.76562   3.88804

Alpha virt. eigenvalues --

4.02048   4.14954

Condensed to atoms (all electrons):

1          2          3          4          5          6

1  C    4.758854   0.621253  -0.041671  -0.093153   0.361879

-0.020294

2  C    0.621253   4.758857   0.361879  -0.093153  -0.041672

0.004721

3  N   -0.041671   0.361879   6.598634   0.427475  -0.071013

0.003616

4  C   -0.093153  -0.093153   0.427475   4.669247   0.427472

-0.026199

5  N    0.361879  -0.041672  -0.071013   0.427472   6.598642

0.319610

6  H   -0.020294   0.004721   0.003616  -0.026199   0.319610

0.307057

7  H    0.375719  -0.027998   0.002859   0.004742  -0.035498

-0.002175

8  H   -0.027998   0.375719  -0.035498   0.004742   0.002859
```

```
-0.000074

9  H    0.004721  -0.020294   0.319612  -0.026200   0.003616

-0.000061

10  H    0.002749   0.002749  -0.031916   0.375634  -0.031917

-0.001049

7          8          9          10

1  C    0.375719  -0.027998   0.004721   0.002749

2  C   -0.027998   0.375719  -0.020294   0.002749

3  N    0.002859  -0.035498   0.319612  -0.031916

4  C    0.004742   0.004742  -0.026200   0.375634

5  N   -0.035498   0.002859   0.003616  -0.031917

6  H   -0.002175  -0.000074  -0.000061  -0.001049

7  H    0.426113  -0.000552  -0.000074  -0.000067

8  H   -0.000552   0.426112  -0.002175  -0.000067

9  H   -0.000074  -0.002175   0.307057  -0.001049

10  H   -0.000067  -0.000067  -0.001049   0.405808

 Mulliken atomic charges:

1

1  C    0.057941

2  C    0.057940

3  N   -0.533979

4  C    0.329393

5  N   -0.533980

6  H    0.414849

7  H    0.256931

8  H    0.256931

9  H    0.414849

10  H    0.279125
```

```
Sum of Mulliken atomic charges =   1.00000
Mulliken charges with hydrogens summed into heavy
atoms:
1
1  C    0.314872
2  C    0.314871
3  N   -0.119131
4  C    0.608517
5  N   -0.119131
Sum of Mulliken charges with hydrogens summed into
heavy atoms =   1.00000
Electronic spatial extent (au):  <R**2>=            283.2593
Charge=              1.0000 electrons
Dipole moment (field-independent basis, Debye):
X=              0.0000    Y=              1.4143
Z=             -0.0001
Tot=              1.4143
Quadrupole moment (field-independent basis, Debye-Ang):
XX=            -12.3528
YY=            -16.2678
ZZ=            -29.7278
XY=              0.0000
XZ=              0.0004
YZ=             -0.0009
Traceless Quadrupole moment (field-independent basis,
Debye-Ang):
XX=              7.0967
YY=              3.1816
```

```
ZZ=            -10.2783
XY=              0.0000
XZ=              0.0004
YZ=             -0.0009
Octapole moment (field-independent basis, Debye-Ang**2):
XXX=             -0.0001
YYY=              5.5696
ZZZ=             -0.0002
XYY=             -0.0001
XXY=              3.4737
XXZ=              0.0002
XZZ=              0.0000
YZZ=              1.4310
YYZ=             -0.0004
XYZ=              0.0001
Hexadecapole moment (field-independent basis, Debye-
Ang**3):
XXXX=            -88.9481
YYYY=           -122.9264
ZZZZ=            -27.4504
XXXY=              0.0000
XXXZ=              0.0003
YYYX=             -0.0003
YYYZ=              0.0010
ZZZX=             -0.0014
ZZZY=              0.0053
XXYY=            -35.4599
XXZZ=            -32.5751
```

```
YYZZ=            -35.2229

XXYZ=              0.0006

YYXZ=             -0.0001

ZZXY=

0.0000

N-N= 1.727668505020D+02

E-N=-8.628661240468D+02

KE= 2.243634271971D+02



 **********************************************************************



            Electrostatic Properties Using The SCF Density



 **********************************************************************



       Atomic Center    1 is at  -0.681675 -0.978140  0.000050

       Atomic Center    2 is at   0.681671 -0.978143  0.000069

       Atomic Center    3 is at   1.074322  0.348446  0.000016

       Atomic Center    4 is at   0.000008  1.142774 -0.000099

       Atomic Center    5 is at  -1.074321  0.348452 -0.000034

       Atomic Center    6 is at  -2.033737  0.679638 -0.000065

       Atomic Center    7 is at  -1.392922 -1.789576  0.000088

       Atomic Center    8 is at   1.392905 -1.789589  0.000130

       Atomic Center    9 is at   2.033734  0.679628  0.000029
```

```
      Atomic Center   10 is at  -0.000008  2.222671 -0.000183
-----------------------------------------------------------------


             Electrostatic Properties (Atomic Units)


-----------------------------------------------------------------
   Center     Electric         -------- Electric Field --------
              Potential          X             Y             Z
-----------------------------------------------------------------
   1 Atom    -14.489758      0.011118     -0.020156       0.000001
   2 Atom    -14.489758     -0.011119     -0.020156       0.000001
   3 Atom    -18.053697      0.004230     -0.003087       0.000002
   4 Atom    -14.431811     -0.000001      0.015744      -0.000001
   5 Atom    -18.053698     -0.004229     -0.003086       0.000001
   6 Atom     -0.764409     -0.044400      0.014598      -0.000002
   7 Atom     -0.873603     -0.023368     -0.030829       0.000002
   8 Atom     -0.873603      0.023368     -0.030828       0.000003
   9 Atom     -0.764409      0.044404      0.014599       0.000000
  10 Atom     -0.836678      0.000001      0.039163      -0.000003
-----------------------------------------------------------------
-----------------------------------------------------
   Center         ---- Electric Field Gradient ----
                    XX            YY            ZZ
-----------------------------------------------------
   1 Atom     -492.370043   -492.670708   -492.626546
   2 Atom     -492.370034   -492.670696   -492.626524
```

```
   3 Atom     -798.110755   -798.155064   -797.467103
   4 Atom     -492.441709   -492.137282   -492.442781
   5 Atom     -798.110758   -798.155054   -797.467091
   6 Atom       -1.927259     -1.522899     -1.420397
   7 Atom       -1.760777     -1.815872     -1.540815
   8 Atom       -1.760771     -1.815877     -1.540814
   9 Atom       -1.927285     -1.522907     -1.420404
  10 Atom       -1.564773     -1.986947     -1.532500
-----------------------------------------------------
-----------------------------------------------------
   Center         ---- Electric Field Gradient ----
                    XY            XZ            YZ
-----------------------------------------------------
   1 Atom        0.174050     -0.000001     -0.000003
   2 Atom       -0.174054      0.000012     -0.000011
   3 Atom        0.050085     -0.000055      0.000049
   4 Atom       -0.000004     -0.000002     -0.000020
   5 Atom       -0.050084      0.000023      0.000057
   6 Atom        0.158536     -0.000016      0.000009
   7 Atom       -0.214924      0.000010      0.000013
   8 Atom        0.214924     -0.000017      0.000020
   9 Atom       -0.158541     -0.000007      0.000002
  10 Atom        0.000005     -0.000001      0.000035
-----------------------------------------------------
-----------------------------------------------------
   Center         ---- Electric Field Gradient ----
                  ----       Eigenvalues       ----
-----------------------------------------------------
```

```
   1 Atom     -492.750361   -492.626546   -492.290390
   2 Atom     -492.750352   -492.626524   -492.290378
   3 Atom     -798.187676   -798.078143   -797.467103
   4 Atom     -492.442781   -492.441709   -492.137282
   5 Atom     -798.187669   -798.078144   -797.467091
   6 Atom       -1.982004     -1.468154     -1.420397
   7 Atom       -2.005007     -1.571642     -1.540815
   8 Atom       -2.005006     -1.571641     -1.540814
   9 Atom       -1.982031     -1.468162     -1.420404
  10 Atom       -1.986947     -1.564773     -1.532500
-----------------------------------------------------
-----------------------------------------------------
   Center         ---- Electric Field Gradient ----
                      ( tensor representation )
                  3XX-RR        3YY-RR        3ZZ-RR
-----------------------------------------------------
   1 Atom        0.185722     -0.114942     -0.070780
   2 Atom        0.185717     -0.114944     -0.070773
   3 Atom       -0.199781     -0.244090      0.443871
   4 Atom       -0.101118      0.203308     -0.102190
   5 Atom       -0.199790     -0.244087      0.443877
   6 Atom       -0.303741      0.100619      0.203121
   7 Atom       -0.054956     -0.110051      0.165006
   8 Atom       -0.054950     -0.110056      0.165007
   9 Atom       -0.303753      0.100625      0.203128
  10 Atom        0.129967     -0.292207      0.162240
-----------------------------------------------------
-----------------------------------------------------
```

```
   Center         ---- Electric Field Gradient ----
                      ( tensor representation )
                  ----       Eigenvalues       ----
 -----------------------------------------------------
   1 Atom       -0.194595     -0.070780      0.265375
   2 Atom       -0.194601     -0.070773      0.265374
   3 Atom       -0.276702     -0.167169      0.443871
   4 Atom       -0.102190     -0.101118      0.203308
   5 Atom       -0.276701     -0.167176      0.443877
   6 Atom       -0.358486      0.155364      0.203121
   7 Atom       -0.299186      0.134179      0.165006
   8 Atom       -0.299186      0.134179      0.165007
   9 Atom       -0.358499      0.155371      0.203128
  10 Atom       -0.292207      0.129967      0.162240
 -----------------------------------------------------
 1\1\GINC-E0002\SP\RB3LYP\6
 31G(d)\C3H5N2(1+)\ROOT\08-Aug-2019\0\\# nmr
 =giao b3lyp/6-31g(d) prop=(read,efg)\\DFT optimisatised
 NMR\\1,1\C,0,0
.681658,0.978152,0.00005\C,0,-0.681688,0.978131,0.000069\N,
0,-1.0
74316
,-0.348465,0.000016\C,0,0.000012,-1.142774,-0.000099\N,0,1.0
7432
7,-0.3


 48433,-0.000034\H,0,2.033749,-0.679602,-0.000065\H,0,1.392
```

```
 8
 9,1.7
 896,0.




000088\H,0,-1.392937,1.789564,0.00013\H,0,-2.033722,-0.679
6
 64,0.
 000029
 \H,0,0.000047,-2.222671,-0.000183\\Version=EM64L-
 G09RevC.01\State=1-A\
 HF=-226.5921732\RMSD=4.674e-
 09\Dipole=0.0000108,-0.5564373,-0.0000382\

 Quadrupole=5.2762011,2.3654635,-7.6416645,0.0000327,-0.000
 2718,
 0.00067
 11\PG=C01 [X(C3H5N2)]\\@




 ON A TOMBSTONE, "HERE LIES LESTER MOORE,
 FOUR SLUGS FROM A 44, NO LES, NO MORE".
 Job cpu time:  0 days  0 hours  0 minutes  9.3 seconds.
 File lengths (MBytes):  RWF=      9 Int=      0 D2E=      0 Chk=
```

```
8

Scr=      1

Normal termination of Gaussian 09 at Thu Aug  8 16:26:59

2019.
```

A.2 Topology File for Im

```
; Imd_GMX.top created by acpype (Rev: 0)

on Mon Sep 24 14:13:15 2018


[ moleculetype ]

;name            nrexcl

 Imd              3


[ atoms ]

;   nr  type  resi  res  atom  cgnr     charge      mass

; qtot   bond_type

     1   cc     1   Imd    C1    1

     0.069250     12.01000

     ; qtot 0.069

     2   cc     1   Imd    C2    2

     -0.123052     12.01000

     ; qtot -0.054

     3   cd     1   Imd    C3    3

     -0.123052     12.01000

     ; qtot -0.177

     4   na     1   Imd    N1    4

     -0.158974     14.01000

     ; qtot -0.336

     5   hn     1   Imd    H1    5

     0.374831      1.00800

     ; qtot 0.039

     6   h5     1   Imd    H2    6
```

```
     0.243370      1.00800
     ; qtot 0.282
     7   hn      1   Imd    H3    7
     0.374831      1.00800
     ; qtot 0.657
     8   h4      1   Imd    H4    8
     0.250885      1.00800
     ; qtot 0.908
     9   h4      1   Imd    H5    9
     0.250885      1.00800
     ; qtot 1.159
    10   na      1   Imd    N2   10
    -0.158974     14.01000
    ; qtot 1.000

[ bonds ]
;   ai      aj funct   r              k
     1       4   1
     1.3802e-01    3.5631e+05

     ;      C1 - N1
     1       6   1
     1.0819e-01    2.9430e+05

     ;      C1 - H2
     1      10   1
     1.3802e-01    3.5631e+05
```

```
;      C1 - N2

2       3   1

1.3729e-01    4.1915e+05


;      C2 - C3

2       8   1

1.0817e-01    2.9455e+05


;      C2 - H4

2      10   1

1.3802e-01    3.5631e+05


;      C2 - N2

3       4   1

1.3802e-01    3.5631e+05


;      C3 - N1

3       9   1

1.0817e-01    2.9455e+05


;      C3 - H5

4       5   1

1.0100e-01    3.4175e+05


;      N1 - H1

7      10   1

1.0100e-01    3.4175e+05
```

```
     ;     H3 - N2


[ pairs ]

;   ai      aj     funct

     1       8       1 ;      C1 - H4

     1       9       1 ;      C1 - H5

     2       5       1 ;      C2 - H1

     3       7       1 ;      C3 - H3

     4       7       1 ;      N1 - H3

     4       8       1 ;      N1 - H4

     5       9       1 ;      H1 - H5

     6       2       1 ;      H2 - C2

     6       3       1 ;      H2 - C3

     6       5       1 ;      H2 - H1

     6       7       1 ;      H2 - H3

     7       8       1 ;      H3 - H4

     8       9       1 ;      H4 - H5

     9      10       1 ;      H5 - N2

    10       5       1 ;      N2 - H1


[ angles ]

;   ai      aj      ak     funct   theta          cth

     1       4       3       1

     1.2801e+02    5.3095e+02

     ;     C1 - N1     - C3

     1       4       5       1

     1.2550e+02    3.9120e+02

     ;     C1 - N1     - H1
```

```
1      10       2       1

1.0990e+02    5.7304e+02

;      C1 - N2      - C2

1      10       7       1

1.2550e+02    3.9120e+02

;      C1 - N2      - H3

2       3       4       1

1.0699e+02    6.1446e+02

;      C2 - C3      - N1

2       3       9       1

1.2848e+02    3.9556e+02

;      C2 - C3      - H5

2      10       7       1

1.2550e+02    3.9120e+02

;      C2 - N2      - H3

3       2       8       1

1.2848e+02    3.9556e+02

;      C3 - C2      - H4

3       2      10       1

1.0699e+02    6.1446e+02

;      C3 - C2      - N2

3       4       5       1

1.2550e+02    3.9120e+02

;      C3 - N1      - H1

4       1       6       1

1.2155e+02    4.1489e+02

;      N1 - C1      - H2

4       1      10       1
```

```
     1.0660e+02    6.2902e+02

     ;      N1 - C1      - N2

     4       3       9       1

     1.2053e+02    4.1664e+02

     ;      N1 - C3      - H5

     6       1      10       1

     1.2155e+02    4.1489e+02

     ;      H2 - C1      - N2

     8       2      10       1

     1.2053e+02    4.1664e+02

     ;      H4 - C2      - N2


[ dihedrals ] ; propers

; treated as RBs in GROMACS to use combine multiple

AMBER torsions per quartet

;     i       j       k       l    func     C0          C1          C2

C3          C4          C5

1       4       3       2       3

14.22560    0.00000   -14.22560

0.00000     0.00000     0.00000

;      C1-     N1-     C3-     C2

1       4       3       9       3

14.22560    0.00000   -14.22560

0.00000     0.00000     0.00000

;      C1-    N1-     C3-     H5

1      10       2       3       3

14.22560    0.00000   -14.22560

0.00000     0.00000     0.00000
```

```
;      C1-    N2-     C2-     C3
1      10       2       8       3
14.22560    0.00000  -14.22560
0.00000    0.00000    0.00000 ;
C1-    N2-     C2-     H4
2       3       4       5       3
14.22560    0.00000  -14.22560
0.00000    0.00000    0.00000 ;
C2-    C3-     N1-     H1
3       2      10       7       3
14.22560    0.00000  -14.22560
0.00000    0.00000    0.00000 ;
C3-    C2-     N2-     H3
4       1      10       2       3
14.22560    0.00000  -14.22560
0.00000    0.00000    0.00000 ;
N1- C1-     N2-    C2
4       1      10       7       3
14.22560    0.00000  -14.22560
0.00000    0.00000    0.00000 ;
N1- C1-     N2-    H3
 4       3       2       8       3
 33.47200    0.00000  -33.47200
 0.00000    0.00000    0.00000 ;
 N1-     C3-     C2-     H4
4       3       2      10       3
33.47200    0.00000  -33.47200
0.00000    0.00000    0.00000 ;
```

```
N1-    C3-    C2-    N2
5      4      3      9      3
14.22560    0.00000  -14.22560
0.00000    0.00000    0.00000 ;
H1-    N1-    C3-    H5
6      1      4      3      3
14.22560    0.00000  -14.22560
0.00000    0.00000    0.00000 ;
H2-    C1-    N1-    C3
6      1      4      5      3
14.22560    0.00000  -14.22560
0.00000    0.00000    0.00000 ;
H2-    C1-    N1-    H1
6      1     10      2      3
14.22560    0.00000  -14.22560
0.00000    0.00000    0.00000 ;
H2-    C1-    N2-    C2
6      1     10      7      3
14.22560    0.00000  -14.22560
0.00000    0.00000    0.00000 ;
H2-    C1-    N2-    H3
7     10      2      8      3
14.22560    0.00000  -14.22560
0.00000    0.00000    0.00000 ;
H3- N2-    C2-    H4
8      2      3      9      3
33.47200    0.00000  -33.47200
0.00000    0.00000    0.00000 ;
```

```
H4- C2-    C3-    H5
9      3      2     10       3
33.47200    0.00000  -33.47200
0.00000    0.00000    0.00000 ;
H5- C3-    C2-    N2
10      1      4      3      3
14.22560    0.00000  -14.22560
0.00000    0.00000    0.00000 ;
N2- C1-    N1-    C3
10      1      4      5      3
14.22560    0.00000  -14.22560
0.00000    0.00000    0.00000 ;
N2- C1-    N1-    H1

[ dihedrals ] ; impropers
; treated as propers in GROMACS to use correct AMBER
analytical function
;    i      j      k      l   func   phase     kd      pn
; Dennis added the last 3 dihedrals on oct 8th 2018
     1      2     10      7      1
     180.00   4.60240   2 ;
     C1-    C2-    N2-    H3
     1      3      4      5      1
     180.00   4.60240   2 ;
     C1-    C3-    N1-    H1
;     6      1      4     10      1
180.00   4.60240   2 ;
H6-    C1-   N10-    N4
```

```
;     8      2      3     10      1

180.00   4.60240   2 ;

H8-    C2-    C3-   N10

;     9      3      2      4      1

180.00   4.60240   2 ;

H9-    C3-    C2-   N10
```

A.3 Topology file for TPA

```
; HTp_GMX.top created by acpype (Rev: 0) on Mon Sep 24 14:33:08 2018

[ moleculetype ]
;name            nrexcl
 HTp              3

[ atoms ]
;   nr  type  resi  res  atom  cgnr     charge      mass
; qtot   bond_type
     1    ca     1   HTp    C1    1
     -0.147815     12.01000
     ; qtot -0.148
     2    ca     1   HTp    C2    2
     -0.200250     12.01000
     ; qtot -0.348
     3    ca     1   HTp    C3    3
     0.092635     12.01000
     ;qtot -0.255
     4    ca     1   HTp    C4    4
     -0.200250     12.01000
     ; qtot -0.456
     5    ca     1   HTp    C5    5
     -0.147815     12.01000
     ; qtot -0.603
     6    ca     1   HTp    C6    6
     -0.098594     12.01000
```

```
 ; qtot -0.702
 7   ha     1   HTp   H1    7
 0.140937      1.00800
 ; qtot -0.561
 8   ha     1   HTp   H2    8
 0.143673      1.00800
 ; qtot -0.417
 9   ha     1   HTp   H3    9
 0.143673      1.00800
 ; qtot -0.274
10   ha     1   HTp   H4   10
0.140937      1.00800
; qtot -0.133
11    c     1   HTp   C7   11
0.766855     12.01000
; qtot 0.634
12    o     1   HTp   O1   12
-0.634101     16.00000
; qtot -0.000
13   oh     1   HTp   O2   13
-0.660660     16.00000
; qtot -0.661
14   ho     1   HTp   H5   14
0.435810      1.00800
; qtot -0.225
15    c     1   HTp   C8   15
0.767597     12.01000
; qtot 0.543
```

```
    16     o      1    HTp     O3    16
    -0.771316      16.00000
    ; qtot -0.229
    17     o      1    HTp     O4    17
    -0.771316      16.00000
    ; qtot -1.000

[ bonds ]
;    ai      aj funct    r              k
      1       2    1     1.3984e-01     3.8585e+05
      ;      C1 - C2
      1       6    1     1.3984e-01     3.8585e+05
      ;      C1 - C6
      1       7    1     1.0860e-01     2.8937e+05
      ;      C1 - H1
      2       3    1     1.3984e-01     3.8585e+05
      ;      C2 - C3
      2       8    1     1.0860e-01     2.8937e+05
      ;      C2 - H2
      3       4    1     1.3984e-01     3.8585e+05
      ;      C3 - C4
      3      15    1     1.4906e-01     2.8945e+05
      ;      C3 - C8
      4       5    1     1.3984e-01     3.8585e+05
      ;      C4 - C5
      4       9    1     1.0860e-01     2.8937e+05
      ;      C4 - H3
      5       6    1     1.3984e-01     3.8585e+05
```

```
     ;      C5 - C6

     5      10   1    1.0860e-01    2.8937e+05

     ;      C5 - H4

     6      11   1    1.4906e-01    2.8945e+05

     ;      C6 - C7

    11      12   1    1.2183e-01    5.3363e+05

    ;      C7 - O1

    11      13   1    1.3513e-01    3.3480e+05

    ;      C7 - O2

    13      14   1    9.7300e-02    3.1079e+05

    ;      O2 - H5

    15      16   1    1.2183e-01    5.3363e+05

    ;      C8 - O3

    15      17   1    1.2183e-01    5.3363e+05

    ;      C8 - O4


[ pairs ]

;   ai      aj    funct

     1       4      1 ;      C1 - C4

     1      10      1 ;      C1 - H4

     1      12      1 ;      C1 - O1

     1      13      1 ;      C1 - O2

     1      15      1 ;      C1 - C8

     2       5      1 ;      C2 - C5

     2       9      1 ;      C2 - H3

     2      11      1 ;      C2 - C7

     2      16      1 ;      C2 - O3

     2      17      1 ;      C2 - O4
```

```
     3      10       1 ;      C3 - H4

     4       8       1 ;      C4 - H2

     4      11       1 ;      C4 - C7

     4      16       1 ;      C4 - O3

     4      17       1 ;      C4 - O4

     5      12       1 ;      C5 - O1

     5      13       1 ;      C5 - O2

     5      15       1 ;      C5 - C8

     6       3       1 ;      C6 - C3

     6       8       1 ;      C6 - H2

     6       9       1 ;      C6 - H3

     6      14       1 ;      C6 - H5

     7       3       1 ;      H1 - C3

     7       5       1 ;      H1 - C5

     7       8       1 ;      H1 - H2

     7      11       1 ;      H1 - C7

     8      15       1 ;      H2 - C8

     9      10       1 ;      H3 - H4

     9      15       1 ;      H3 - C8

    10      11       1 ;      H4 - C7

    12      14       1 ;      O1 - H5


[ angles ]

;   ai      aj      ak    funct   theta           cth

     1       2       3       1

     1.2002e+02    5.5748e+02

     ;      C1 - C2      - C3

     1       2       8       1
```

```
1.1988e+02    4.0317e+02

;      C1 - C2      - H2

1       6       5       1

1.2002e+02    5.5748e+02

;      C1 - C6      - C5

1       6      11       1

1.2033e+02    5.3790e+02

;      C1 - C6      - C7

2       1       6       1

1.2002e+02    5.5748e+02

;      C2 - C1      - C6

2       1       7       1

1.1988e+02    4.0317e+02

;      C2 - C1      - H1

2       3       4       1

1.2002e+02    5.5748e+02

;      C2 - C3      - C4

2       3      15       1

1.2033e+02    5.3790e+02

;      C2 - C3      - C8

3       2       8       1

1.1988e+02    4.0317e+02

;      C3 - C2      - H2

3       4       5       1

1.2002e+02    5.5748e+02

;      C3 - C4      - C5

3       4       9       1

1.1988e+02    4.0317e+02
```

```
;      C3 - C4      - H3

3      15      16       1

1.2260e+02    5.7505e+02

;      C3 - C8      - O3

3      15      17       1

1.2260e+02    5.7505e+02

;      C3 - C8      - O4

4       3      15       1

1.2033e+02    5.3790e+02

;      C4 - C3      - C8

4       5       6       1

1.2002e+02    5.5748e+02

;      C4 - C5      - C6

4       5      10       1

1.1988e+02    4.0317e+02

;      C4 - C5      - H4

5       4       9       1

1.1988e+02    4.0317e+02

;      C5 - C4      - H3

5       6      11       1

1.2033e+02    5.3790e+02

;      C5 - C6      - C7

6       1       7       1

1.1988e+02    4.0317e+02

;      C6 - C1      - H1

6       5      10       1

1.1988e+02    4.0317e+02

;      C6 - C5      - H4
```

```
     6      11      12       1
     1.2260e+02    5.7505e+02
     ;      C6 - C7      - O1
     6      11      13       1
     1.1345e+02    5.7865e+02
     ;      C6 - C7      - O2
    11      13      14       1
    1.0655e+02    4.1740e+02
    ;      C7 - O2      - H5
    12      11      13       1
    1.2210e+02    6.3530e+02
    ;      O1 - C7      - O2
    16      15      17       1
    1.3025e+02    6.5220e+02
    ;      O3 - C8      - O4

[ dihedrals ] ; propers
; treated as RBs in GROMACS to use combine multiple
AMBER torsions per quartet
;    i      j      k      l   func    C0         C1
C2          C3          C4          C5
     1      2      3      4      3
     30.33400    0.00000  -30.33400
     0.00000    0.00000    0.00000
     ;      C1-    C2-    C3-    C4
     1      2      3     15      3
     30.33400    0.00000  -30.33400
     0.00000    0.00000    0.00000
```

```
;      C1-     C2-     C3-     C8

1       6       5       4       3

30.33400    0.00000  -30.33400

0.00000    0.00000    0.00000

C1-     C6-     C5-     C4

1       6       5      10       3

30.33400    0.00000  -30.33400

0.00000    0.00000    0.00000

;      C1-     C6-     C5-     H4

1       6      11      12       3

8.36800    0.00000   -8.36800

0.00000    0.00000    0.00000

;      C1-     C6-     C7-     O1

1       6      11      13       3

8.36800    0.00000   -8.36800

0.00000    0.00000    0.00000

;      C1-     C6-     C7-     O2

2       1       6       5       3

30.33400    0.00000  -30.33400

0.00000    0.00000    0.00000

;      C2-     C1-     C6-     C5

2       1       6      11       3

30.33400    0.00000  -30.33400

0.00000    0.00000    0.00000

;      C2-     C1-     C6-     C7

2       3       4       5       3

30.33400    0.00000  -30.33400

0.00000    0.00000    0.00000
```

```
;      C2-     C3-     C4-     C5
2       3       4       9       3
30.33400    0.00000  -30.33400
0.00000    0.00000    0.00000
;      C2-     C3-     C4-     H3
2       3      15      16       3
8.36800    0.00000   -8.36800
0.00000    0.00000    0.00000
;      C2-     C3-     C8-     O3
2       3      15      17       3
8.36800    0.00000   -8.36800
0.00000    0.00000    0.00000
;      C2-     C3-     C8-     O4
3       4       5       6       3
30.33400    0.00000  -30.33400
0.00000    0.00000    0.00000
;      C3-     C4-     C5-     C6
3       4       5      10       3
30.33400    0.00000  -30.33400
0.00000    0.00000    0.00000
;      C3-     C4-     C5-     H4
4       3       2       8       3
30.33400    0.00000  -30.33400
0.00000    0.00000    0.00000
;      C4-     C3-     C2-     H2
4       3      15      16       3
8.36800    0.00000   -8.36800
0.00000    0.00000    0.00000
```

```
;      C4-     C3-     C8-     O3
4       3      15      17       3
8.36800     0.00000    -8.36800
0.00000     0.00000     0.00000
;      C4-     C3-     C8-     O4
4       5       6      11       3
30.33400     0.00000  -30.33400
0.00000     0.00000     0.00000
;      C4-     C5-     C6-     C7
5       4       3      15       3
30.33400     0.00000  -30.33400
0.00000     0.00000     0.00000
;      C5-     C4-     C3-     C8
5       6      11      12       3
8.36800     0.00000    -8.36800
0.00000     0.00000     0.00000
;      C5-     C6-     C7-     O1
5       6      11      13       3
8.36800     0.00000    -8.36800
0.00000     0.00000     0.00000
;      C5-     C6-     C7-     O2
6       1       2       3       3
30.33400     0.00000  -30.33400
0.00000     0.00000     0.00000
;      C6-     C1-     C2-     C3
6       1       2       8       3
30.33400     0.00000  -30.33400
0.00000     0.00000     0.00000
```

```
;     C6-    C1-    C2-    H2
6      5      4      9      3
30.33400    0.00000  -30.33400
0.00000    0.00000    0.00000
;     C6-    C5-    C4-    H3
6     11     13     14      3
19.24640    0.00000  -19.24640
0.00000    0.00000    0.00000
;     C6-    C7-    O2-    H5
7      1      2      3      3
30.33400    0.00000  -30.33400
0.00000    0.00000    0.00000
;     H1-    C1-    C2-    C3
7      1      2      8      3
30.33400    0.00000  -30.33400
0.00000    0.00000    0.00000
;     H1-    C1-    C2-    H2
7      1      6      5      3
30.33400    0.00000  -30.33400
0.00000    0.00000    0.00000
;     H1-    C1-    C6-    C5
7      1      6     11      3
30.33400    0.00000  -30.33400
0.00000    0.00000    0.00000
;     H1-    C1-    C6-    C7
8      2      3     15      3
30.33400    0.00000  -30.33400
0.00000    0.00000    0.00000
```

```
     ;     H2-    C2-    C3-    C8
     9      4      3     15      3
     30.33400    0.00000  -30.33400
     0.00000    0.00000    0.00000
     ;     H3-    C4-    C3-    C8
     9      4      5     10      3
     30.33400    0.00000  -30.33400
     0.00000    0.00000    0.00000
     ;     H3-    C4-    C5-    H4
    10      5      6     11      3
    30.33400    0.00000  -30.33400
    0.00000    0.00000    0.00000
    ;     H4-    C5-    C6-    C7
    12     11     13     14      3
    27.19600   -7.94960  -19.24640
    0.00000    0.00000    0.00000
    ;     O1-    C7-    O2-    H5

[ dihedrals ] ; impropers
; treated as propers in GROMACS to use correct AMBER
analytical function
;    i      j      k      l
func   phase     kd      pn
     1      3      2      8      1
     180.00   4.60240   2
     ;     C1-    C3-    C2-
     H2
     3      5      4      9      1
```

```
180.00   4.60240   2

;      C3-    C5-    C4-

H3

3      16      15      17       1

180.00   4.60240   2

;      C3-    O3-

C8-    O4

4       6       5      10       1

180.00   4.60240   2

;      C4-    C6-

C5-    H4

6      13      11      12       1

180.00  43.93200   2

;      C6-    O2-

C7-    O1

7       1       6       2       1

180.00   4.60240   2

;      H1-    C1-

C6-    C2
```

Abbreviations

Abbreviation	Meaning
ACF	Autocorrelation Function
AMBER	Assisted Model Building with Energy Refinement
CCDC	Cambridge Crystallographic Data Centre
CF	Cone Frame
DFT	Density Function Theory
DP	Direct Propagation
EFG	Electric Field Gradient
EPR	Electron Paramagnetic Resonance Spectroscopy
FFT	Fast Fourier Transform
FID	Free Induction Decay
FML	Fast Motional Limit
GROMACS	GROningen MAchine for Chemical Simulations
Im	Imidazolium Cation
LAB	Laboratory Frame
LINCS	LINear Constraint Solver
MD	Molecular Dynamics
NMR	Nuclear Magnetic Resonance Spectroscopy

Table A.1: List of Abbreviations

PAS	Principle Axis system
r.f	Radio Frequency
SLE	Stochastic Liouville Equation
TPA	Hydrogen Terephthalate Anion
VMD	Visual Molecular Dynamics

Table A.1: List of Abbreviations

Bibliography

---

[1] Vasily S. Oganesyan. A general approach for prediction of motional epr spectra from molecular dynamics (md) simulations: application to spin labelled protein. *Phys. Chem. Chem. Phys.*, 13:4724–4737, 2011.

[2] Ryogo Kubo. Stochastic liouville equations. *Journal of Mathematical Physics*, 4(2):174–183, 1963.

[3] Trivikram R. Molugu, Soohyun Lee, and Michael F. Brown. Concepts and methods of solid-state nmr spectroscopy applied to biomembranes. *Chemical Reviews*, 117(19):12087–12132, 2017. PMID: 28906107.

[4] V. Macho, L. Brombacher, and H. W. Spiess. The nmr-weblab: An internet approach to nmr lineshape analysis. *Applied Magnetic Resonance*, 20(3):405–432, Apr 2001.

[5] Chao Shi, Xi Zhang, Chun-Hua Yu, Ye-Feng Yao, and Wen Zhang. Geometric isotope effect of deuteration in a hydrogen-bonded hostâeur"guest crystal. *Nature Communications*, 9(1):481, 2018.

[6] B. I. Ionin and B. A. Ershov. *The Fundamentals of NMR Spectroscopy*, pages 1–59. Springer US, Boston, MA, 1970.

[7] Nikolay V. Anisimov and Olga S. Pavlova. Simultaneous recording of nmr signals from nuclei with different gyromagnetic ratios using

undersampling technique. *Applied Magnetic Resonance*, 49(5):523–532, May 2018.

[8] T Vosegaard, IP Byriel, L Binet, D Massiot, and HJ Jakobsen. Crystal structure studies by single-crystal NMR spectroscopy. Ga-71 and Ga-69 single-crystal NMR of beta-Ga(2)0(3) twins. *JOURNAL OF THE AMERICAN CHEMICAL SOCIETY*, 120(32):8184–8188, AUG 19 1998.

[9] Robin K. Harris, Edwin D. Becker, Sonia M. Cabral De Menezes, Pierre Granger, Roy E. Hoffman, and Kurt W. Zilm. Further conventions for NMR shielding and chemical shifts (IUPAC recommendations 2008). *PURE AND APPLIED CHEMISTRY*, 80(1):59–84, JAN 2008.

[10] E. L. Hahn and D. E. Maxwell. Spin echo measurements of nuclear spin coupling in molecules. *Phys. Rev.*, 88:1070–1084, Dec 1952.

[11] Piotr Tekely. Malcolm h. levitt. spin dynamics: basics of nuclear magnetic resonance. john wiley & sons, chichester, uk, 2001, 686 pp. price £34.95. isbn 0-471-48921-2. *Magnetic Resonance in Chemistry*, 40(12):800–800, 2002.

[12] J. A. S. Smith. Nuclear quadrupole resonance spectroscopy. general principles. *Journal of Chemical Education*, 48(1):39, 1971.

[13] J. C. Bevington, J. R. Ebdon, and T. N. Huckerby. *Solution-state NMR determination of polymer end-groups, substituents and minor structures*, pages 80–124. Springer Netherlands, Dordrecht, 1993.

[14] GJ MARTIN, ML MARTIN, and BL ZHANG. SITE-SPECIFIC NATURAL ISOTOPE FRACTIONATION OF HYDROGEN IN PLANT-PRODUCTS STUDIED BY NUCLEAR-MAGNETIC-

RESONANCE. *PLANT CELL AND ENVIRONMENT*, 15(9):1037–1050, DEC 1992.

[15] BQ SUN, PR COSTA, D KOCISKO, PT LANSBURY, and RG GRIFFIN. INTERNUCLEAR DISTANCE MEASUREMENTS IN SOLID-STATE NUCLEAR-MAGNETIC-RESONANCE - DIPOLAR RECOUPLING VIA ROTOR SYNCHRONIZED SPIN LOCKING. *JOURNAL OF CHEMICAL PHYSICS*, 102(2):702–707, JAN 8 1995.

[16] Robert "Graf, D. Demco, J. Gottwald, Siegfried Hafner, and Hans" Spiess. Dipolar couplings and internuclear distances by double-quantum nuclear magnetic resonance spectroscopy of solids. *The Journal of Chemical Physics*, 106:885–895, 01 1997.

[17] Francis Cloran, Ian Carmichael, and Anthony S. Serianni. 2jcoc spin-spin coupling constants across glycosidic linkages exhibit a valence bond-angle dependence. *Journal of the American Chemical Society*, 122(2):396–397, 2000.

[18] Sophie Lau, Naomi Stanhope, John Griffin, Eleri Hughes, and David A. Middleton. Drug orientations within statin-loaded lipoprotein nanoparticles by 19f solid-state nmr. *Chem. Commun.*, 55:13287–13290, 2019.

[19] Federico M. Paruzzo, Brennan J. Walder, and Lyndon Emsley. Line narrowing in 1h nmr of powdered organic solids with top-ct-mas experiments at ultra-fast mas. *Journal of Magnetic Resonance*, 305:131 – 137, 2019.

[20] Nonappa . and Erkki Kolehmainen. Caffeine as a gelator. *Gels*, 2:9, 03 2016.

[21] Maggy Hologne and J Hirschinger. Molecular dynamics as studied by static-powder and magic-angle spinning 2h nmr. *Solid state nuclear magnetic resonance*, 26:1–10, 09 2004.

[22] Marica Cutajar, Sharon E. Ashbrook, and Stephen Wimperis. H-2 double-quantum MAS NMR spectroscopy as a probe of dynamics on the microsecond timescale in solids. *CHEMICAL PHYSICS LETTERS*, 423(4-6):276–281, JUN 1 2006. 4th Alpine Conference on Solid-State NMR, Chamonix, FRANCE, SEP 11-15, 2005.

[23] Sasa Antonijevic, Sharon E. Ashbrook, Silke Biedasek, Richard I. Walton, Stephen Wimperis, and Huaixin Yang. Dynamics on the microsecond timescale in microporous aluminophosphate alpo-14 as evidenced by 27al mqmas and stmas nmr spectroscopy. *Journal of the American Chemical Society*, 128(24):8054–8062, 2006. PMID: 16771521.

[24] Jaclyn Catalano, Anna Murphy, Yao Yao, Nicholas Zumbulyadis, Silvia A. Centeno, and Cecil Dybowski. Molecular dynamics of palmitic acid and lead palmitate in cross-linked linseed oil films: Implications from deuterium magnetic resonance for lead soap formation in traditional oil paintings. *SOLID STATE NUCLEAR MAGNETIC RESONANCE*, 89:21–26, FEB 2018.

[25] R. Eckman and A. J. Vega. Deuterium nmr study of organic molecules absorbed by zeolites. *Journal of the American Chemical Society*, 105(14):4841–4842, 1983.

[26] "Scott Sneddon, Juergen Kahr, Angelica F. Orsi, David J. Price, Daniel M. Dawson, Paul A. Wright, and Sharon E." Ashbrook. Investigation of zeolitic imidazolate frameworks using 13c and 15n solid-state nmr

spectroscopy". *"Solid State Nuclear Magnetic Resonance"*, 87":54–64", 10" 2017".

[27] Junichi. Fukasawa, Chi Duen. Poon, and Edward T. Samulski. Deuterium nmr investigation of benzene adsorbed on boehmite glasses. *Langmuir*, 7(8):1727–1733, 1991.

[28] Bryan E. G. Lucier, Yue Zhang, Kelly J. Lee, Yuanjun Lu, and Yining Huang. Grasping hydrogen adsorption and dynamics in metal–organic frameworks using 2h solid-state nmr. *Chem. Commun.*, 52:7541–7544, 2016.

[29] Robert M. Marti, Joshua D. Howe, Cody R. Morelock, Mark S. Conradi, Krista S. Walton, David S. Sholl, and Sophia E. Hayes. Co2 dynamics in pure and mixed-metal mofs with open metal sites. *The Journal of Physical Chemistry C*, 121(46):25778–25787, 2017.

[30] Theodore P. Trouard, Alexander A. Nevzorov, Todd M. Alam, Constantin Job, Jaroslav Zajicek, and Michael F. Brown. Influence of cholesterol on dynamics of dimyristoylphosphatidylcholine bilayers as studied by deuterium nmr relaxation. *The Journal of Chemical Physics*, 110(17):8802–8818, 1999.

[31] Mehran Shaghaghi, Amir Keyvanloo, Zhaohua Huang, Francis C. Szoka, and Jenifer L. Thewalt. Constrained versus free cholesterol in dppc membranes: A comparison of chain ordering ability using deuterium nmr. *Langmuir*, 33(50):14405–14413, 2017. PMID: 29120186.

[32] Matthew R. Elkins, Jonathan K. Williams, Martin D. Gelenter, Peng Dai, Byungsu Kwon, Ivan V. Sergeyev, Bradley L. Pentelute, and Mei Hong. Cholesterol-binding site of the influenza m2 protein in lipid

bilayers from solid-state nmr. *Proceedings of the National Academy of Sciences*, 114(49):12946–12951, 2017.

[33] Ishita Sengupta, Philippe S. Nadaud, and Christopher P. Jaroniec. Protein structure determination with paramagnetic solid-state nmr spectroscopy. *Accounts of Chemical Research*, 46(9):2117–2126, 2013. PMID: 23464364.

[34] Frédéric Bouyer, Gérard Picard, and Jean-Jacques Legendre. Computational chemistry: A way to reach spectroscopic and thermodynamic data for exotic compounds. *Journal of Chemical Information and Computer Sciences*, 36(4):684–693, 1996.

[35] P. Hebert, Sebastien and H. Bernhard Schlegel. Computational study of the ph-dependent competition between carbonate and thymine addition to the guanine radical. *Chemical Research in Toxicology*, 32(1):195–210, 2019.

[36] Suvonil Sinha Ray. Ab initio diagnosis of isomerization pathway of diphosphene and diphosphinylidene. *Chemical Physics*, 529:110555, 2020.

[37] Xuan Guo, Rui Ming Zhang, Lu Gem Gao, Xin Zhang, and Xuefei Xu. Computational kinetics of the hydrogen abstraction reactions of n-propanol and iso-propanol by oh radical. *Phys. Chem. Chem. Phys.*, 21:24458–24468, 2019.

[38] María A. Izquierdo, Junqing Shi, Sangyoon Oh, Soo Young Park, Begoña Milián-Medina, Johannes Gierschner, and Daniel Roca-Sanjuán. Excited-state non-radiative decay in stilbenoid compounds: an ab initio quantum-chemistry study on size and substituent effects. *Phys. Chem. Chem. Phys.*, 21:22429–22439, 2019.

[39] F. Ruipérez. Application of quantum chemical methods in polymer chemistry. *International Reviews in Physical Chemistry*, 38(3-4):343–403, 2019.

[40] Christopher Robertson and Scott Habershon. Fast screening of homogeneous catalysis mechanisms using graph-driven searches and approximate quantum chemistry. *CATALYSIS SCIENCE & TECHNOLOGY*, 9(22):6357–6369, NOV 21 2019.

[41] Ralf Meyer, Klemens S. Schmuck, and Andreas W. Hauser. Machine learning in computational chemistry: An evaluation of method performance for nudged elastic band calculations. *Journal of Chemical Theory and Computation*, 15(11):6513–6523, 2019. PMID: 31553610.

[42] Peter Gast and Edgar J.J. Groenen. *EPR Interactions – g -Anisotropy*, pages 1435–1444. American Cancer Society, 2016.

[43] Joshua Telser. *EPR Interactions – Zero-Field Splittings*, pages 207–234. American Cancer Society, 2017.

[44] Débora M. Martino, Mario C.G. Passeggi, Rafael Calvo, and Otaciro R. Nascimento. Epr spectroscopy and exchange interaction parameters in cu(glycine)2·h2o. *Physica B: Condensed Matter*, 225(1):63 – 75, 1996.

[45] Marina Bennati. *EPR Interactions – Hyperfine Couplings*, pages 271–282. American Cancer Society, 2017.

[46] C. Prior, L. Danilāne, and V. S. Oganesyan. All-atom molecular dynamics simulations of spin labelled double and single-strand dna for epr studies. *Phys. Chem. Chem. Phys.*, 20:13461–13472, 2018.

[47] Andrea Catte, Gaye F. White, Mark R. Wilson, and Vasily S. Oganesyan. Direct prediction of epr spectra from lipid bilayers

: understanding structure and dynamics in biological membranes. *ChemPhysChem.*, 19(7):2183–2193, September 2018.

[48] Vasily S. Oganesyan, Fatima Chami, Gaye F. White, and Andrew J. Thomson. A combined EPR and MD simulation study of a nitroxyl spin label with restricted internal mobility sensitive to protein dynamics. *Journal of Magnetic Resonance*, 274:24–35, Jan 2017.

[49] H. Bernhard Schlegel. Geometry optimization. *WIREs Computational Molecular Science*, 1(5):790–809, 2011.

[50] H. Bernhard Schlegel. Optimization of equilibrium geometries and transition structures. *Journal of Computational Chemistry*, 3(2):214–218, 1982.

[51] J. J. Hernández, Gómez, V. Marquina, and R. Gómez. Algorithm to compute the electric field gradient tensor in ionic crystals. *Revista Mexicana de Fisica*, 2011.

[52] F. Chami, M. R. Wilson, and V. S. Oganesyan. Molecular dynamics and epr spectroscopic studies of 8cb liquid crystal. *Soft Matter*, 8:6823–6833, 2012.

[53] M J. Duer. *Introduction to Solid State NMR Spectroscopy.* Blackwell Publishing, 2004.

[54] Uwe Semmelmann and Gregor Weingart. The standard laplace operator. *manuscripta mathematica*, 158(1):273–293, Jan 2019.

[55] Derick Kaseman and Meghan McKenney, 2019.

[56] C. M. Gall, J. A. DiVerdi, and S. J. Opella. Phenylalanine ring dynamics by solid-state deuterium nmr. *Journal of the American Chemical Society*, 103(17):5039–5043, 1981.

[57] Robert G. Bryant. The nmr time scale. *Journal of Chemical Education*, 60(11):933, 1983.

[58] Yannick Millot and Pascal P. Man. Active and passive rotations with euler angles in nmr. *Concepts in Magnetic Resonance Part A*, 40A(5):215–252, 2012.

[59] Brian C. Hall. *Systems and Subsystems, Multiple Particles*, pages 419–440. Springer New York, New York, NY, 2013.

[60] Mark W. Maciejewski, Harry Z. Qui, Iulian Rujan, Mehdi Mobli, and Jeffrey C. Hoch. Nonuniform sampling and spectral aliasing. *Journal of magnetic resonance (San Diego, Calif. : 1997)*, 2009.

[61] Mei Hong, Xiaolan Yao, Karen Jakes, and Daniel Huster. Investigation of molecular motions by lee-goldburg cross-polarization nmr spectroscopy. *The Journal of Physical Chemistry B*, 106(29):7355–7364, 2002.

[62] C M Gall, T A Cross, J A DiVerdi, and S J Opella. Protein dynamics by solid-state nmr: aromatic rings of the coat protein in fd bacteriophage. *Proceedings of the National Academy of Sciences*, 79(1):101–105, 1982.

[63] H BEKKER, HJC BERENDSEN, EJ DIJKSTRA, S ACHTEROP, R VONDRUMEN, D VANDERSPOEL, A SIJBERS, H Keegstra, and MKR RENARDUS. Gromacs - a parallel computer for molecular-dynamics simulations. In RA DeGroot and J Nadrchal, editors, *PHYSICS COMPUTING '92*, pages 252–256. World Scientific Publishing, 1993.

[64] Junmei Wang, Wei Wang, Peter A. Kollman, and David A Case. Automatic atom type and bond type perception in molecular

mechanical calculations. *Journal of molecular graphics & modelling*, 25 2:247–60, 2006.

[65] D.J. Thouless and J.G. Valatin. Time-dependent hartree-fock equations and rotational states of nuclei. *Nuclear Physics*, 31:211 – 230, 1962.

[66] Benedict J. Leimkuhler, Sebastian Reich, and Robert D. Skeel. *Integration Methods for Molecular Dynamics*, pages 161–185. Springer New York, New York, NY, 1996.

[67] Stewart A. Adcock and J. Andrew McCammon. Molecular dynamics Survey of methods for simulating the activity of proteins. *Chemical Reviews*, 106(5):1589–1615, 2006. PMID: 16683746.

[68] William Humphrey, Andrew Dalke, and Klaus Schulten. Vmd: Visual molecular dynamics. *Journal of Molecular Graphics*, 14(1):33 – 38, 1996.

[69] F. Bloch. Nuclear induction. *Phys. Rev.*, 70:460–474, Oct 1946.

[70] I. P. Gerothanassis and C. G. Tsanaktsidis. Nuclear electric quadrupole relaxation. *Concepts in Magnetic Resonance*, 8(1):63–74, 1996.

[71] Jeffery B. Klauda, Mary F. Roberts, Alfred G. Redfield, Bernard R. Brooks, and Richard W. Pastor. Rotation of lipids in membranes: Molecular dynamics simulation, 31p spin-lattice relaxation, and rigid-body dynamics. *Biophysical Journal*, 94(8):3074 – 3083, 2008.

[72] M. J. Frisch et al. Gaussian˜16 Revision C.01, 2016.